2017-08-01

Ion Trap Miniaturization Considerations: Space-Charge Effects in Cylindrical Ion Traps and Misalignment Effects in a Two-Plate Linear Ion Trap

Yuan Tian
Brigham Young University

Ion Trap Miniaturization Considerations: Space-Charge Effects in Cylindrical Ion Traps and Misalignment Effects in a Two-Plate Linear Ion Trap

Yuan Tian

A dissertation submitted to the faculty of
Brigham Young University
in partial fulfillment of the requirements for the degree of

Doctor of Philosophy

Daniel E. Austin, Chair
David V. Dearden
Steven R. Goates
Jaron C. Hansen
Brian F. Woodfield

Department of Chemistry and Biochemistry

Brigham Young University

ABSTRACT

Ion Trap Miniaturization Considerations: Space-Charge Effects in Cylindrical Ion Traps and Misalignment Effects in a Two-Plate Linear Ion Trap

Yuan Tian
Department of Chemistry and Biochemistry, BYU
Doctor of Philosophy

Portable mass spectrometers provide convenience for applications where conventional mass spectrometers are not suitable. However, a series of miniaturization issues show up in small mass spectrometers, specifically mass analyzers, that need to be thoroughly addressed before further miniaturization. The work in this dissertation focuses on miniaturization issues of ion trap mass analyzers.

Space-charge is one of the major issues in small ion traps affecting their analytical performance. It limits ion trapping capacity when ion-ion repulsion causes spreading of a packet of ions. Simulation studies on the relationship between different trap dimensions and trapping capacity was done on a geometry-optimized cylindrical ion trap. A reasonable way of scaling the two important operating parameters (trapping voltage and trapping frequency as functions of the trap dimension) was discussed and applied in the simulation. The trapping capacity (N) decreased with the physical trap dimension (r_0) as expected, and N is scaled exponentially as r_0. Scaling laws for trapping parameters are proposed, confirmed by SIMION simulations that evaluate the space charge issue in small ion traps. This effect represents a practical limit in ion trap miniaturization. Geometry deviation is another issue that cannot be neglected in miniaturized ion traps, especially in small linear ion traps (LIT). The LIT our group is working on consists of an assembly of two plates, of which each was made by lithographically patterning a series of electrodes on an insulating plate. It is a promising way of expanding the trap capacity at a small trap dimension. However, misalignment of the two plates might seriously affect its performance, specifically resolution and signal intensity. Simulations were done on the misalignment of two-plate planar LIT in the six possible degrees of freedom (DOF) of misalignment between the two plates. Each DOF's influence on the mass resolution and the ion detection efficiency were discussed. Preliminary data from a previous ceramic plate design was collected while most of the misalignment experiments were done on an improved version. A platform was designed incorporating four motorized stages to precisely control the alignment of the ion trap in vacuum. The new plate design was demonstrated to achieve a better than unit resolution for toluene and deuterated toluene after the plates were aligned. The impact on the resolution and signal intensity from pitch, x-, y- and z-displacement were also experimentally studied.

Keywords: miniaturization, space charge, trap dimension, trap capacity, linear ion trap, misalignment, wire ion trap

ACKNOWLEDGEMENTS

First, I'd like to thank Dr. Austin for providing this precious opportunity of studying here at BYU. The past few years of study not only enriched my research and life experience, but also led me to be of an independent mind when facing problems, of which I will benefit a lot for all aspects of life in the future. Dr. Austin is a patient, kind and knowledgeable mentor who gave me tremendous support when I fell in trouble. It's my honor and fortune to study under his direction.

I'd like to thank Dr. Lee, Dr. Dearden, Dr. Hansen, Dr. Goates and Dr. Woodfield for serving on my committee and taking time out of busy schedules each year to view my progress in research, point out the drawbacks and propose insightful suggestions for my future work. I'd also like to thank Dr. Hawkins in the Department of Electrical Engineering and his group members Justin Sorensen, Derek Andrew, Trevor Decker and Joshua McClellan for the guidance and great help on the instrumentation, including fabricating ion trap plates and overcoming any electrical problems confronted in the experiment. Experiments cannot be done without their technical help.

My work cannot be done without the generous assistance from my group members Dr. Qinghao Wu, Jessica Higgs and Ailin Li on the software that is necessary for simulation and experiment. Dr. Qinghao Wu and Dr. Zhiping Zhang's contribution of their knowledge and experience on my experiment can never be overestimated.

I’m grateful for the Precision Machining Lab (PML) for the machining job in mounting platform, the National Science Foundation (NSF), U.S. Department of Defense (DoE), and PerkinElmer (PE) for the financial support of this project.

Last but not least, I would express my appreciation on the emotional support from my family and friends, especially my parents. I’d like to thank them for their accompanying when I went through ups and downs during my study here.

TABLE OF CONTENTS

LIST OF ACRONYMS, SYMBOLS, AND UNITS

a_z	stability parameter in z (axial) direction
a.m.u.	atomic mass unit
AC	alternative current, the supplementary voltage for resonance ejection
APT	Thorlab's APT suite, the software used to control the movement of the motorized actuator
BNC	Berkeley Nucleonic Corporation, a pulse/delay generator
CAD	computer-aided design
CIT	cylindrical ion trap
CSG	constructive solid geometry
d	duty cycle
$\bar{D}$	pseudopotential well depth
Da	Dalton, another name for atomic mass unit
DC	direct current, the voltage applied on the end-cap electrode or endbars on the planar plate
DESI	desorption electrospray ionization
DIT	digital ion trap
DOF	degree of freedom
e	the charge of an electron in coulombs
E-gun	Electron-gun
EI	electron ionization

eV	electron volt
FWHM	full width of a peak at its half maximum
GEM	geometry file, the extension of the file to define the electrode points in SIMION
HMCO	high-mass-cut-off, the higher boundary of a mass range
HS	hard-sphere
ISIS	Integrated System for Ion Simulation, simulation program
ITSIM	Ion Trajectory Simulation, simulation program
IUPAC	International Union of Pure and Applied Chemistry
LIT	linear ion trap
LMCO	low-mass-cut-off, the lower boundary of a mass range
m	ion mass, in kilograms
m/z	mass-to-charge ratio
MEMS	micro-electro mechanical system
MFP	mean-free-path
MOSFET	metal-oxide-semiconductor field-effect transistor
MS	mass spectrometer
N	number of ions being trapped
PA	potential array
PCB	printed circuit board
PS	paper spray
PTFE	polytetrafluoroethylene
q_z	stability parameter in z (axial) direction

QIT	quadrupole ion trap
QMF	quadrupole mass filter
r_0	trapping dimension, the radius of the ring electrode
RF	radio frequency, the trapping voltage
RIT	rectilinear ion trap
S/N	signal-to-noise ratio
SIMION	Ion and the electron optics simulation package, simulation program
SPI	single photon ionization
T	period in rectangular waveforms
Th	Thompson, a unit of mass-to-charge ratio
TOF	time-of-flight, a type of mass analyzer
U	the offset voltage of the trapping voltage
UV	ultra violet
V / $V_{0\text{-}p}$	the amplitude of the RF sinewave / zero to peak amplitude in volt
WIT	wire ion trap
x_0	the half distance between the two opposite electrodes with ejection slits in two-dimensional ion traps
y_0	the half distance between the two opposite electrodes without ejection slits in two-dimensional ion traps
z_0	the half distance between the two end-cap electrodes in three-dimensional ion traps
β	a trapping parameter that is related to q and a

ΔM	resolving power
ω	ion's secular frequency
Ω	frequency of the RF signal

LIST OF TABLES

LIST OF FIGURES

1.Portable Mass Spectrometry

1.1 Towards a Portable Mass Spectrometer

Mass spectrometry is one of the most important techniques in analytical chemistry given its excellent chemical specificity and sensitivity. Its capability of fast analysis makes it an ideal choice for coupling with chromatographic instruments that have been applied in various fields. Conventional mass spectrometers (MSs) are expensive, laboratory-scale instruments, which means that samples must be brought to the lab for mass spectrometric analysis. This drawback prevents them from characterizing those samples that must be preserved in their native chemical environment, otherwise they may change during transport or are impractical to conduct laboratory analysis. Portable MSs that enable the instruments to be brought to the sample overcome this limitation.

The motivation for developing portable MSs was first driven by space exploration[1-2], but the current generation of portable MSs find their ways in many other fields such as threat detection[3-5], environmental monitoring[6-8], clinical diagnosis[9-11] and oceanography[12-13] in addition to a continued effort on space missions[14-15].

Though small size and light weight for portability are the main goals for miniaturizing mass spectrometers, other factors must be taken into account. Ease of use is necessary, since users will

be mostly in other fields and may have little technical training on MS. Analytical performance might be sacrificed from laboratory-scale instruments but still needs to be good enough to answer relevant questions. Power consumption and battery life for continuity, robustness in transport, durability in harsh environment, and low cost are important considerations for portable MSs to become prevalent and applicable.

More than just developing a small mass analyzer, miniaturization of a mass spectrometer involves miniaturizing the vacuum chamber, pump, sample inlet, ionization source, detector, power supplies, and control and acquisition electronics. One prominent problem confronted in small mass spectrometers is ionizing samples in the field. Efforts have been made on developing new sampling and ionization techniques to couple with the reduced-size mass spectrometers, including DESI (desorption electrospray ionization)[16], PS (paper spray)[17-20] and plasma ionization[21-24]. An equally important issue is the interface between the sample inlet and the vacuum parts. As the pumping capacities in portable mass spectrometers should be small, vacuum chambers are more likely to be overwhelmed by the common continuous sample introduction methods. Solutions are using capillary tubes[25] and discontinuous introduction systems[26]. Vacuum pumps are typically the heaviest part in mass spectrometers. Development of vacuum pumps with reduced weight, size and power consumption is underway[27]. A reduction in the physical dimension of a mass analyzer loosens the requirements on operating pressure and power consumption, and tends to correlate with many other miniaturization benefits. Much of the attention thus has been paid to miniaturizing mass analyzers as a starting point in developing portable MSs.

1.2 Mass Analyzers for Miniaturization

Early efforts on miniaturizing mass analyzers were made on magnetic sectors[28-30] and quadrupole mass analyzers[28]. After the breakthrough invention of the reflectron[31], time-of-flight (TOF) started to play a role in MS due to its relative simple instrument design and electronic requirements. Since then, developing portable MS based on miniaturized TOF has become attractive. However, most of the recent progresses were made with radio frequency (RF) quadrupole mass analyzers, including quadrupole mass filters (QMF)[32-37] and especially quadrupole ion traps (QIT)[3, 5, 14, 17, 38-125].

Magnetic Sector

Magnetic sectors were the dominant type of mass analyzer used in mass spectrometers in the last century. However, miniaturizing them to the same scale as other mass analyzers is more challenging, since they are typically large, heavier, and more utility dependent. This is mainly due to the electromagnet or superconducting magnet used. Nevertheless, these issues didn't impede researchers' steps in exploring ways of miniaturization[126-132], specifically when considering the its attractive characteristic that all ions can be simultaneously detected at an appropriate plane with an array detector.

TOF

TOF mass analyzers have the advantage of unlimited mass range since ions are separated based on how long they take to pass through field-free drift regions and reach detectors. Resolution in miniaturized-TOF is limited by factors contributing to the uncertainty in arrival time, such as the variation in ions' initial kinetic energy, time when ions are formed or accelerated and slight

differences in the distance ions travel before reaching the detector. Remarkable achievements on miniaturizing TOF have been done[133-137] and developing TOF-based MSs is still moving forward[138-140].

QMF and QIT

QMFs represent the earliest form of quadrupole instrument and many efforts on miniaturizing QMFs were made in the 1990s[141-144]. In recent years most of the published research has been focused on ion trap miniaturization[89]. Compared to other mass analyzers, quadrupole instruments are of particular promise because of several key characteristics: their simple structure allows stringent electrode alignment; their tolerance to high pressure helps reduce the vacuum requirements; and their light weight and compact size. Although the resolution in quadrupole mass analyzers is typically lower than that in other mass analyzers, they have nonetheless seen a fast pace of development for portable MS[145]. The content of this dissertation only focuses on RF-based quadrupole ion traps and their derivatives.

1.3 Principles of quadrupole ion traps

A typical view of a conventional quadrupole ion trap is seen in Figure 1-1. It is composed of one ring electrode sandwiched by two end-cap electrodes on top. all of which are shaped as a hyperbolic surface of revolution on their inner surfaces.

The radius of the ring electrode is r_0, which is taken as the characteristic trap dimension in the following chapters; the half distance between the two end-caps is represented as z_0. Typically, RF

trapping voltage is applied to the ring electrode with the two end-cap electrodes nominally grounded.

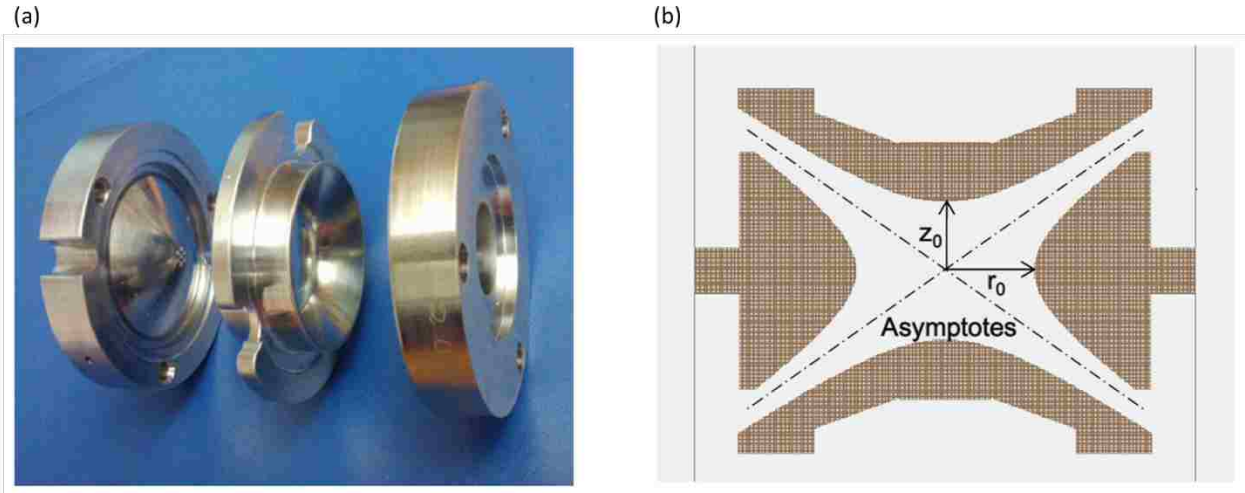

Figure 1-1. (a) Photo of a commercial quadrupole ion trap; (b) Cross section view of a quadrupole ion trap. (Adapted from Peng, Y. Novel Ion Trap Made Using Lithographically Patterned Plates. Ph.D. dissertation, Brigham Young University, 2011)

To generate a pure quadrupole electric field, the two geometric parameters should satisfy Equation 1-1.

$$r_0^2 = 2z_0^2 \qquad \textit{Equation 1-1}$$

assuming no electrode truncation or ejection holes are involved. This is because any geometry defect may introduce higher-order fields that change ions' movement and influence ion traps' performances.

A typical 3-D view of the quadrupolar field looks like a saddle as shown in Figure 1-2, when the RF signal alternates between the positive and negative part of a sine wave, the "saddle" orientation varies at the same frequency, forming a pseudopotential well that holds ions inside the trap region.

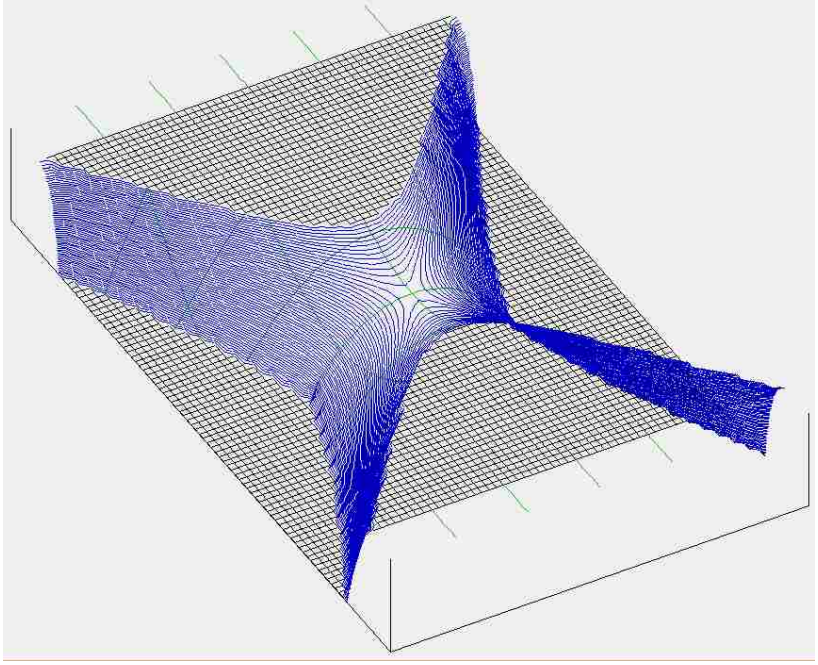

Figure 1-2. Quadupolar field in a quadrupole ion trap. The four poles of the potential surface vary with time at a static trapping frequency.

Stability diagram and pseudopotential well

To determine whether an ion with a given mass can be trapped under a given condition, a parameter ***q*** is commonly used which is derived from the Mathieu Equation and is expressed as

$$q_z = \frac{8eV}{m(r_0^2+2z_0^2)\Omega^2} \qquad \textit{Equation 1-2}$$

to describe ion stability, where ***V*** is the zero-to-peak RF trapping voltage, **Ω** is the RF angular frequency, ***m*** and ***e*** are the mass and charge of an ion, the subscript ***z*** indicates the axial direction. Similarly, another stability parameter ***a*** can be expressed as

$$a_z = -\frac{16eU}{m(r_0^2+2z_0^2)\Omega^2} \qquad \textit{Equation 1-3}$$

in which ***U*** is a DC offset of the RF signal. There are axial (***z***) stable regions described by Equation 1-2 and radial (***r***) stable regions described by Equation 1-3.

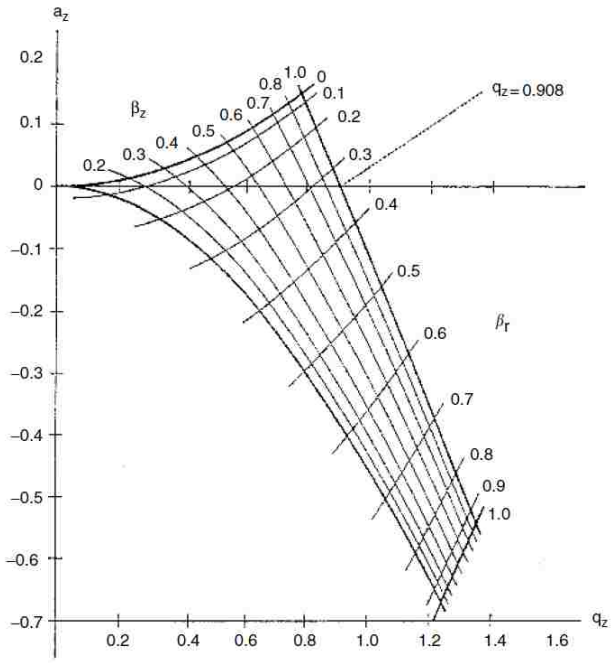

Figure 1-3. Stability diagram near origin in a conventional quadrupole ion trap. (Adapted from March, R.E.; Todd, J. F. J., Quadrupole Ion Trap Mass Spectrometry, *John Wiley & Sons, Inc.*, **2005**, pp 34-72.)

Only ions that are stable in both regions are considered trapped. The stability diagram shown in Figure 1-3 is one of the overlapping regions from these two directions. In fact, there are several overlapped regions, but routine operating points fall in this one which is near the origin. When $\boldsymbol{U}$ = 0 (End-caps are grounded), $\boldsymbol{a}$ is always 0, and when $\boldsymbol{q}$ is larger than 0.908, ions are no longer stable in the trap. $\boldsymbol{\beta}$ is another commonly used trapping parameter that is determined by a complex continued-fraction function of $\boldsymbol{a}$ and $\boldsymbol{q}$, but it can be approximated as

$$\beta_u \approx \sqrt{\left(a_u + \frac{1}{2}q_u^2\right)} \qquad \textit{Equation 1-4}$$

when $\boldsymbol{q_u} < 0.4$, which is well-known as the *Dehmelt approximation*[146].

A pseudopotential well model is a quantitative way of describing the trap capacity of an ion trap. The approximate well depth can be represented as Equation 1-5 by the *Dehmelt approximation*. It

appeared the trap capacity is proportional to both the trapping voltage V and the stability parameter q.

$$\overline{D_z} = \frac{1}{8} V q_z \qquad \textit{Equation 1-5}$$

Secular frequency

The trajectory of an ion in the quadrupolar field is a combination of low-frequency oscillation (Lissajous curve) and high-frequency ripple as shown in Figure 1-4. The low-frequency oscillation is the secular motion, and it is composed of two independent frequencies in the r direction and the z direction, represented as ω_r and ω_z, respectively. Secular frequencies are related to the RF trapping frequency. The general expressions for secular frequencies are

$$\omega_{u,n} = \left(n + \frac{1}{2}\beta_u\right)\Omega \qquad 0 \le n < \infty \qquad \textit{Equation 1-6}$$

$$\omega_{u,n} = -\left(n + \frac{1}{2}\beta_u\right)\Omega \qquad -\infty < n < 0 \qquad \textit{Equation 1-7}$$

When $n = 0$, ω is the fundamental secular frequency.

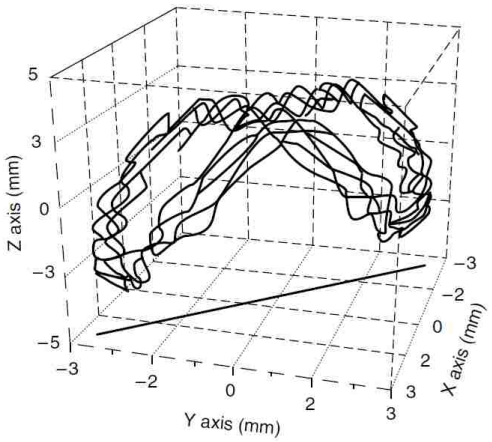

Figure 1-4. Simulated ion trajectory in quadrupole ion trap. (Adapted from Nappi, M.; Weil, C.; Cleven, C. D.; Horn, L. A.; Wollnik, H.; Cooks, R. G., Visual representations of simulated three-dimensional ion trajectories in an ion trap mass spectrometer. *Int. J. Mass Spectrom. Ion Processes*, **1997**, *161*, 77–85.)

Collisional cooling

Wherever sample molecules are ionized, inside or outside the trap region, ions possess some initial kinetic energy due to the thermal energy of the neutral molecules. If the kinetic energy is too large, ions may escape the trapping space. A higher trapping voltage enables trapping ions with higher kinetic energy, but a more efficient way is introducing some cooling gas. The cooling gas used the most is helium. Nitrogen and argon are alternatives for He but are not ideal for small analyte molecules. This is because the cooling effect relies on the ion mass m_i and the molecular mass of the cooling gas m_c. If m_i is much lighter than m_c, the outcome is an ion packet that is more scattered as the initial trajectories of ions in that packet are severely changed, whereas if m_i is much larger than m_c, ions are cooled down as the initial kinetic energy is gradually passed to the cooling gas molecules. The presence of helium buffer gas can both increase sensitivity and resolution[39]: typically the longer time ions reside in the trap, the better the resolution will be as ions are more "cooled" to the trap center and are better controlled by the electric field instead of traveling randomly.

Scan mode

As ions with different mass-to-charge ratios are trapped together in the trap, the way that they are selectively ejected affects the performance, particularly peak width and peak position. A straight-forward method for mass analysis is by scanning the trapping voltage $\boldsymbol{V}$ to move the stability parameter $\boldsymbol{q}$ out of the stable region in Figure 1-3. As $\boldsymbol{q_z}$ values are different for different ion masses at the same trapping voltage, when the voltage is scanned linearly from the low end to the high end, low mass ions are ejected first and sequentially followed by high mass ions. This

scan mode is named boundary ejection, since ions are ejected by approaching the boundary of the stability region.

Another way to eject ions is applying a supplementary AC signal on one of the endcaps at a frequency equal to the ions' secular frequency. Ions resonate with that tickle voltage, and are oscillated out of the trap region. Spectra obtained in this way typically have narrower and higher peaks than by boundary ejection. This is called resonant ejection. There are several modes of resonant ejection: "monopole" ejection is done by grounding one of the end-caps and applying AC on the other; "dipole" ejection means applying AC on both end-caps: the AC amplitudes are the same, but phases are different by 180 degrees; "quadrupole" ejection refers to applying exactly the same AC on two endcaps. Monopole and dipole ejections are used most commonly. The resolution obtained by resonant ejection is so much better than by boundary ejection that almost all the commercial QITs have applied resonant voltages for MS analysis. A particularly useful point for dipole resonant ejection corresponds to the natural nonlinear resonance line at $\beta = 2/3$, as seen in Figure 1-3. Substituting that value in Equation 1-6, we can see the fundamental secular frequency is 1/3 of the RF trapping frequency.

Mass resolution and mass range

Mass resolution is one of the most important parameters to evaluate the performance of a mass spectrometer, which is also an important consideration during the miniaturization process. Mass resolution represents the ability of a mass spectrometer to separate two ions with slight mass difference.

According to the definition given by IUPAC (International Union of Pure and Applied Chemistry), the expression of the resolution (***R***) is written as

$$R = \frac{M}{\Delta M} \qquad \textit{Equation 1-8}$$

in which M is the mass of the second peak, ΔM is the resolving power or the minimum peak separation. There are two definitions for ΔM. One is the width of a mass peak at 50% of the peak height, which is FWHM (full width of a peak at its half maximum), the other is the closest distance of two peaks having the same intensity. Though some scientists[147-148] take ΔM as the resolution and ***R*** as the resolving power, they are commonly used interchangeably in practice. In this dissertation, the resolution is mostly calculated based on Equation 3-1, taking FWHM as the ΔM.

Mass range limits the types of samples being analyzed. The lower limit is called the low mass cut off (LMCO), and the higher limit of a mass range is called the high mass cut off (HMCO). LMCO is the mass-to-charge ratio (***m/z***) when the working point of the ions with that ratio is where $\boldsymbol{\beta} = 1$ curve (stability boundary) intersects the $\boldsymbol{q_z}$ axis under the trapping voltage. HMCO is the ***m/z*** when ions with that mass-to-charge ratio reach the same point under the maximum amplitude the RF signal can ramp to. According to the stability diagram shown in Figure 1-3, that cross point is at $\boldsymbol{q_z}$ = 0.908.

1.4 Miniaturization issues

Many problems that are never confronted or are neglectable in conventional ion traps may show up or become serious when the physical dimensions are reduced. These problems generally include electrical issues, pressure, space charge, and mechanical tolerance.

Space-charge

Ion traps are particularly sensitive to charge density as ions have long residence times inside the trap. Each trapped ion strongly affects the electric fields experienced by other ions, perturbing their trajectories. Space charge could be a serious problem for ion traps at small scales. It could limit the storage volume for ions and significantly reduce the signal intensity. It can be seen from the expression of pseudopotential well depth (Equation 1-5) that the trapping capacity is also influenced by the trapping voltage. Chapter 2 talks about a practical way to scale the trapping voltage and trapping frequency as the trap dimension, as demonstrated in a simulation studying on the space charge effect in small ion traps.

Mechanical tolerance

Decreasing physical dimensions would correspondingly decrease the accuracy of the electric field. This is because the absolute dimension is reduced whereas the dimensional tolerance is the same, which is limited by conventional machining techniques. Thus, maintaining a certain level of the relative tolerance becomes more difficult. Tolerance may come from surface roughness[85] or electrode alignment and geometry defects. In the past decades, fabricating small ion traps relies more on microelectromechanical systems (MEMS) and other microfabrication techniques[40, 63-64, 71-72, 74-75, 77-78, 81, 86-87, 91, 149-150], as ion trap miniaturization has progressively challenged the limits of conventional machining.

Electrical issues and vacuum

Portable MSs are expected to be long-lasting and low power-consuming. In fact, vacuum pumps are frequently the most power-hungry parts of a MS. Increasing the operating pressures

enables the use of smaller pumps with lower power consumptions. Small ion traps are also more durable at relatively high pressures since the mean free paths (MFP) of the trapped ions should scale with trap dimensions[50, 151]. However, high pressures may cause electron emissions between electrodes, especially when the electrodes are smaller and closer to each other. On the other hand, small trap dimensions can have serious capacitance issues which would bring down the final voltage delivered to the electrodes and consume more power.

The issues from small trap dimensions are summarized and their correlations are illustrated in Figure 1-5. Red lines indicate positive effects. Blue lines indicate negative effects. Black lines indicate neutral effects.

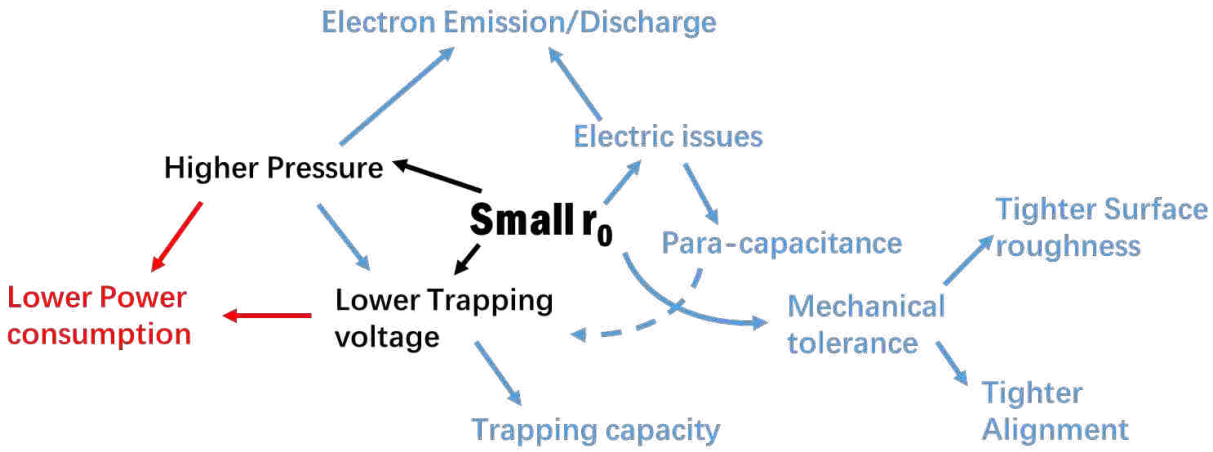

Figure 1-5. Summary of miniaturization issues and their relations with each other.

1.5 Development of miniaturized ion traps

The concept of quadrupole ion traps with hyperbolic inner surfaces was first proposed by Paul and Steinwedel[152]. However, the hyperbolic surfaces presented difficulty with machining at high precision at small scales. Later on, the cylindrical ion trap (CIT) emerged as a derivative of

the quadrupole ion trap but with simpler geometric structure. All the inner surfaces in CITs were flat or cylindrical[44], as seen in Figure 1-6 (b). Since then, a series of miniature ion traps based on cylindrical structures were reported[63, 66, 71, 74]. However, the reduction in ion storage volumes remains a problem in small ion traps. There are two general ways to recover storage volume in the process of miniaturizing ion traps: either by increasing the storage volume using traps with an extended trapping dimension or by paralleling trap arrays.

Traps with large storage volumes

The mechanism of increasing storage volumes is by increasing dimensionalities of trap regions. The representative examples are linear ion traps (LIT) and toroidal ion traps, both of which expand geometries in non-trapping dimensions.

The first model of the linear ion trap was reported by Schwartz in 2002[54]. It was composed of two end sections and one central section. Every section had four electrodes that had hyperbolic surfaces on inner surfaces (see Figure 1-6 (c)). An RF trapping waveform was applied to opposite rods within the central section. The two end sections were applied with RF and also a small DC voltage to confine ions' movements to the central section. Ions were eventually ejected through the slit on one of the electrodes in the central section. Depending on the length of the trap, the number of ions that can be analyzed in a linear-type trap can be 1-3 orders of magnitude larger than in a CIT of similar characteristic trap dimension[57].

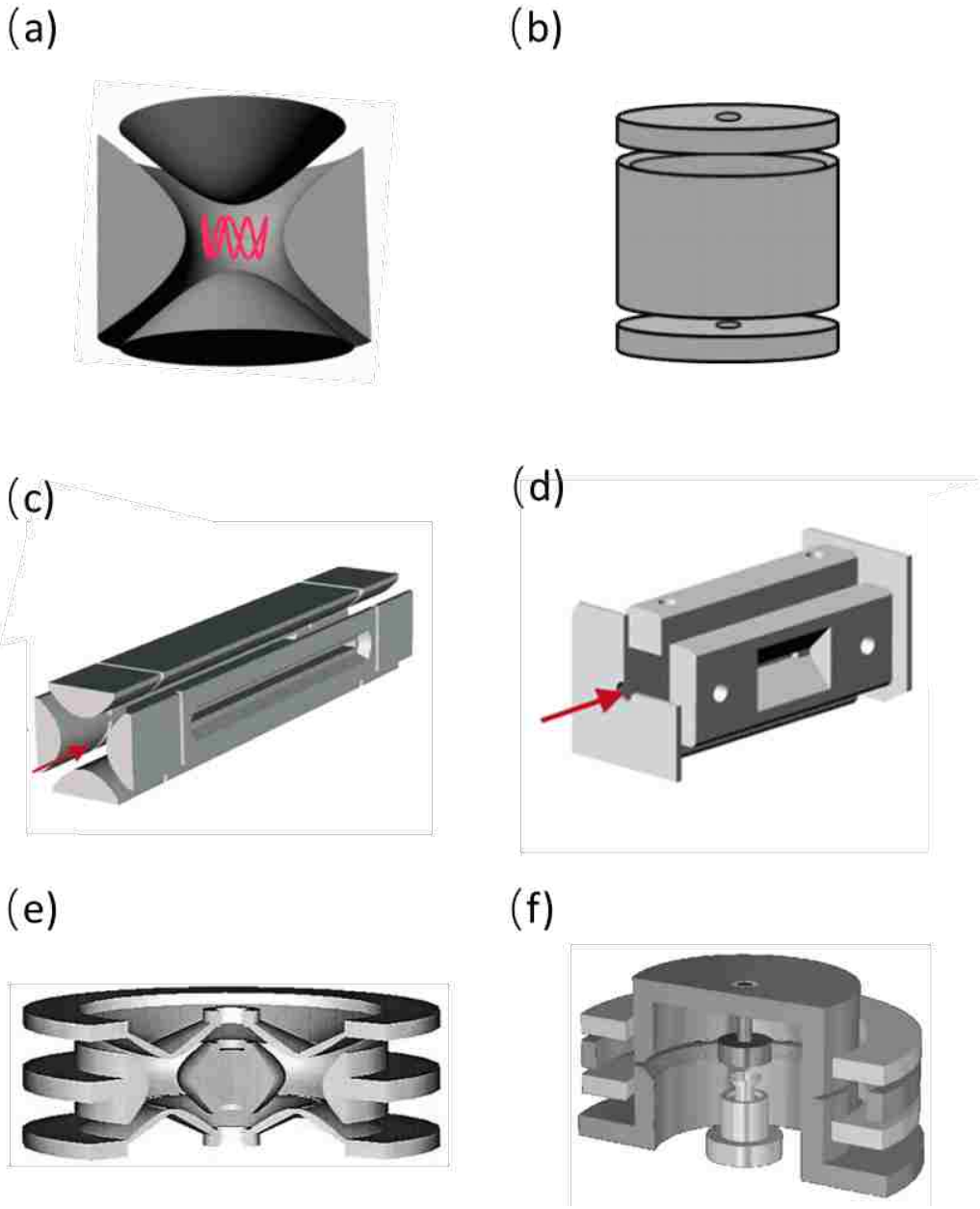

Figure 1-6. Representative model of (a) Quadrupole ion trap; (b) Cylindrical ion trap; (c) Linear ion trap; (d) Rectilinear ion trap; (e) Toroidal ion trap and (f) Toroidal ion trap with cylindrical electrodes. (Adapted from Tian, Y.; Higgs, J.; Li, A.; Barney, B.; Austin, D. E. How far can ion trap miniaturization go? Parameter scaling and space-charge limits for very small cylindrical ion traps. *J. Mass. Spectrom.*, **2014**, *49*(3), 233-240.)

The rectilinear ion trap (RIT), a simplified version of the LIT, was first built by Ouyang in 2004[60]. The two end sections which were composed of eight electrodes in a LIT were replaced by

two rectangular planar plates with holes in the center for ions or electrons to pass through. The four electrodes in the central section were modified into four rectangular electrodes, of which two were cut with ejection slits (see Figure 1-6 (d)). Subsequently, hand-held mass spectrometers based on RITs were made[10, 16, 21, 24, 70].

Lammert first reported the structure of a toroidal ion trap in 2001[52]. The formation of this novel ion trap can be viewed by rotating the cross section of a quadrupole ion trap based on its edge into a torus as shown in Figure 1-7(a). The storage volume was tremendously expanded and good mass resolution was obtained by using an asymmetric version (see Figure 1-7(b)). Miniaturization of toroidal ion traps continued[73] and portable MS based on toroidal ion traps were developed and applied[82, 101]. Later on, a toroidal ion trap with cylindrical electrodes was reported[108] (Figure 1-6(f)).

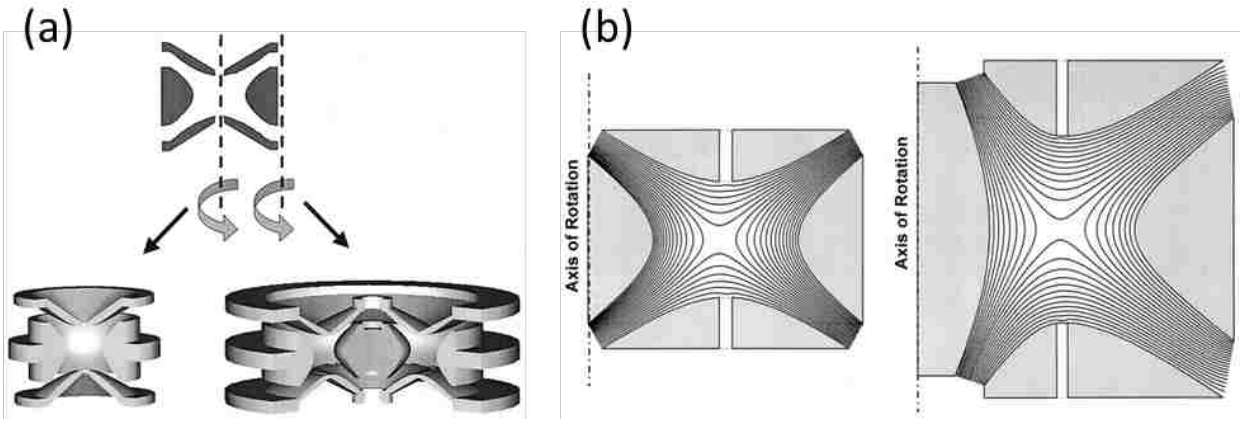

Figure 1-7. (a) Representative for formation of toroidal ion trap; (b) Cross section view of symmetric (left) and asymmetric (right) version in toroidal ion traps. (Adapted from Lammert, S. A.; Plass, W. R.; Thompson, C. V.; Wise, M. B., Design, optimization and initial performance of a toroidal RF ion trap mass spectrometer. *Int. J. Mass Spectrom.* **2001**, *212*(1-3), 25-40.)

Generally, quadrupole ion traps and cylindrical ion traps are classified as 3-D ion traps, linear ion traps and rectilinear ion traps belong to 2-D ion traps. In 2-D ion traps, the dimensional parameter (r_0) is replaced with x_0 and y_0 since there is no concept of radial or axial direction. The dimension x_0 is the half-distance between the two trapping electrodes with slits. The dimension y_0 is the half-distance between the two trapping electrodes without slits.

Parallel trap arrays

The trap array is another way to restore the trapping capacity at small scales. The CIT might be the most suitable choice for MEMS fabrication because of its simple structure. Arrays of CITs have been reported by Cooks[48, 50-51, 58, 65, 68], Ramsey[72], Short[71, 81, 86], and Blain[63, 74, 77]. Arrays of RITs were also introduced by Cooks, Ouyang and Chappell's group[87, 90, 94], Xiao[111] and Chu[110]. Recently 3-D ion trap arrays were introduced by Xu[119] and Wilper[107].

The assembly of a trap array may use multiple ionization sources and/or multiple detectors. Compared to large volume traps, trap arrays operate at relatively higher pressures and under relatively lower voltages because of their small trap dimensions[89]. The mass range could also be readily expanded by arraying traps with various trap dimensions[51]. However, trap arrays may suffer from cross-talk among independent traps, impacting the quality of final spectra obtained[93].

1.6 Conclusion and Outlook

Notable achievements have been obtained on small mass spectrometers based on miniaturized ion traps and other mass analyzers. With advancements in sample introduction methods, ionization techniques and pumping systems, portable mass spectrometers are starting to

make an impact in many fields. Though there are still various obstacles that have to be properly taken care of before further miniaturizing, the desire to build small, light, low-cost and user-friendly mass spectrometers with fast, sensitive and reliable analytical performance is becoming more and more realistic. It is likely in the future that MSs will permeate into many aspects of routine life such as security checkpoints, home health care, or food and drug quality control.

1.7 References

1. Rushneck, D. R.; Diaz, A. V.; Howarth, D. W.; Rampacek, J.; Olson, K. W.; Dencker, W. D.; Smith, P.; McDavid, L.; Tomassian, A.; Harris, M.; Bulota, K.; Biemann, K.; Lafleur, A. L.; Biller, J. E.; Owen, T., Viking gas chromatrograph mass spectrometer. *Rev. Sci. Instrum.* **1978,** *49* (6), 817-834.

2. Hoffman, J. H.; Hodges, R. R.; Duerksen, K. D., Pioneer venus large probe neutral mass spectrometer. *J. Vac. Sci. Technol.* **1979,** *16* (2), 692-694.

3. Graichen, A. M.; Vachet, R. W., Using metal complex ion-molecule reactions in a miniature rectilinear ion trap mass spectrometer to detect chemical warfare agents. *J. Am. Soc. Mass Spectrom.* **2013,** *24* (6), 917-925.

4. Nagashima, H.; Kondo, T.; Nagoya, T.; Ikeda, T.; Kurimata, N.; Unoke, S.; Seto, Y., Identification of chemical warfare agents from vapor samples using a field-portable capillary gas chromatography/membrane-interfaced electron ionization quadrupole mass spectrometry instrument with Tri-Bed concentrator. *J. Chromatogr. A* **2015,** *1406*, 279-290.

5. Smith, P. A.; Lepage, C. J.; Lukacs, M.; Martin, N.; Shufutinsky, A.; Savage, P. B., Field-portable gas chromatography with transmission quadrupole and cylindrical ion trap mass spectrometric detection: Chromatographic retention index data and ion/molecule interactions for chemical warfare agent identification. *Int. J. Mass Spectrom.* **2010,** *295* (3), 113-118.

6. Bouvier-Brown, N. C.; Carrasco, E.; Karz, J.; Chang, K.; Nguyen, T.; Ruiz, D.; Okonta, V.; Gilman, J. B.; Kuster, W. C.; de Gouw, J. A., A portable and inexpensive method for quantifying ambient intermediate volatility organic compounds. *Atmos. Environ.* **2014,** *94*, 126-133.

7. Barreira, L. M. F.; Parshintsev, J.; Karkkainen, N.; Hartonen, K.; Jussila, M.; Kajos, M.; Kulmala, M.; Riekkola, M. L., Field measurements of biogenic volatile organic compounds in the atmosphere by dynamic solid-phase microextraction and portable gas chromatography-mass spectrometry. *Atmos. Environ.* **2015,** *115*, 214-222.

8. Eckenrode, B. A., Environmental and forensic applications of field-portable GC-MS: An overview. *J. Am. Soc. Mass Spectrom.* **2001,** *12* (6), 683-693.

9. Ye, H.; Gemperline, E.; Li, L., A vision for better health: Mass spectrometry imaging for clinical diagnostics. *Clin. Chim. Acta* **2013,** *420*, 11-22.

10. Li, L.; Chen, T.; Ren, Y.; Hendricks, P. I.; Cooks, R. G.; Ouyang, Z., Mini 12, miniature mass spectrometer for clinical and other applications - introduction and characterization. *Anal. Chem.* **2014,** *86* (6), 2909 - 2916.

11. Molina, M. A.; Zhao, W.; Sankaran, S.; Schivo, M.; Kenyon, N. J.; Davis, C. E., Design-of-experiment optimization of exhaled breath condensate analysis using a miniature differential mobility spectrometer (DMS). *Anal. Chim. Acta* **2008,** *628* (2), 155-161.

12. Mach, P. M.; Winfield, J. L.; Aguilar, R. A.; Wright, K. C.; Verbeck, G. F., A portable mass spectrometer study targeting anthropogenic contaminants in Sub-Antarctic Puerto Williams, Chile. *Int. J. Mass Spectrom.* **2016,** *In Press, Corrected Proof, Available online 10 December*

13. Short, R. T.; Toler, S. K.; Kibelka, G. P. G.; Rueda Roa, D. T.; Bell, R. J.; Byrne, R. H., Detection and quantification of chemical plumes using a portable underwater membrane introduction mass spectrometer. *TrAC, Trends Anal. Chem.* **2006,** *25* (7), 637-646.

14. Brinckerhoff, W. B.; van Amerom, F. H. W.; Danell, R. M.; Pinnick, V.; Arevalo, R.; Atanassova, M.; Hovmand, L.; Mahaffy, P. R.; Cotter, R. J.; MOMA Team, A dual source ion trap mass spectrometer for the Mars Organic Molecule Analyzer on ExoMars 2018. *EPC Abstracts* **2011,** *6*, 1337.

15. Siljestrom, S.; Freissinet, C.; Goesmann, F.; Steininger, H.; Goetz, W.; Steele, A.; Amundsen, H.; Amase Team, Comparison of prototype and laboratory experiments on MOMA GCMS: Results from the AMASE11 campaign. *Astrobiology* **2014,** *14* (9), 780-797.

16. Keil, A.; Talaty, N.; Janfelt, C.; Noll, R. J.; Gao, L.; Ouyang, Z.; Cooks, R. G., Ambient mass spectrometry with a handheld mass spectrometer at high pressure. *Anal. Chem.* **2007,** *79* (20), 7734-7739.

17. Pulliam, C. J.; Wei, P.; Snyder, D. T.; Wang, X.; Ouyang, Z.; Pielak, R. M.; Cooks, G. R., Rapid discrimination of bacteria using a miniature mass spectrometer. *Analyst* **2016,** *141* (5), 1633-1636.

18. Bag, S.; Hendricks, P. I.; Reynolds, J. C.; Cooks, G. R., Biogenic aldehyde determination by reactive paper spray ionization mass spectrometry. *Anal. Chim. Acta* **2015,** *860*, 37-42.

19. Jjunju, F. P. M.; Li, A.; Badu-Tawiah, A.; Wei, P.; Li, L.; Ouyang, Z.; Roqan, I. S.; Cooks, G. R., In situ analysis of corrosion inhibitors using a portable mass spectrometer with paper spray ionization. *Analyst* **2013,** *138* (13), 3740-3748.

20. Pulliam, C. J.; Bain, R. M.; Wiley, J. S.; Ouyang, Z.; Cooks, G. R., Mass spectrometry in the home and garden. *J. Am. Soc. Mass Spectrom.* **2015,** *26* (2), 224-230.

21. Dalgleish, J. K.; Hou, K.; Ouyang, Z.; Cooks, G. R., In situ explosive using a miniature plasma ion source and a portable mass spectrometer. *Anal. Lett.* **2012,** *45* (11), 1440-1446.

22. Na, N.; Zhao, M.; Zhang, S.; Yang, C.; Zhang, X., Development of a dielectric barrier discharge ion source for ambient mass spectrometry. *J. Am. Soc. Mass Spectrom.* **2007,** *18* (10), 1859-1862.

23. Harper, J. D.; Charipar, N. A.; Mulligan, C. C.; Zhang, X.; Cooks, G. R.; Ouyang, Z., Low-temperature plasma probe for ambient desorption ionization. *Anal. Chem.* **2008,** *80* (23), 9097-9104.

24. Hendricks, P. I.; Dalgleish, J. K.; Shelley, J. T.; Kirleis, M. A.; McNicholas, M. T.; Li, L. F.; Chen, T. C.; Chen, C. H.; Duncan, J. S.; Boudreau, F.; Noll, R. J.; Denton, J. P.; Roach, T. A.; Ouyang, Z.; Cooks, R. G., Autonomous in situ analysis and real-time chemical detection using a backpack miniature mass spectrometer: Concept, instrumentation development, and performance. *Anal. Chem.* **2014,** *86* (6), 2900-2908.

25. Andres, R. P., Rational inlet design for a portable atmospheric pressure ionization-mass spectrometer (API-MS). *Int. J. Mass Spectrom.* **2011,** *300* (2-3), 194-197.

26. Gao, L.; Cooks, G. R.; Ouyang, Z., Breaking the pumping speed barrier in mass spectrometry: Discontinuous atmospheric pressure interface. *Anal. Chem.* **2008,** *80* (11), 4026-4032.

27. Chen, C. H.; Chen, T. C.; Zhou, X.; Kline-Schoder, R.; Sorensen, P.; Cooks, G. R.; Ouyang, Z., Design of portable mass spectrometers with handheld probes: Aspects of the sampling and miniature pumping systems. *J. Am. Soc. Mass Spectrom.* **2015,** *26* (2), 240-247.

28. Dawson, P. H.; Hedman, J. W.; Whetten, N. R., A miniature mass spectrometer. *Anal. Chem.* **1970,** *42* (12), 103A-108A.

29. Baril, M., Application des Miroirs Electrostatiques a L'elimination de L' effect Chromatique dans les Spectrometers Magnetiques. Deuxieme Partie: les Aberrations. *Can. J. Phys.* **1970,** *48*, 2487-2498.

30. Swingler, D. L., A small magnetic analyzer mass spectrometer with a velocity filter for residual gas analysis. *Vacuum* **1971,** *21* (3-4), 121-125.

31. Mamyrin, B. A.; Karataev, V. I.; Shmikk, D. V.; Zagulin, V. A., The mass-reflectron, a new nonmagnetic time-of-flight mass spectrometer with high resolution. *Sov. Phys. JETP* **1973,** *37*, 45-48.

32. Taylor, S.; Tindall, R. F.; Syms, R. R. A., Silicon based quadrupole mass spectrometry using microelectromechanical systems. *J. Vac. Sci. Technol. B* **2001,** *19* (2), 557-562.

33. Boumsellek, S.; Ferran, R. J., Trade-offs in miniature quadrupole designs. *J. Am. Soc. Mass Spectrom.* **2001,** *12* (6), 633-640.

34. Geear, M.; Syms, R. R. A.; Wright, S.; Holmes, A. S., Monolithic MEMS quadurpole mass spectrometers by deep silicon etching. *J. Microelectromech. Syst.* **2005,** *14* (5), 1156-1166.

35. Velasquez-Garcia, L. F.; Cheung, K.; Akinwande, A. I., An application of 3-D MEMS packaging: Out-of-plane quadrupole mass filters. *J. Microelectromech. Syst.* **2008,** *17* (6), 1430-1438.

36. Taylor, S.; Tunstall, J. J.; Leck, J. H.; Tindall, R. F.; P., J. J.; Batey, J.; Syms, R. R. A.; Tate, T. J.; Ahmad, M. M., Performance improvements for a miniature quadrupole with a micromachined mass filter. *Vacuum* **1999,** *53* (1-2), 203-206.

37. Wang, J.; Zhang, X.; Mao, F.; Xiao, M.; Cui, Y.; den Engelsen, D.; Lei, W., Study of a micro chamber quadrupole mass spectrometer. *J. Vac. Sci. Technol.* **2008,** *26* (2), 239-243.

38. Knight, R. D., The general form of the quadrupole ion trap potential. *Int. J. Mass Spectrom. Ion Phys.* **1983,** *51* (1), 127-131.

39. Stafford Jr., G. C.; Kelley, P. E.; Syka, J. E. P.; Reynolds, W. E.; Todd, J. F. J., Recent improvements in an analytical application of advanced ion trap technology. *Int. J. Mass Spectrom.* **1984,** *60*, 85-98.

40. Brewer, R. G.; DeVoe, R. G.; Kallenbach, R., Planar ion trap. *Phys. Rev. A* **1992,** *46*, R6781 (5 pgs).

41. Londry, F. A.; Alfred, R. L.; March, R. E., Computer simulation of single-ion-trajectories in Paul-type ion traps. *J. Am. Soc. Mass Spectrom.* **1993,** *4* (9), 687-705.

42. Guan, S.; Marshall, A. G., Equilibrium space charge distribution in a quadrupole ion trap. *J. Am. Soc. Mass Spectrom.* **1994,** *5* (2), 64-71.

43. He, L.; Lubman, D. M., Simulation of external ion injection, cooling and extraction processes with SIMION 6.0 for the ion trap/reflectron time-of-flight mass spectrometer. *Rapid Commun. Mass Spectrom.* **1997,** *11* (13), 1467-1477.

44. Badman, E. R.; Johnson, R. C.; Plass, W. R.; Cooks, R. G., A miniature cylindrical quadrupole ion trap: Simulation and experiment. *Anal. Chem.* **1998,** *70* (23), 4896-4901.

45. Bui, A. H.; Cooks, G. R., Windows version of the ion trap simulation program ITSIM: A powerful heuristic and perdictive tool in ion trap mass spectrometry. *J. Mass Spectrom.* **1998,** *33* (4), 297-304.

46. Gill, L. A.; Amy, J. W.; Vaughn, W. E.; Cooks, R. G., In situ optimization of the electrode geometry of the quadrupole ion trap1. *Int. J. Mass Spectrom.* **1999,** *188* (1–2), 87-93.

47. Kornienko, O.; Reilly, P. T. A.; Whitten, W. B.; Ramsey, J. M., Micro ion trap mass spectrometry. *Rapid Commun. Mass Spectrom.* **1999,** *13* (1), 50-53.

48. Ouyang, Z.; Badman, E. R.; Cooks, R. G., Characterization of a serial array of miniature cylindrical ion trap mass analyzers. *Rapid Commun. Mass Spectrom.* **1999,** *13* (24), 2444-2449.

49. Forbes, M. W.; Sharifi, M.; Croley, T.; Lausevic, Z.; March, R. E., Simulation of ion trajectories in a quadrupole ion trap: A comparison of three simulation programs. *J. Mass Spectrom.* **1999,** *34* (12), 1219-1239.

50. Badman, E. R.; Cooks, R. G., A parallel miniature cylindrical ion trap array. *Anal. Chem.* **2000,** *72* (14), 3291-3297.

51. Badman, E. R.; Cooks, R. G., Cylindrical ion trap array with mass selection by variation in trap dimensins. *Anal. Chem.* **2000,** *72* (20), 5079-5086.

52. Lammert, S. A.; Plass, W. R.; Thompson, C. V.; Wise, M. B., Design, optimization and initial performance of a toroidal rf ion trap mass spectrometer. *Int. J. Mass Spectrom.* **2001,** *212* (1-3), 25-40.

53. Schwartz, J. C.; Syka, J. E. P.; Jardine, I., High-resolution on a quadrupole ion trap mass-spectrometer. *J. Am. Soc. Mass Spectrom.* **2001,** *2* (3), 198-204.

54. Schwartz, J. C.; Senko, M. W.; Syka, J. E. P., A two-dimensional quadrupole ion trap mass spectrometer. *J. Am. Soc. Mass Spectrom.* **2002,** *13* (6), 659-669.

55. Ding, L.; Sudakov, M.; Kumashiro, S., A simulation study of the digital ion trap mass spectrometry. *Int. J. Mass Spectrom.* **2002,** *221* (2), 117 - 138.

56. Moxom, J.; Reilly, P. T. A.; Whitten, W. B.; Ramsey, J. M., Double resonance ejection in a micro ion trap mass spectrometer. *Rapid Commun. Mass Spectrom.* **2002,** *16* (8), 755-760.

57. Hager, J. W., A new linear ion trap mass spectrometer. *Rapid Commun. Mass Spectrom.* **2002,** *16* (6), 512-526.

58. Tabert, A. M.; Greip-Raming, J.; Guymon, A. J.; Cooks, R. G., High-throughput miniature cylindrical ion trap array mass spectrometer. *Anal. Chem.* **2003,** *75* (21), 5656-5664.

59. Ding, L.; Sudakov, M.; Brancia, F. L.; Giles, R.; Kumashiro, S., A digital ion trap mass spectrometer coupled with atmospheric pressure ion sources. *J. Mass Spectrom.* **2004,** *39* (5), 471-484.

60. Ouyang, Z.; Wu, G.; Song, Y.; Li, H.; Plass, W. R.; Cooks, R. G., Rectilinear ion trap: Concepts, calculations, and analytical performance of a new mass analyzer. *Anal. Chem.* **2004,** *76* (16), 4595 - 4605.

61. Moxom, J.; Reilly, P. T. A.; Whitten, W. B.; Ramsey, J. M., Sample pressure effects in a micro ion trap mass spectrometer. *Rapid Commun. Mass Spectrom.* **2004,** *18* (6), 721-723.

62. Whitten, W. B.; Reilly, P. T. A.; Ramsey, J. M., High-pressure ion trap mass spectrometry. *Rapid Commun. Mass Spectrom.* **2004,** *18* (15), 1749-1752.

63. Blain, M. G.; Riter, L. S.; Cruz, D.; Austin, D. E.; Wu, G. X.; Plass, W. R.; Cooks, R. G., Towards the hand-held mass spectrometer: Design considerations, simulation, and fabrication of micrometer-scaled cylindrical ion traps. *Int. J. Mass Spectrom.* **2004,** *236* (1-3), 91-104.

64. Madsen, M. J.; Hensinger, W. K.; Stick, D.; Rabchuk, J. A.; Monroe, C., Planar ion trap geometry for microfabrication. *Appl. Phys. B* **2004,** *78*, 639-651.

65. Tabert, A. M.; Misharin, A. S.; Cooks, G. R., Performance of a multiplexed chemical ionization miniature cylindrical ion trap array mass spectrometer. *Analyst* **2004,** *129* (4), 323-330.

66. Wu, G.; Cooks, R. G.; Ouyang, Z., Geometery optimization for the cylindrical ion trap: Field calculations, simulations and experiments. *Int. J. Mass Spectrom.* **2005,** *241* (2-3), 119-132.

67. March, R. E.; Todd, J. F. J., Theory of Quadrupole Instruments. In *quadrupole ion trap mass spectrometry*, John Wiley & Sons, Inc.: Hoboken, New Jersey, 2005; Vol. 165, pp 34-72.

68. Misharin, A. S.; Laughlin, B. C.; Vilkov, A.; Takats, Z.; Ouyang, Z.; Cooks, R. G., High-throughput mass spectrometer using atmospheric pressure ionization and a cylindrical ion trap array. *Anal. Chem.* **2005,** *77* (2), 459-470.

69. Ding, L.; Kumashiro, S., Ion motion in the rectangular wave quadrupole field and digital operation mode of a quadrupole ion trap mass spectrometer. *Rapid Commun. Mass Spectrom.* **2006,** *20* (1), 3-8.

70. Gao, L.; Song, Q.; Patterson, G. E.; Cooks, R. G.; Ouyang, Z., HandHeld recilinear ion trap mass spectrometer. *Anal. Chem.* **2006,** *78* (17), 5994 - 6002.

71. Chaudhary, A.; van Amerom, F.; Short, R.; Bhansali, S., Fabrication and testing of a miniature cylindrical ion trap mass spectrometer constructed from low temperature co-fired ceramics. *Int. J. Mass Spectrom.* **2006,** *251* (1), 32-39.

72. Pau, S.; Pai, C. S.; Low, Y. L.; Moxom, J.; Reilly, P. T. A.; Whitten, W. B.; Ramsey, J. M., Microfabricated quadrupole ion trap for mass spectrometer applications. *Phys. Rev. Lett.* **2006,** *96* (12), 120801.

73. Lammert, S. A.; Rockwood, A. A.; Wang, M.; Lee, M. L.; Lee, E. D.; Tolley, S. E.; Oliphant, J. R.; Jones, J. L.; Waite, R. W., Miniature toroidal radio frequency ion trap mass analyzer. *J. Am. Soc. Mass Spectrom.* **2006,** *17* (7), 916-922.

74. Austin, D. E.; Cruz, D.; Blain, M. G., Simulations of Ion Trapping in a micrometer-sized cylindrical ion trap. *J. Am. Soc. Mass Spectrom.* **2006,** *17*, 430-441.

75. Yu, M.; Fico, M.; Kothari, S.; Ouyang, Z.; Chappell, W. J., Polymer-based ion trap chemical sensor. *IEEE Sensors J.* **2006,** *6*, 1429-1434.

76. Austin, D. E.; Wang, M.; Tolley, S. E.; Maas, J. D.; Hawkins, A. R.; Rockwood, A. L.; Tolley, H. D.; Lee, E. D.; Lee, M. L., Halo ion trap mass spectrometer. *Anal. Chem.* **2007,** *79* (7), 2927-2932.

77. Cruz, D.; Chang, J. P.; Fico, M.; Guymon, A. J.; Austin, D. E.; Blain, M. G., Design, microfabrication, and analysis of micrometer-sized cylindrical ion trap arrays. *Rev. Sci. Instrum.* **2007,** *78* (1), 015107.

78. Wan, J.; Qu, Q.; Zhou, Z.; Li, Z.; Wang, Y.; Liu, L., Surface Planar ion chip for linear radio-frequency paul traps. *Chin. Phys. Lett.* **2007,** *24*, 1238-1241.

79. Zhao, X.; Douglas, D. J., Dipole excitation of ions in linear radio frequency quadrupole ion traps with added multipole fields. *Int. J. Mass Spectrom.* **2008,** *275* (1–3), 91-103.

80. Janfelt, C.; Graesboll, R.; Lauritsen, F. R., Characterization and optimization of membrane inlets for a miniature ion trap mass spectrometer operating at a high background pressure of humid air. *Int. J. Mass Spectrom.* **2008,** *276* (1), 17-23.

81. van Amerom, F. H. W.; Chaudhary, A.; Cardenas, M.; Bumgarner, J.; Short, R. T., Microfabrication of cylindrical ion trap mass spectrometer arrays for handheld chemical analyses. *Chem. Eng. Commun.* **2008,** *195* (2), 98 - 114.

82. Contreras, J. A.; Murray, J. A.; Tolley, S. E.; Oliphant, J. L.; Tolley, H. D.; Lammert, S. A.; Lee, E. D.; Later, D. W.; Lee, M. L., Hand-portable gas chromatograph-toroidal ion trap mass spectrometer (GC-TMS) for detection of hazardous compounds. *J. Am. Soc. Mass Spectrom.* **2008,** *19* (10), 1425-1434.

83. Yang, M.; Kim, T.; Hwang, H.; Yi, S.; Kim, D., Development of a palm portable mass spectrometer. *J. Am. Soc. Mass Spectrom.* **2008,** *19* (10), 1442-1448.

84. Koizumi, H.; Whitten, W. B.; Reilly, P. T. A.; Koizumi, E., The effect of endcap electrode holes on the resonant ejection from an ion trap. *Int. J. Mass Spectrom.* **2009,** *281* (3), 108-114.

85. Xu, W.; Chappell, W. J.; Cooks, R. G.; Ouyang, Z., Characterization of electrode surface roughness and its impact on ion trap mass analysis. *J. Mass Spectrom.* **2009,** *44* (3), 353-360.

86. Chaudhary, A.; van Amerom, F. H. W.; Short, R. T., Development of microfabricated cylindrical ion trap mass spectrometer arrays. *J. Microelectromech. Syst.* **2009,** *18* (2), 442 - 448.

87. Fico, M.; Maas, J. D.; Smith, S. A.; Costa, A. B.; Ouyang, Z.; Chappell, W. J.; Cooks, R. G., Circular arrays of polymer-based miniature rectilinear ion traps. *Analyst* **2009,** *134* (7), 1338-1347.

88. Li, X.; Jiang, G.; Luo, C.; Xu, F.; Wang, Y.; Ding, L.; Ding, C., Ion trap array mass analyzer: Structure and performance. *Anal. Chem.* **2009,** *81* (12), 4840-4846.

89. Ouyang, Z.; Gao, L.; Fico, M.; Chappell, W. J.; Noll, R. J.; Cooks, R. G., Quadrupole ion traps and trap arrays: Geometry, material, scale, performane. *Eur. J. Mass Spectrom.* **2009,** *13*, 13-18.

90. Kothari, S.; Song, Q. Y.; Xia, Y.; Fico, M.; Taylor, D.; Amy, J. W.; Stafford, G.; Cooks, R. G., Multiplexed four-channel rectilinear ion trap mass spectrometer. *Anal. Chem.* **2009,** *81* (4), 1570-1579.

91. Fico, M.; Yu, M.; Ouyang, Z.; Cooks, G. R.; Chappell, W. J., Miniaturization and geometry optimization of a polymer-based rectilinear ion trap. *Anal. Chem.* **2009,** *79*, 8076-8082.

92. Jesseph, A. V.; Fox, J. D.; Verbecj IV, G. F., Ion isolation and collision-induced dissociation in a 0.5 mm r0 cylindrical ion trap. *Int. J. Mass Spectrom.* **2010,** *295* (3), 149-152.

93. Smith, S. A.; Mulligan, C. C.; Song, Q.; Noll, R. J.; Cooks, R. G.; Ouyang, Z., Ion traps for miniature, multiplexed, and soft-landing technologies. In *practical aspects of trapped ion mass spectrometry*, March, R. E.; Todd, J. F. J., Eds. CRC Press: Boca Raton, FL, 2010; Vol. IV, pp 170-247.

94. Maas, J. D.; Hendricks, P. I.; Ouyang, Z.; Cooks, R. G.; Chappell, W. J., Miniature Monolithic rectilinear ion trap arrays by stereolithography on printed circuit board. *J. Microelectromech. Syst.* **2010,** *19* (4), 951-960.

95. Zhang, Z.; Quist, H.; Peng, Y.; Hansen, B. J.; Wang, J.; Hawkins, A. R.; Austin, D. E., Effects of higher-order multipoles on the performance of a two-plate quadrupole ion trap mass analyzer. *Int. J. Mass Spectrom.* **2011,** *299* (2–3), 151-157.

96. Ziaeian, I.; Sadat Kiai, S. M.; Ellahi, M.; Sheibani, S.; Safarian, A.; Farhangi, S., Theoretical study of the effect of ion trap geometry on the dynamic behavior of ions in a Paul trap. *Int. J. Mass Spectrom.* **2011,** *304* (1), 25-28.

97. Sokol, E.; Noll, R. J.; Cooks, R. G.; Beegle, L. W.; Kim, H. I.; Kanik, I., Miniature mass spectrometer equipped with electrospray and desorption electrospray ionization for direct analysis of organics from solids and solutions. *Int. J. Mass Spectrom.* **2011,** *306* (2–3), 187-195.

98. Hendricks, P.; Duncan, J.; Noll, R. J.; Ouyang, Z.; Cooks, R. G., Performance of a low voltage ion trap. *Int. J. Mass Spectrom.* **2011,** *305* (2-3), 69-73.

99. Maas, J. D.; Chappell, W. J., RF planar ion trap for chemical sensing In *IEEE MTT-S International*, 2011.

100. Peng, Y.; Hansen, B. J.; Quist, H.; Zhang, Z. P.; Wang, M.; Hawkins, A. R.; Austin, D. E., Coaxial ion trap mass spectrometer: Concentric toroidal and quadrupolar trapping regions. *Anal. Chem.* **2011,** *83* (14), 5578-5584.

101. Smith, P. A.; Lepage, C. R. J.; Savage, P. B.; Bowerbank, C. R.; Lee, E. D.; Lukacs, M. J., Use of a hand-portable gas chromatograph-toroidal ion trap mass spectrometer for self-chemical

ionization identification of degradation products related to O-ethyl S-(2-diisopropylaminoethyl) methyl phosphonothiolate (VX). *Anal. Chim. Acta* **2011,** *690* (2), 215-220.

102. Wang, M.; Quist, H.; Hansen, B. J.; Peng, Y.; Zhang, Z.; Hawkins, A. R.; Rockwood, A. L.; Austin, D. E.; Lee, M. L., Performance of a halo ion trap mass analyzer with exit slits for axial ejection. *J. Am. Soc. Mass Spectrom.* **2011,** *22* (2), 369-378.

103. Peng, Y., Novel ion trap made using lithographically patterned plates. BYU ScholarsArchive: Brigham Young University, Provo, UT, 2011.

104. Wang, L.; Xu, F.; Ding, C., Performance and geometry optimization of the ceramic-based rectilinear ion traps. *Rapid Commun. Mass Spectrom.* **2012,** *26* (17), 2068-2074.

105. Xiong, X.; Xu, W.; Fang, X.; Deng, Y.; Ouyang, Z., Accelerated simulation study of space charge effects in quadrupole ion traps using GPU techniques. *J. Am. Soc. Mass Spectrom.* **2012,** *23* (10), 1799-1801.

106. Misharin, A.; Novoselov, K.; Laiko, V.; Doroshenko, V. M., Development and characterization of a field-deployable ion-trap mass spectrometer with an atmospheric pressure interface. *Anal. Chem.* **2012,** *84* (22), 10105-10112.

107. Wilpers, G.; See, P.; Gill, P.; Sinclair, A. G., A monolithic array of three-dimensional ion traps fabricated with conventional semiconductor technology. *Nat. Nanotechnol.* **2012,** *7* (9), 572-576.

108. Taylor, N.; Austin, D. E., A simplified toroidal ion trap mass analyzer. *Int. J. Mass Spectrom.* **2012,** *321*, 25-32.

109. Hansen, B. J.; Niemi, R. J.; Hawkins, A. R.; Lammert, S. A.; Austin, D. E., A lithographically patterned discrete planar electrode linear ion trap mass spectrometer. *J. Microelectromech. Syst.* **2013,** *22* (4), 876-883.

110. Chu, Y.; Xiao, Y.; Ling, X.; Ding, C., Analytical performance of printed circuit board ion trap array mass analyzer with electrospray ionization. *Chinese J. Anal. Chem. (Fenxi Huaxue)* **2013,** *41* (1), 152 - 158.

111. Yu, X.; Chu, Y.; Ling, X.; Ding, Z.; Xu, C.; Ding, L.; Ding, C., Multiple mass analysis using an ion trap array (ITA) mass analyzer. *J. Am. Soc. Mass Spectrom.* **2013,** *24* (9), 1420-1427.

112. Tian, Y.; Higgs, J.; Li, A.; Barney, B.; Austin, D. E., How far can ion trap miniaturization go? Parameter scaling and space-charge limits for very small cylindrical ion traps. *J. Mass Spectrom.* **2014,** *49* (3), 233-240.

113. Wang, Y.; Zhang, X.; Feng, Y.; Shao, R.; Xiong, X.; Fang, X.; Deng, Y.; Xu, W., Characterization of geometry deviation effects on ion trap mass analysis: A comparison study. *Int. J. Mass Spectrom.* **2014,** *370*, 125-131.

114. Remes, P. M.; Syka, J. E. P.; Kovtoun, V. V.; Schwartz, J. C., Insight into the resonance ejection process during mass analysis through simulations for improved linear quadrupole ion trap mass spectrometer performance. *Int. J. Mass Spectrom.* **2014,** *370*, 44-57.

115. Chaudhary, A.; van Amerom, F. H. W.; Short, R. T., Experimental evaluation of micro-ion trap mass spectrometer geometries. *Int. J. Mass Spectrom.* **2014,** *371*, 17-27.

116. Brkić, B.; Giannoukos, S.; France, N.; Murcott, R.; Siviero, F.; Taylor, S., Optimized DLP linear ion trap for a portable non-scanning mass spectrometer. *Int. J. Mass Spectrom.* **2014,** *369*, 30-35.

117. Li, A.; Hansen, B. J.; Powell, A. T.; Hawkins, A. R.; Austin, D. E., Miniaturization of a planar-electrode linear ion trap mass spectrometer. *Rapid Commun. Mass Spectrom.* **2014,** *28* (12), 1338-1344.

118. Wang, Y.; Zhang, X.; Zhai, Y.; Jiang, Y.; Fang, X.; Zhou, M.; Deng, Y.; Xu, W., Mass selective ion transfer and accumulation in ion trap arrays. *Anal. Chem.* **2014,** *86* (20), 10164-10170.

119. Xu, W.; Li, L.; Zhou, X.; Ouyang, Z., Ion sponge: A 3-dimentional array of quadrupole ion traps for trapping and mass-selectively processing ions in gas phase. *Anal. Chem.* **2014,** *86* (9), 4102-4109.

120. Wu, Q.; Tian, Y.; Li, A.; Austin, D. E., Simulations of electrode misalignent effects in two-plate linear ion traps. *Int. J. Mass Spectrom.* **2015,** *393*, 52-57.

121. Dang, Q. K.; Xu, F. X.; Huang, X. H.; Fang, X.; Wang, R. Z.; Ding, C. F., Linear ion trap with added octopole field component: The property and method. *J. Mass Spectrom.* **2015,** *50* (12), 1400-1408.

122. Wu, Q.; Li, A.; Tian, Y.; Zare, R. N.; Austin, D. E., Miniaturized linear wire ion trap mass analyzer. *Anal. Chem.* **2016,** *88* (15), 7800-7806.

123. Huo, X.; Tang, F.; Chen, J.; Zhang, X.; Wang, X., Characterization of the impact of the ejection slit on miniature rectilinear ion trap analysis. *Int. J. Mass Spectrom.* **2016,** *399–400*, 44-50.

124. Ma, Q.; Bai, H.; Li, W.; Wang, C.; Li, X.; Cooks, R. G.; Ouyang, Z., Direct identification of prohibited substances in cosmetics and foodstuffs using ambient ionization on a miniature mass spectrometry system. *Anal. Chim. Acta* **2016,** *912*, 65-73.

125. Xue, B.; Sun, L. L.; Huang, Z. X.; Gao, W.; Fan, R. R.; Cheng, P.; Ding, L.; Ma, L.; Zhou, Z., A hand-portable digital linear ion trap mass spectrometer. *Analyst* **2016,** *141* (19), 5535-5542.

126. Wahlin, L., The colutron, a zero deflection isotope separator. *Nucl. Instrum. Methods* **1964,** *27*(1), 55-60.

127. Freidhoff, C. B.; Young, R. M.; Sriram, S.; Braggins, T. T.; O'Keefe, T. W.; Adam, J. D.; Nathanson, H. C.; Syms, R. R. A.; Tate, T. J.; Ahmad, M. M.; Taylor, S.; Tunstall, J. J., Chemical sensing using nonoptical microelectromechanical systems. *J. Vac. Sci. Technol. A* **1999,** *17*, 2300-2307.

128. Sillon, N.; Baptist, R., Micromachined mass spectrometer. *Sens. Act. B* **2002,** *83*, 129-137.

129. Diaz, J. A.; Giese, C. F.; gentry, W. R., Sub-miniature ExB sector-field mass spectrometer. *J. Am. Soc. Mass Spectrom.* **2001,** *12*, 619-632.

130. Diaz, J. A.; Giese, C. F.; Gentry, W. R., Portable double-focusing mass-spectrometer system for field gas monitoring. *Field Anal. Chem. Technol.* **2001,** *5* (156-167).

131. Diaz, J. A.; Daley, P.; Miles, R.; Rohrs, H.; Polla, D., Integration test of a low-cost, portable, chemical-detection system. *Trends Anal. Chem.* **2004,** *23*, 314-321.

132. Berger, P. S., A compact, stand-alone, integrated ms/vacuum package. In *Harsh Environment Mass Spectrometry Workshop*, Santa Barbara, CA, 2009; pp 21-24.

133. Berkout, V. D.; Cotter, R. J.; Segers, D. P., Miniaturized EI/Q/oa TOF mass spectrometer. *J. Am. Soc. Mass Spectrom.* **2001,** *12*, 641-647.

134. Syage, J. A.; Hanning-Lee, M. A.; Hanold, K. A., A man-portable, photoionization time-of-flight mass spectrometer. *Field Anal. Chem. Technol.* **2000,** *4* (4), 204-215.

135. Cotter, R. J.; English, R. D.; Warscheid, A. H.; Gardner, B. D., Miniaturized time-of-flight mass spectrometers for bioagent detection and identification. *J. Am. Soc. Mass Spectrom.* **2003,** *51* (1), 36-40.

136. Austin, D. E.; Ahrens, T. J.; Beauchamp, J. L., Dustbuster: A compact impact-ionization time-of-flight mass spectrometer for in situ analysis of cosmic dust. *Rev. Sci. Instrum.* **2002,** *73*, 185-189.

137. Austin, D. E.; Beauchamp, J. L.; Manning, H. L. K.; Bailey, C. L., A compact time-of-flight mass spectrometer for high-flux cosmic dust analysis. *J. Geophys. Res. Planets* **2004,** *109*, E07S07(5 pgs).

138. Huang, Z.; Tan, G.; Zhou, Z.; Chen, L.; Cheng, L.; Jin, D.; Tan, X.; Xie, C.; Li, L.; Dong, J.; Fu, Z.; Cheng, P.; Gao, W., Development of a miniature time-of-flight mass/charge spectrometer for ion beam source analyzing. *Int. J. Mass Spectrom.* **2015,** *379*, 60-64.

139. Gao, W.; Tan, G.; Hong, Y.; Li, M.; Nian, H.; Guo, C.; Huang, Z.; Fu, Z.; Dong, J.; Xu, X.; Cheng, P.; Zhou, Z., Development of portable single photon ionization time-of-flight mass spectrometer combined with membrane inlet. *Int. J. Mass Spectrom.* **2013,** *334*, 8-12.

140. Getty, S. A.; Brinckerhoff, W. B.; Cornish, T.; Ecelberger, S.; Floyd, M., Compact two-step laser time-of-flight mass spectrometer for in situ analyses of aromatic organics on planetary missions. *Rapid Commun. Mass Spectrom.* **2012,** *26* (23), 2786-2790.

141. Syms, R. R. A.; Tate, T. J.; Ahmad, M. M.; Taylor, S., Fabrication of a microengineered quadrupole electrostatic lens. *Electron. Lett.* **1996,** *32*, 2094-2095.

142. Syms, R. R. A.; Tate, T. J.; Ahmad, M. M.; Taylor, S., Design of a microengineered electrostatic quadrupole lens. *IEEE Trans. Electron Dev.* **1998,** *45*, 2304-2311.

143. Holkeboer, D. H.; Karandy, T. L.; Currier, F. C.; Frees, L. C.; Ellefson, R. E., Miniature quadrupole residual gas analyzer for process monitoring at millitorr pressures. *J. Vac. Sci. Technol. A* **1998,** *16* (3), 1157-1162.

144. Orient, O. J.; Chutjian, A.; Garkanian, V., Miniature, high-resolution, quadrupole mass-spectrometer array. *Rev. Sci. Instrum.* **1997,** *68* (3), 1393-1397.

145. Ouyang, Z.; Noll, R. J.; Cooks, G. R., Handheld miniature ion trap mass spectrometers. *Anal. Chem.* **2009,** *81* (7), 2421-2425.

146. Dehmelt, H. G., Radiofrequency spectroscopy of stored ions I: Storage. *Adv. At. and Mol. Phy.* **1967,** *3*, 53-72.

147. Dass, C., Fundamentals of contemporary mass spectrometry. John Wiley and Sons: Chichester, 2007.

148. Sparkman, O. D.; Watson, J. T., Introduction to mass spectrometry: Instrumentation, applications and strategies for data interpretation. John Wiley and Sons: Chichester, 2008.

149. Drndic, M.; Lee, C. S.; Westervelt, R. M., Three-dimensional microelectromagnet traps for neutral and charged particles. *Phys. Rev. B* **2001,** *63*, 085321 (5 pgs).

150. Fox, J.; Saini, R.; Tsui, K.; Verbeck, G., Microelectromechanical system assembled ion optics: An advance to miniaturization and assembly of electron and ion optics. *Rev. Sci. Instrum.* **2009,** *80*, 093302 (6 pgs).

151. Ferran, R. J.; Boumsellek, S., High-pressure effects in miniature arrays of quadrupole analyzers for residual gas analysis from 10^{-9} to 10^{-2} Torr. *J. vac. Sci. Tech. A* **1996,** *14* (3), 1258.

152. Paul, W.; Steinwedel, H. Apparatus for separating charged particles of different specific charges. US2939952, 1956.

2. Simulation Study on Space Charge Effect on Cylindrical Ion Traps with Different Trap Dimensions

(This Chapter has been published as an article: "Tian, Y.; Higgs, J. M.; Barney, L. B; Li, A.; Austin, D. E. How far can miniaturized ion trap go? Parameter scaling and space-charge limits for very small cylindrical ion traps. Journal of Mass Spectrometry, 2014, 49(3), 233-240 (featured as the cover article of this issue)". My individual contribution was building the simulation model, running the experiment, plotting the resulting figures, and writing the draft manuscript.)

2.1 Introduction

Space charge is one of the prominent problems in the process of miniaturizing ion traps as mentioned in the first chapter. Serious space charges will significantly reduce ion traps' trapping capacity, reducing signal intensities or making the signals too weak to be seen. Mass resolution may also be affected as the trapped ion packet is more scattered instead of being focused around the trap center with less kinetic energy. It is shown in Chapter 1 that pseudopotential well depth is a quantitation method to approximately describe ion traps' trapping ability. According to Equation 1-5, trapping capacities are proportional to the amplitude of trapping voltages. Efforts have been made on miniaturizing different ion traps' sizes to different degrees as shown in Table 2-1. The experimental operating parameters had been explored to reach the best condition, yet how the RF trapping voltage should vary theoretically with the trap size is still unknown. There might be a

correlation between trapping capacities and trap sizes or the amplitudes of trapping voltages. Since experiments usually involve many unexpected factors that contribute uncertainties to the results, simulations turned out to be appropriate and simple methods to reveal these relationships if any.

Table 2-1. Representative efforts at miniaturization of several types of radiofrequency ion traps, including a summary of operating parameters.

Ion trap type	Trap size/r_0 or y_0 (mm)	RF frequency/ω (mhz)	RF amplitude/v_{p-p} (v)	Maximum RF amplitude/v_{p-p} (v)	Reference and location
Cylindrical	5	1.1	—	—	Purdue Univ.[1]
	3.88	0.82	240		Beijing Inst. Tech.[2]
	2.5	2	—	810	Purdue Univ.[3]
	2.5	2	150	—	South Korea[4]
	1.375	2.79	114	770	Univ. South Florida[5]
	0.5	8.1	—	500	Oak Ridge National Lab.[6]
	0.02	100	45	90	Univ. North. Carolina Chapel Hill[7]
	0.001	1200	8	—	Sandia National Labs[8]
Linear	4	1	600	5000	Thermo Finnigan[9]
	3	0.7	30	—	NASA Goddard Space Flight Center[10]
	2.2	2.3	300	1200	Brigham Young Univ.[11]
Rectilinear	7.6	0.881	—	1500	Purdue Univ.[12]
	5	0.97	200	650	Purdue Univ.[13]
	6	0.768	—	—	Fudan Univ.[14]
	1.66	1.105	68	610	Purdue Univ.[15]
Toroidal	10	1.038	—	—	Oak Ridge National Lab.[16]
	2	2	400	400	Torion Technologies, Inc.[17]

Simulations have always been competent assistants in designing instrument geometries involving ion optics and exploring their operating parameters before they are built and tested. The most famous three simulation programs in ion optics are the Integrated System for Ion Simulation (ISIS) developed by Raymond March's group[18-19], the Ion Trajectory SIMulation (ITSIM)[20] developed at Purdue University and the ION and the electron optics SIMulation package

(SIMION)[21] developed originally by David Dahl at the Idaho National Laboratory, and subsequently improved and distributed by Scientific Instrument Service, Inc. (SIS). ISIS is seldom used due to its limited function and the archaic DOS platform it runs on[19]. Though ITSIM is suitable for trap-based instruments, SIMION is more widely used since it is able to simulate complicated configurations[19]. The simulation program used in this dissertation is SIMION.

SIMION creates electric fields by calculating potentials at every point in a Potential Array(PA), which is a 3-D rectangular grid of points in space. Potentials at each point are determined by solving the Laplace equation using a fourth-order Runge-Kutta integration. Ion trajectories are calculated based on classical mechanics. Ion trajectories are thus determined by the potentials they experience at their positions at every time step. Calculating electric fields requires a PA carrying pre-defined electrodes. Methods to construct electrodes include directly modifying the potentials on the desired grid points, drawing electrodes from a GEM geometry file that defines the geometry by constructive solid geometry (CSG) primitive, and importing the desired model from a 3D CAD file.

Helium is most frequently used as the cooling gas in both experiments and simulations. There have been several collision models proposed for simulations[22-24]. One of the most frequently used is the hard-sphere collision model, which takes the collision between an ion and a neutral molecule as elastic. In other words, there is no kinetic energy loss during the collision. A user program based on the hard-sphere collision model, which is taken from SIMION install package, isused in the experiments throughout this dissertation.

In this chapter, the ways of scaling the amplitudes and frequencies of RF signals as the trap sizes are discussed and a reasonable scaling scheme is suggested. The simulation model is a

cylindrical ion trap. The space charge effects in various trap sizes are studied by scaling the trapping parameters based on the method suggested.

2.2 Scaling operating parameters in small ion traps

The choice of the two chief operating parameters, voltage and frequency of the RF applied to ion traps, are dependent on several factors. Substituting Equation 1-1 into 1-2 and 1-3, the stability of trapped ions in the axial direction in a 3-D QIT with ideal geometry is governed by the transformed relations:

$$q_z = \frac{4eV}{mr_0^2\Omega^2} \qquad \textit{Equation 2-1}$$

$$a_z = \frac{-8eU}{mr_0^2\Omega^2} \qquad \textit{Equation 2-2}$$

The acceptable ranges of these dimensionless parameters $\boldsymbol{q}$ and $\boldsymbol{a}$ do not change as the dimensions of traps are reduced. Analogous relationships exist for other ion trap geometries. The equation for $\boldsymbol{q}_z$, one of the stability parameters, can be rearranged to illustrate the general relationship between voltage, frequency and size in a small ion trap:

$$r_0 \propto \frac{\sqrt{V}}{\Omega} \qquad \textit{Equation 2-3}$$

for a given mass-to-charge range. A reduction in the physical dimensions of the trap must be accompanied with a reduction in RF amplitude or an increase in RF frequency, or some combination of the two. Note that there are still two independent variables in this equation – for a given size ion trap, an infinite range of voltage/frequency combinations will satisfy this equation. However, there are several practical considerations that constrain a fairly narrow range for the RF frequencies and voltages used in miniaturized ion traps. These include electrical power, electrical

discharge and breakdown, the pseudopotential well depth, the size of the ion cloud within the trap, desired mass resolution and availability/performance of RF power supplies.

Within an ion trap, ions typically are collisionally cooled to a small volume at the trap center using helium or another background gas. The presence of helium greatly improves mass resolution[25], and also makes collision-induced dissociation possible for MS/MS. The size of the cooled ion cloud at the trap center is dependent on the strength of the trapping field and the trapping frequency. Stronger fields or higher frequencies are required to squeeze the ions into a smaller volume, but there is a limit to the magnitude of electric field that can be maintained across a given gap between electrodes. Ultimately, the maximum maintainable field strength may limit the extent to which the size of the ion trajectories can be reduced and, hence, limit the extent to which ion traps can be miniaturized. This important factor will be explored in the simulations later.

The question whether the cooled ion cloud will fit within the trap volume is a consequence of the pseudopotential well constraint. The pseudopotential well depth, given by Dehmelt for low values of $\boldsymbol{q}$ is as Equation 1-5. For ions to be trapped, the product of the well depth $\overline{\boldsymbol{D}}$ and the electronic charge, $\boldsymbol{e}$, must be greater than the kinetic energies of the ions – which in turn is a combination of collisional cooling and the energy obtained from acceleration in the trapping field. If the ions have a kinetic energy larger than this, or if the pseudopotential well depth is too small, ions will strike the trap electrodes and be lost. In this case, the motion of ions is still bounded (i.e. they still fall within the stability region given by the Mathieu equation), but the trajectories exceed the physical dimensions of the trap. Higher electric fields are needed to confine the ions into a smaller space.

A further driver for higher voltages and frequencies is mass resolution, which is improved as trap frequency increases for a given trap size[7]. As noted, voltages cannot be increased without limit due to problems associated with electrical breakdown. Gas-ionization discharges limit electric fields in the presence of low pressures of gases, although miniaturized ion traps may avoid the problem region in the Paschen curve. Still, even under high vacuum, field emission limits applied voltages, as demonstrated for micron-sized CIT[26]. In addition, electrical power decreases as the RF amplitude and frequency decrease, providing motivation to reduce these parameters.

Table 2-2. Several options for scaling the trapping RF amplitude with trap size. Note that the RF amplitude given is the trapping voltage and not the maximum RF voltage that would be applied at the end of an RF ramp.

	Case A: Constant V		Case B: Constant Ω		Case C: V scales with r_0		Case D: V scales as 1/3 power of r_0		Case E: V scales as 1/2 power of r_0		Case F: V scales as 2/3 power of r_0	
r_0	$V_{0\text{-}p}$ (V)	Ω (MHz)	$V_{0\text{-}p}$ (V)	Ω (MHz)	$V_{0\text{-}p}$ (V)	Ω (MHz)	$V_{0\text{-}p}$ (V)	Ω (MHz)	$V_{0\text{-}p}$ (V)	Ω (MHz)	$V_{0\text{-}p}$ (V)	Ω (MHz)
1 cm	1000	1	1000	1	1000	1	1000	1	1000	1	1000	1
1 mm	1000	10	10	1	100	3	464	7	316	6	215	5
100 µm	1000	100	0.1	1	10	10	215	46	100	32	46	22
10 µm	1000	1000	0.001	1	1	32	100	316	32	178	10	100
1 µm	1000	10000	0.00001	1	0.1	100	46	2155	10	1000	2	464

Producing an ion trap with reduced physical dimensions includes determining what RF frequency and RF amplitudes will be used. These parameters will be scaled based on the equations and constraints presented above. Taking voltage as the independent variable, for a given ***m/z*** range, the RF frequency and pseudopotential well depth are constrained. The question that remains is how voltage should scale with trap size, and what will be the corresponding consequences for power, performance and trapping capacity. Below are several test cases to explore this question. Table 2-2 shows several possible ways that RF amplitude can scale with size in miniaturized ion traps. These are shown graphically in Figure 2-1. In all cases, the same ***m/z*** range is used. The

values of RF frequency are determined directly from Equation 2-3 for a given size/voltage relationship.

Case A attempts to keep the applied RF amplitude constant and adjust only the RF frequency. The pseudopotential well depth remains constant for ions of the same ***m/z*** range. This scenario has been proposed[7] for ion trap miniaturization, but the resulting fields are not sustainable. For full-sized ion traps, the applied RF amplitudes pose no problems, but for very small traps, these same voltages are too large to be maintained across small electrode gaps. The same applied voltage at smaller size scales would also require higher frequencies and more electric power, obviating possible electric advantages to portability.

Case B attempts to keep the RF frequency constant and adjust only the RF amplitude with trap size. The RF amplitude then scales as the square of the trap radius, r_0. For very small ion traps, this case results in a pseudopotential well that is too shallow to contain ions at typical thermal energies. In this case, the electric field at and near the trap center is invariant as the trap is made smaller. Hence, ion trajectories are not reduced in physical dimensions compared with full-sized traps. When the trap becomes smaller than these dimensions, the ions are no longer trapped.

Cases A and B represent extremities in the parameter space of interest. In one case, the voltages are too high, and in the other, the voltages are too small. The remaining cases fall between these two examples.

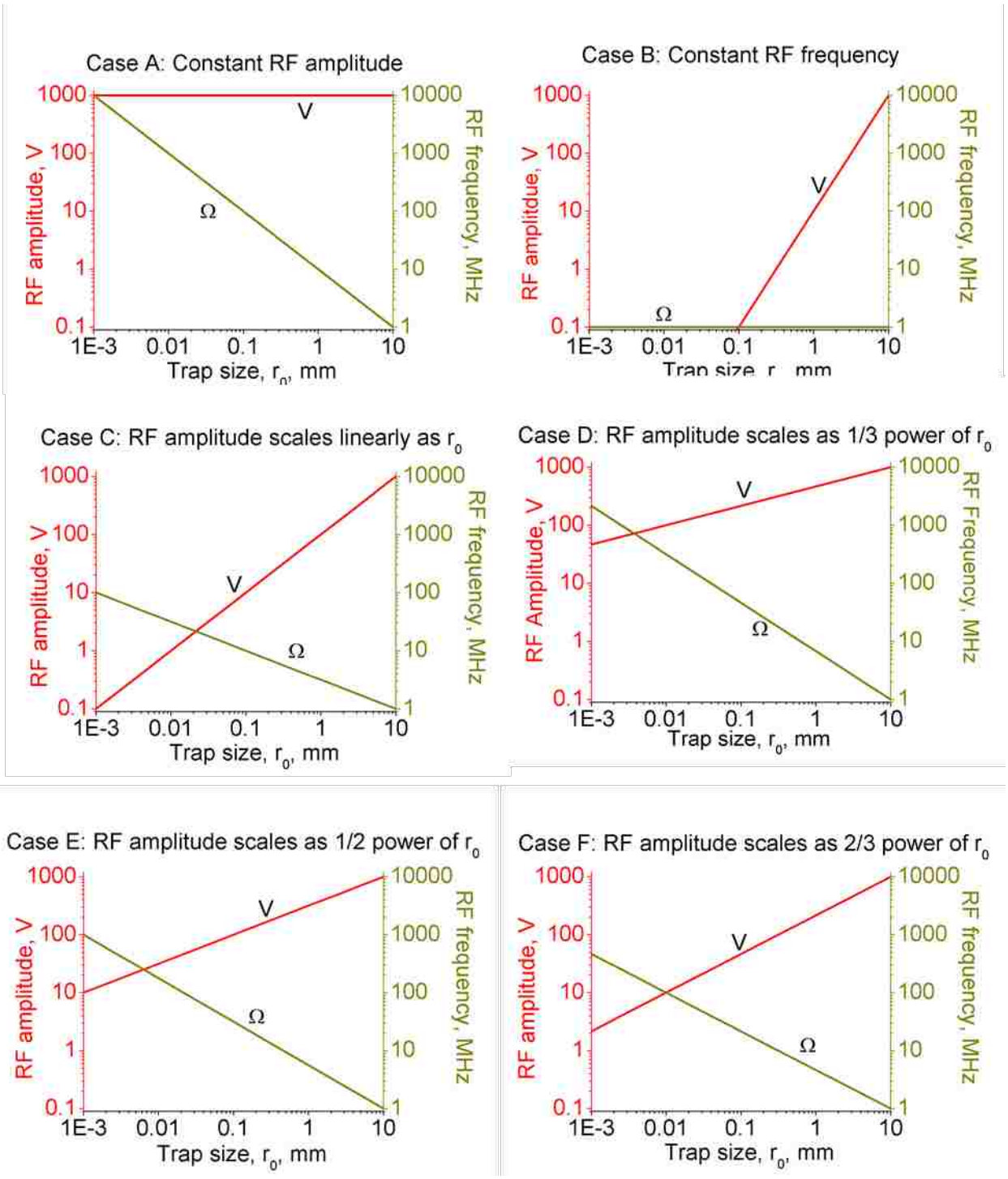

Figure 2-1. Plots showing several ways in which RF amplitude and RF frequency can be varied for smaller-size cylindrical ion traps. These values retain the same q_z value for a given m/z and are based on the cases presented in Table 2-2.

In Case C, the RF amplitude scales linearly with r_0. This scaling maintains a constant electric field regardless of device size and makes sense from the standpoint of avoiding field effects such as electric discharge in very small traps. This case has a deeper pseudopotential well than Case B, but it would be desirable to use a higher voltage if possible.

The last three scenarios show intermediate proportions, with the trapping RF amplitude scaling as the 1/3, 1/2 and 2/3 power of r_0. The electric field among electrode elements increases for smaller traps, so these cases may present engineering and/or electrical challenges, but may still be feasible depending on fabrication methods and electrode geometry. On the other hand, these cases should have a higher trapping capacity compared with a trap scaled with Case C.

None of the reported miniaturization efforts follow strictly any of these scaling cases, and significant variation exists throughout the literature. Still, these cases allow us to explore the general question of ion trap miniaturization and the resulting expectations on trapping capacity and device sensitivity.

2.3 Simulation of trapping capacity in small ion traps

It is expected that trapping capacity is reduced in smaller ion traps, but it is not clear how this effect scales with trap size. Dehmelt's original treatment discussed a maximum density of ions that can be trapped as a function of trap size[27]. Guan and Marshall[28] showed calculations of maximum ion density in different trap sizes, but the number of ions is still unknown unless the ion cloud volume and ion density distribution are determined. Other groups have suggested that the number of ions that can be analyzed in an ion trap mass spectrometer scales[7] as r_0, or alternatively as r_0^3, the trap volume[29-30]. This issue is further complicated by the dependence on voltage and frequency

scaling, which, as we have seen in the cases above, must be taken into account to answer this question. Further, the maximum number or density of ions that can be trapped is not the same as the maximum number of ions that can be analyzed in an ion trap mass spectrometer. Space charge begins to degrade ion trap mass analysis at charge densities that are orders of magnitude below the absolute trapping capacities[9]. The trapping advantages of linear-type ion traps are only partially understood, as ions are not spread equally through the trapping volume. Finally, the trapping capacity of toroidal-type traps has not been adequately explored. For the purposes of this study, we are concerned only with the maximum number of ions that still result in a useful mass spectrum.

The number of ions that can be analyzed in a miniaturized ion trap can be estimated using SIMION ion trajectory software. The intent is not to provide precise numerical limits but rather to explore in a general sense how this important variable scales with trap size. Specifically, the following simulations seek to identify the scaling of (1) the number of ions that can be analyzed and (2) the effect of trapping in the context of the pseudopotential well and the size of the collisionally cooled ion cloud for ion traps ranging in size down to the micrometer scale.

2.4 Simulations

Computer simulations of space-charge effects in a series of CITs with sizes ranging from r_0 = 1 cm to r_0 = 1μm were carried out using SIMION 8.0 ion trajectory software (Scientific Instrument Services, Ringoes, NJ). The design of the CIT in these simulations is taken from the design by Wu et al.[31], which was optimized experimentally to give the best mass resolution. In addition to the other dimensions provided in Wu et al., the inner radius of the ring electrode r_0 was 5.0 mm, and the center to end-cap distance z_0 was 5.0 mm. This design was reported as having a mass resolution,

m/Δm, of 100 during boundary ejection for ions with m/z = 146[32]. The same relative dimensions were used for all trap sizes in our simulations, ensuring that the higher-order terms in the trapping potential are the same in all simulations. The CIT was represented as a 2-D, cylindrically symmetric potential array in SIMION with both r_0 and z_0 represented by 50 grid units from trap center to electrodes, and a total array size of 95 grid units radially by 55 grid unit axially. The trap size was varied by adjusting the grid-unit-to-mm scaling factor. Scaling the size in this way ensured that higher-order fields and effects were the same among traps of differing size. Whereas the theoretical treatment (Equation 2-1, 2-2) is strictly true only for an ideal quadrupole, the following simulations take into account the higher-order field components arising from the non-ideal (cylindrical) electrode shape, ejection holes, truncation of electrodes, etc. These higher-order terms have little effect on the scaling of major variables (frequency, voltage, size) but have significant effect on mass resolution.

An RF potential was simulated using a modified version of the ion trap demo program supplied with the software and was applied to the ring electrode, while the two end-cap electrodes were set to ground. Ions were ejected axially by ramping the RF amplitude at a rate corresponding to 5 000 RF periods for the m/z 140 ion, starting from a q_z value of 0.697.

In the presence of a buffer gas ions in an RF trap will be collisionally cooled to the center of the trap. Commercial ion traps typically use helium in the pressure range of 1mTorr to cool ions, thereby improving mass resolution and accuracy[25]. As the size of the ion cloud may be closely related to space-charge effects, the choice of collision models for these simulations is important. For example, viscous damping will tend to cool the simulated ions to temperatures well below thermal equilibrium, leading to a cloud size that is much smaller than is observed. The present

simulations employed a hard-sphere collision model and full 3-D treatment of collision mechanics based on the user program HS1 supplied with the software. Helium at room temperature was used as the collision gas. The collision frequency was increased proportionally with the RF frequency, simulating higher pressure operation for smaller traps[7]. For the largest trap (r_0 = 1 cm), the helium pressure was set to 1 mTorr.

It has been shown in both experiments and simulations that ion traps with too many ions exhibit both reduced mass resolution and shifted peaks[14, 29, 33]. In the present simulations, the mass resolution was used to predict the onset of space-charge effects. Space-charge effects were approximated using the 'factor repulsion' feature in SIMION with a limited number of simulated ions. For each size trap, 100 ions at ***m/z*** 140 and 50 ions at ***m/z*** 141 were used with repulsion factor turned off in order to determine the baseline mass resolution. Then, the simulation was repeated several times with different values of the charge repulsion factor to estimate the point at which mass resolution decreased to half the baseline value. While this approach is less accurate than explicit calculation of space charge for every ion in the trap, the wide range of ion populations (from 1 to over 106) made explicit calculations impractical, and this approach allowed consistency among all simulations. For very small traps, the repulsion factor was set to 1, and the number of ions was varied from 1 to 150 to find the number of ions for which mass resolution was decreased to half the baseline value. Mass resolution was determined as $M/\Delta M$, with ΔM, the full-width at half max, calculated as 2.355 s, where s was the observed standard deviation of the ejections of all ions of a given ***m/z***. Ions originated with no initial kinetic energy in the center of each trap, distributed randomly within a sphere with a radius of $r_0/10$. Collisional cooling increased or decreased the ion cloud to an equilibrium size before ejection. The size of the ion cloud was

estimated by observing the ion trajectories for a period of roughly 100 RF cycles after the size of the cloud reached a constant value.

Most of the simulations employed the voltage and frequency scaling given in Case E above. Table 2-3 shows the key operating parameters for each trap size with RF amplitude scaling as the square root of the trap radius. In addition to the values in Table 2-3, several simulations were carried out using RF amplitude scaling as the 1/3 and the 2/3 power of r_0 for comparison and to determine the robustness of the obtained scaling rule to the choice of the voltage–size relationship.

Table 2-3. Parameters used in simulations of CIT with voltage scaled as 1/2 power of r_0.

r_0 (μm)	RF voltage ($V_{0\text{-}p}$, initial)	RF frequency (MHz)	Mean free path (mm)
10000	1000.00	1.00	14.43
3000	547.72	2.47	5.85
1000	316.23	5.62	2.57
300	173.21	13.87	1.04
100	100.00	31.62	0.46
30	54.77	78.01	0.19
10	31.62	177.83	0.08
3	17.32	438.69	0.03
1	10.00	1000.00	0.01

2.5 Results and discussion

As expected, the number of ions that can be analyzed decreases in smaller traps. Of greater interest, though, is the functional form of this relationship. Figure 2-2 shows a log–log plot of the number of analyzable ions as a function of r_0, the trap radius, for CITs ranging from 10 mm down to 30 microns.

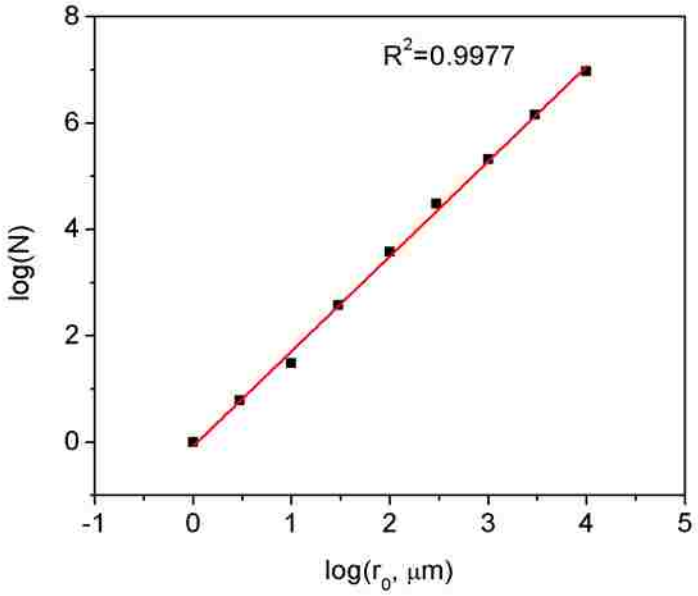

Figure 2-2. Log–log plot of maximum number of analyzable ions as a function of trap size. r_0, from 1 μm to 1 cm, as determined using SIMION 8.0. Also shown is the best fit line and corresponding R^2 parameter.

Only the trials shown in Table 2-2, with voltage scaling as $r_0^{0.5}$, are shown in this figure. The data points are strongly correlated as a straight line (R^2 = 0.9977), implying that the scaling is approximated by a function of the form $N = Ar_0^k$, where A and k are parameters that can be determined from the slope and intercept of the fit line. In this case, k = 1.70, and A = 1.3. This strongly suggests that the number of ions varies as $1.3r_0^{1.7}$.

Figure 2-3 shows these same data points displayed in linear coordinates, along with the best fit curve. Similar analysis in which the voltage scales as the 1/3 and 2/3 powers of r_0 yields values of k of 1.55 and 1.75, respectively.

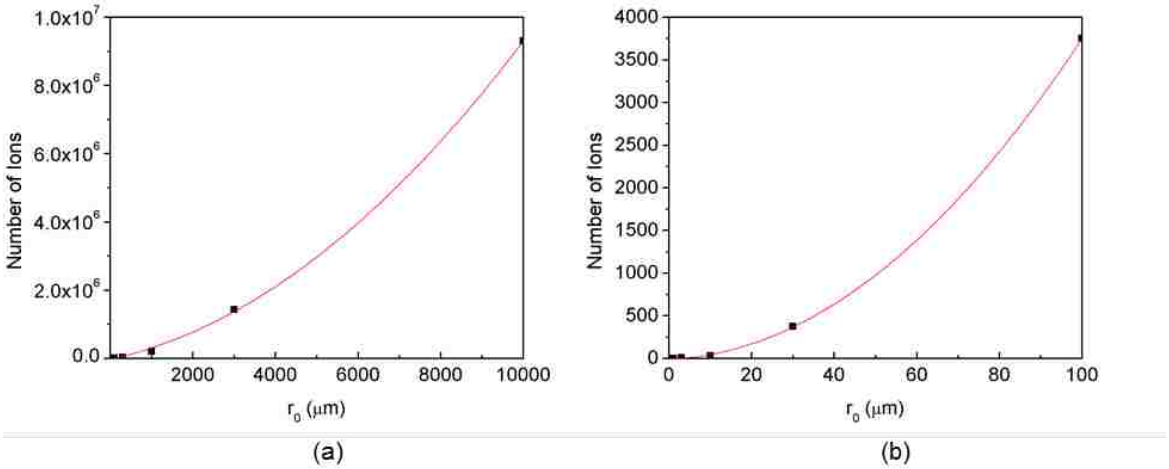

Figure 2-3. The maximum number of analyzable ions as a function of r_0 from (a) 1–10 000 μm and (b) 1–100 μm. Also shown in both graphs is the curve $\mathbf{N = 1.3r_0^{1.70}}$ (r_0 in microns), which is the best fit power function to these data.

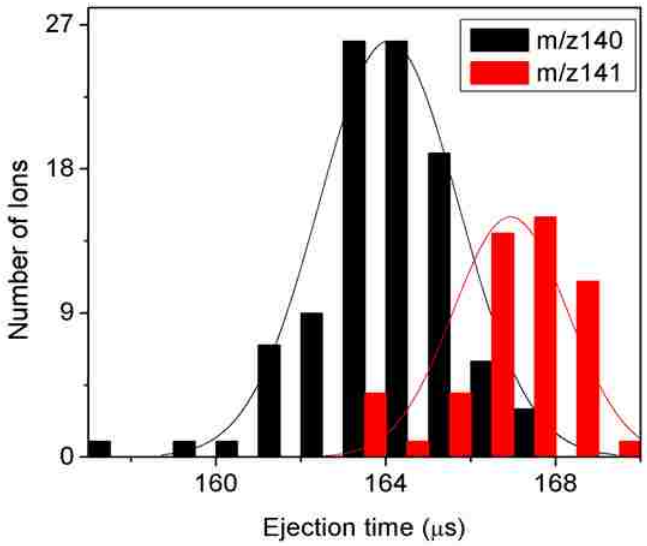

Figure 2-4. Typical simulated mass spectral in a 100-μm trap with a scan rate of 349 000 Th/s. The resolutions for ***m/z*** 140 and ***m/z*** 141 are 103 and 127, respectively.

Figure 2-4 shows typical simulated peaks for ***m/z*** 140 and 141 from simulations of a CIT with r_0 of 0.1mm and a scan rate of 349 000 Th/s. Measured mass resolution for the ***m/z*** 140 peak is 103 (m/Δm).

In these simulations, we have assumed that scan rates scale with the RF frequency, according to the equation given by Pau[7]. Higher RF frequencies will use faster scans in terms of Th/s but not necessarily in V/s due to the smaller voltages used. In these simulations, the ramp rate of the RF amplitude was adjusted for each trap size so that ions experienced the same number of RF cycles prior to ejection. In order to test this, we carried out additional simulations at other ramp rates and observed the expected increase/decrease in resolution for slower/faster ramps. Keeping the number of RF cycles constant for each simulation provides some consistency among these simulations, did not result in significant differences in baseline resolution for different trap sizes and is therefore not expected to significantly affect the results.

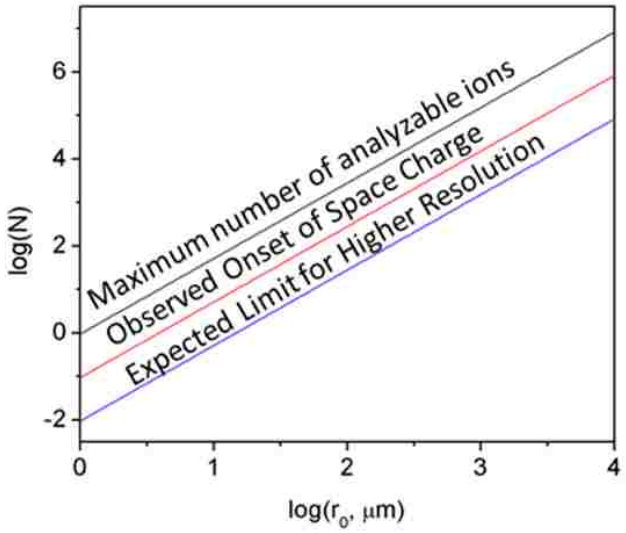

Figure 2-5. A comparison of the maximum number of analyzable ions, observed onset of space charge in simulations and expected limit for higher resolution (100× lower than maximum) in different trap sizes.

The above results represent modest mass resolution and a system with significant space charge. In fact, initial peak broadening was observable at roughly an order of magnitude fewer ions than are shown in Figs 2-2, 2-3. For higher-performance ion traps (or improvements such as resonant

ejection or slower ramp rates), the achievable mass resolution may be significantly higher than what was used in these simulations, and the corresponding trapping limit may be 2 or more orders of magnitude lower than are shown in Figs 2-2, 2-3, according to the observations of Schwartz[9]. However, the scaling relationship is likely to hold. Figure 2-5 summarizes these results, showing the numbers of ions for different levels of performance within the range of CIT sizes studied. At the low end of the size range, these results compare well with the experimental results of Pau et al., who observed that approximately 10 ions could be trapped and analyzed in a CIT with $r_0 = 20$ μm[7].

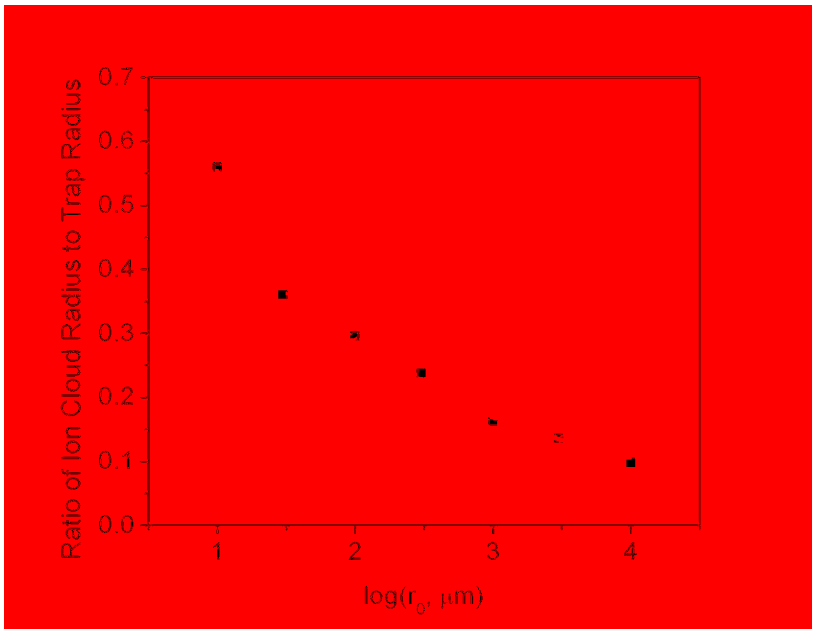

Figure 2-6. Ion cloud size as a function of trap size in the absence of space-charge effects, based on scaling of operating parameters shown in Table 3-3. Cloud size is measured as the maximum excursion of 150 stably trapped ions over 100 RF cycles after reaching equilibrium through collisional cooling. A best fit power function is shown as a visual guide.

In the absence of space-charge effects, the size of the cloud of trapped ions is a function of the pseudopotential well depth, in turn determined by the RF amplitude and the ***a***- and ***q***-stability parameters in Equations 2-2 and 2-3). Because the high voltages used in full-sized ion traps cannot

be used with the small electrode spacings of miniaturized ion traps, the pseudopotential well must necessarily become shallower. As a result, the collisionally cooled ion cloud occupies a larger fraction of the total trap volume. Figure 2-6 shows the equilibrium ion cloud radius as a fraction of r_0 for different sized traps using the voltage/frequency scaling in Table 2-3.

It is apparent that ion cloud size becomes larger relative to the trap size when the trap becomes smaller. At some point, the ion cloud becomes larger than the trap and ions are lost to the electrodes. This process sets a limit on miniaturization ultimately governed by the strength of electric field that can be created in small traps before field emission or electrical breakdown occur. In experiments with micron-sized CITs,[34] field emission was observed at applied potentials in a range of 100 V.

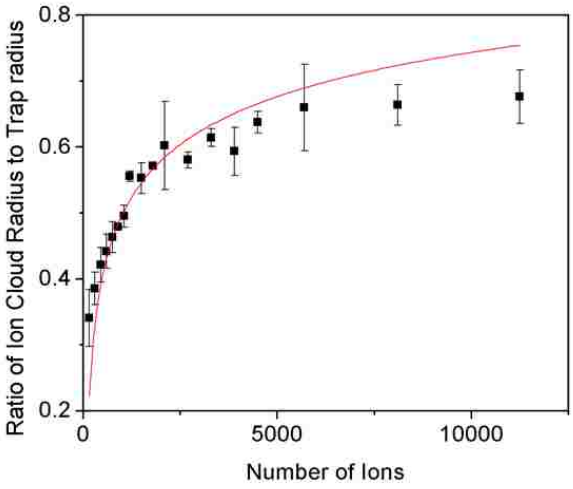

Figure 2-7. Ion cloud size as a fraction of trap size for different ion populations in a 100-μm CIT. A best fit population growth curve is shown as a visual guide.

With large numbers of trapped ions, the ion cloud expands due to the Coulombic force created by the presence of other trapped ions. Simulations explored this process. As shown in Figure 2-7,

the ion cloud size in a 100-micron trap grows rapidly with the ion number below 5000, then the size approaches the maximum gradually. Each data point is the mean value of three trials. The errors are the standard deviations of the three trials. A larger cloud of trapped, collisionally cooled ions, expanded either due to space charge or due to a shallower pseudopotential well, may create difficulties in ejection through a small end-cap aperture and may require redesign of the trap.

Obviously, the development of miniaturized ion traps represented in Table 2-1 does not follow exactly any of the cases in Table 2-2. There is much variety in the literature. But the trends of lower voltage and higher frequency are clearly seen. Electric breakdown in small ion traps is dependent on many factors such as surface preparation, materials, contamination and electrode oxidation. Capacitance and consequent electrical power depend strongly on instrument design.

Having too few ions presents several obvious challenges ranging from accurate isotope ratios to being able to see fragment ions in MS/MS analysis. Increasing the integration or analysis time may improve the situation through averaging, but for some applications, such as using the ion trap to analyze species separated by gas or liquid chromatography, there may not be time for extensive averaging. Options such as mass selective trapping or pre-concentration may prove useful.

The above simulations have assumed that RF trapping occurs at a relatively low RF amplitude and that the RF is ramped as part of the mass scan. Some advantage may be gained by using a fixed RF amplitude all the time and effecting mass-selective ejection by scanning the frequency of the resonant ejection signal. This approach is used in at least one portable MS system, resulting in reduced electrical power[17].

While the capacitance of a single ion trap may represent a negligible load to an RF power supply, an array of traps is a different story. In this case, the capacitance, and hence the power required, scale linearly with the number of arrayed traps – and may even be larger depending on the arrangement of wiring among traps. Similarly, increasing the aspect ratio of a linear or toroidal ion trap may increase ion capacity but comes at the cost of increased power. Here, it must be remembered that the goal of miniaturization is not a smaller trap *per se* but a more portable overall mass spectrometer system, including power supplies. Capacitance is a critical issue in designing any miniaturized ion trap system.

A surprising result of these simulations is that the number of ions does not scale as an integral power of the trapping dimension, as might be expected based solely on volume or size arguments. Several factors contribute to this result, including the necessity that the RF amplitude cannot remain constant as trap size is reduced. In addition, the observation that the ion cloud size does not scale proportionally with the trap size may contribute to the non-integral power relationship between ion number and trap size.

Thorough calculations of space-charge effects in ion traps can be very time consuming, especially for large numbers of ions. The present study has used only a modest number of independent, explicit ions, relying on a charge factor – a computational shortcut – to simulate larger ion populations. For the very small ion traps simulated in this study, explicit ion–ion repulsion among all ions increases the fidelity of the results. For larger ion traps simulated, the space-charge effects are less accurately modeled. As it is the small traps that are of the greatest interest in the question of miniaturization, the shortcut is appropriate. These simulations have also

not explored the possibility of trapping both positively and negatively charged ions simultaneously as a route to reduce space-charge effects and increase the trapping capacity in miniaturized devices.

2.6 Conclusions

All efforts to create very small ion trap mass analyzers face the issue of reduced ion counts and the associated loss in sensitivity. We have shown in simulations that the ion populations scale as the 1.55–1.75 power of the characteristic trapping dimension, r_0, for the CIT for a constant but marginal level of performance. At sizes in the range of 4–20 μm, the space charge caused by more than one ion in a CIT degrades resolution. The simulations above did not examine the space-charge limits in linear or toroidal ion traps, but these likely would offer improvements in trapping capacity at these small scales, as they do at larger size scales. Although performance of ion traps is best at the highest practical frequency and voltage[7], this voltage is limited both by the requirement that portable devices consume little power and also by the maximum voltage that can be supported by small electrodes in close proximity. As a result, the pseudopotential well becomes shallower and the ion cloud occupies a larger proportion of the trap. Ion traps that have an extended trapping dimension, such as rectilinear or toroidal, as well as arrays of traps, can be used to increase the number of trapped ions, but are only useful to the extent that precise dimensions can be maintained throughout the device. Despite these challenges, progress continues to be made on many fronts.

2.7 References

1. Ouyang, Z.; Badman, E. R.; Cooks, R. G., Characterization of a serial array of miniature cylindrical ion trap mass analyzers. *Rapid Commun. Mass Spectrom.* **1999,** *13* (24), 2444-2449.

2. Xu, W.; Li, L.; Zhou, X.; Ouyang, Z., Ion sponge: A 3-dimentional array of quadrupole ion traps for trapping and mass-selectively processing ions in gas phase. *Anal. Chem.* **2014,** *86* (9), 4102-4109.

3. Badman, E. R.; Cooks, R. G., A parallel miniature cylindrical ion trap array. *Anal. Chem.* **2000,** *72* (14), 3291-3297.

4. Lee, W-W.; Oh, C-H.; Kim, P-S.; Song, K., Characteristic of cylindrical ion trap. *Int. J. Mass Spectrom.* **2003,** *230* (1), 25-31.

5. Chaudhary, A.; van Amerom, F.; Short, R.; Bhansali, S., Fabrication and testing of a miniature cylindrical ion trap mass spectrometer constructed from low temperature co-fired ceramics. *Int. J. Mass Spectrom.* **2006,** *251* (1), 32-39.

6. Moxom, J.; Reilly, P. T. A.; Whitten, W. B.; Ramsey, J. M., Double resonance ejection in a micro ion trap mass spectrometer. *Rapid Commun. Mass Spectrom.* **2002,** *16* (8), 755-760.

7. Pau, S.; Pai, C. S.; Low, Y. L.; Moxom, J.; Reilly, P. T. A.; Whitten, W. B.; Ramsey, J. M., Microfabricated Quadrupole Ion Trap for Mass Spectrometer Applications. *Phys. Rev. Lett.* **2006,** *96* (12), 120801.

8. Austin, D. E.; Cruz, D.; Blain, M. G., Simulations of ion trapping in a micrometer-sized cylindrical ion trap. *J. Am. Soc. Mass Spectrom.* **2006,** *17*, 430-441.

9. Schwartz, J. C.; Senko, M. W.; Syka, J. E. P., A two-dimensional quadrupole ion trap mass spectrometer. *J. Am. Soc. Mass Spectrom.* **2002,** *13* (6), 659-669.

10. Brinckerhoff, W. B.; van Amerom, F. H. W.; Danell, R. M.; Pinnick, V.; Arevalo, R.; Atanassova, M.; Hovmand, L.; Mahaffy, P. R.; Cotter, R. J.; team, M., A dual source ion trap mass spectrometer for the Mars Organic Molecule Analyzer on ExoMars 2018. *EPC Abstracts* **2011,** *6*, 1337.

11. Hansen, B. J.; Niemi, R. J.; Hawkins, A. R.; Lammert, S. A.; Austin, D. E., A lithographically patterned discrete planar electrode linear ion trap mass spectrometer. *J. Microelectromech. Syst.* **2013,** *22* (4), 876-883.

12. Chen, H.; Xu, R.; Chen, H.; Cooks, R. G.; Ouyang, Z., Ion/molecule reactions in a miniature RIT mass spectrometer. *J. Mass Spectrom.* **2005,** *40* (11), 1403-1411.

13. Keil, A.; Talaty, N.; Janfelt, C.; Noll, R. J.; Gao, L.; Ouyang, Z.; Cooks, R. G., Ambient mass spectrometry with a handheld mass spectrometer at high pressure. *Anal. Chem.* **2007,** *79* (20), 7734-7739.

14. Wang, L.; Xu, F.; Ding, C., Performance and geometry optimization of the ceramic-based rectilinear ion traps. *Rapid Commun. Mass Spectrom.* **2012,** *26* (17), 2068-2074.

15. Hendricks, P.; Duncan, J.; Noll, R. J.; Ouyang, Z.; Cooks, R. G., Performance of a low voltage ion trap. *Int. J. Mass Spectrom.* **2011,** *305* (2-3), 69-73.

16. Kornienko, O.; Reilly, P. T. A.; Whitten, W. B.; Ramsey, J. M., Micro ion trap mass spectrometry. *Rapid Commun. Mass Spectrom.* **1999,** *13* (1), 50-53.

17. Contreras, J. A.; Murray, J. A.; Tolley, S. E.; Oliphant, J. L.; Tolley, H. D.; Lammert, S. A.; Lee, E. D.; Later, D. W.; Lee, M. L., Hand-portable gas chromatograph-toroidal ion trap mass spectrometer (GC-TMS) for detection of hazardous compounds. *J. Am. Soc. Mass Spectrom.* **2008,** *19* (10), 1425-1434.

18. Londry, F. A.; Alfred, R. L.; March, R. E., Computer simulation of single-ion-trajectories in Paul-type ion traps. *J. Am. Soc. Mass Spectrom.* **1993,** *4* (9), 687-705.

19. Forbes, M. W.; Sharifi, M.; Croley, T.; Lausevic, Z.; March, R. E., Simulation of ion trajectories in a quadrupole ion trap: A comparison of three simulation programs. *J. Mass Spectrom.* **1999,** *34* (12), 1219-1239.

20. Bui, A. H.; Cooks, G. R., Windows version of the ion trap simulation program ITSIM: A powerful heuristic and perdictive tool in ion trap mass spectrometry. *J. Mass Spectrom.* **1998,** *33* (4), 297-304.

21. Manura, D. J.; Dah, D. A., *SIMION 8.0 User Manual*. Scientific Instrument Services, Inc.: Ringoes, NJ, 2008.

22. Mahan, B. H., Collinear collision chemistry: I. A simple model for inelastic and reactive collision dynamics. *J. Chem. Educ.* **1974,** *51* (5), 308.

23. Gilbert, R. G., Collisional energy exchange in highly vibrationally excited molecules: The biased random walk model. *J. Chem. Phys.* **1984,** *80* (11), 5501.

24. He, L.; Lubman, D. M., Simulation of external ion injection, cooling and extraction processes with SIMION 6.0 for the ion trap/reflectron time-of-flight mass spectrometer. *Rapid Commun. Mass Spectrom.* **1997,** *11* (13), 1467-1477.

25. March, R. E.; Todd, J. F. J., Theory of quadrupole instruments. In *Quadrupole Ion Trap Mass Spectrometry*, John Wiley & Sons, Inc.: Hoboken, New Jersey, 2005; Vol. 165, pp 34-72.

26. Cruz, D.; Chang, J. P.; Fico, M.; Guymon, A. J.; Austin, D. E.; Blain, M. G., Design, microfabrication, and analysis of micrometer-sized cylindrical ion trap arrays. *Rev. Sci. Instrum.* **2007,** *78* (1), 015107.

27. Dehmelt, H. G., Radiofrequency spectroscopy of stored ions I: Storage. *Adv. At. and Mol. Phy.* **1967,** *3*, 53-72.

28. Guan, S.; Marshall, A. G., Equilibrium space charge distribution in a quadrupole ion trap. *J. Am. Soc. Mass Spectrom.* **1994,** *5* (2), 64-71.

29. Hager, J. W., A new linear ion trap mass spectrometer. *Rapid Commun. Mass Spectrom.* **2002,** *16* (6), 512-526.

30. Maas, J. D.; Chappell, W. J., RF planar ion trap for chemical sensing in *IEEE MTT-S International*, 2011.

31. Wu, G.; Cooks, R. G.; Ouyang, Z., Geometery optimization for the cylindrical ion trap: Field calculations, simulations and experiments. *Int. J. Mass Spectrom.* **2005,** *241* (2-3), 119-132.

32. Badman, E. R.; Johnson, R. C.; Plass, W. R.; Cooks, R. G., A miniature cylindrical quadrupole ion trap: Simulation and experiment. *Anal. Chem.* **1998,** *70* (23), 4896-4901.

33. Xiong, X.; Xu, W.; Fang, X.; Deng, Y.; Ouyang, Z., Accelerated simulation study of space charge effects in quadrupole ion traps using gpu techniques. *J. Am. Soc. Mass Spectrom.* **2012,** *23* (10), 1799-1801.

34. Cruz, D.; Chang, J. P.; Blain, M. G., Field emission characteristics of a tungsten microelectromechanical system device. *Appl. Phys. Lett.* **2005,** *86* (15), 153502.

3.Two-Plate Ceramic Planar Linear Ion Trap and Its Geometry Deviation

(The simulation work in this chapter is taken from "Wu, Q.; Tian, Y.; Li, A.; Austin, D. E. Simulations of electrode misalignment effects in two-plate linear ion traps. International Journal of Mass Spectrometry. 2015, 393, 52-57". My contributions to this paper are proposing the idea to explore the misalignment problem of two-plate LIT in SIMION and offering the simulation specifications during the experiment. The rest of this chapter are my individual efforts, including constructing the vacuum chamber, designing the first-generation alignment platform, designing the second alignment platform with the help of Dr. Qinghao Wu (a postdoctoral researcher in the Austin group), and conducting the preliminary experiment on the two-plate ceramic LIT.)

3.1 Introduction

As mentioned in Chapter 1, electrodes with hyperbolic inner surfaces are hard to machine with high precision at small scales. Thanks to the prevalence of MEMS techniques, which provide a high precision level far beyond what conventional techniques could reach, miniaturized ion traps and trap arrays especially based on cylindrical traps had great progress in the past two decades [1-16]. Though trap arrays can effectively restore the ion storage volume at micron scale, the requirement on the uniformity among arrayed trap sizes is tighter. This is because, to obtain good resolution, ions with the same mass-to-charge ratio should undergo the same field environment in different traps to be simultaneously detected. On the other hand, assembling the electrodes in a trap array becomes more challenging as trap dimensions are reduced.

Most microfabrication techniques, including MEMS, are in-plane processes that provide high precision and accuracy in two dimensions, but limited capabilities in the third (out-of-plane)

dimension. The relative accuracy of in-plane features is extremely high, whereas out-of-plane features typically suffer from tapering, layer misalignment, undercutting and inconsistent depth. The key to high performance in microfabricated mass analyzers is to leverage the high precision of in-plane features, and reduce or eliminate dependence on out-of-plane fabrication. Our group developed a two-plate technique to microfabricate ion traps. Each of the two plates in the ion trap assembly is lithographically patterned with sets of electrodes that are used to produce a well-defined potential distribution on the surface of each plate. The combination of two plates produces the desired potential distribution in the space between the plates. Complex electric fields with high accuracy can be produced.

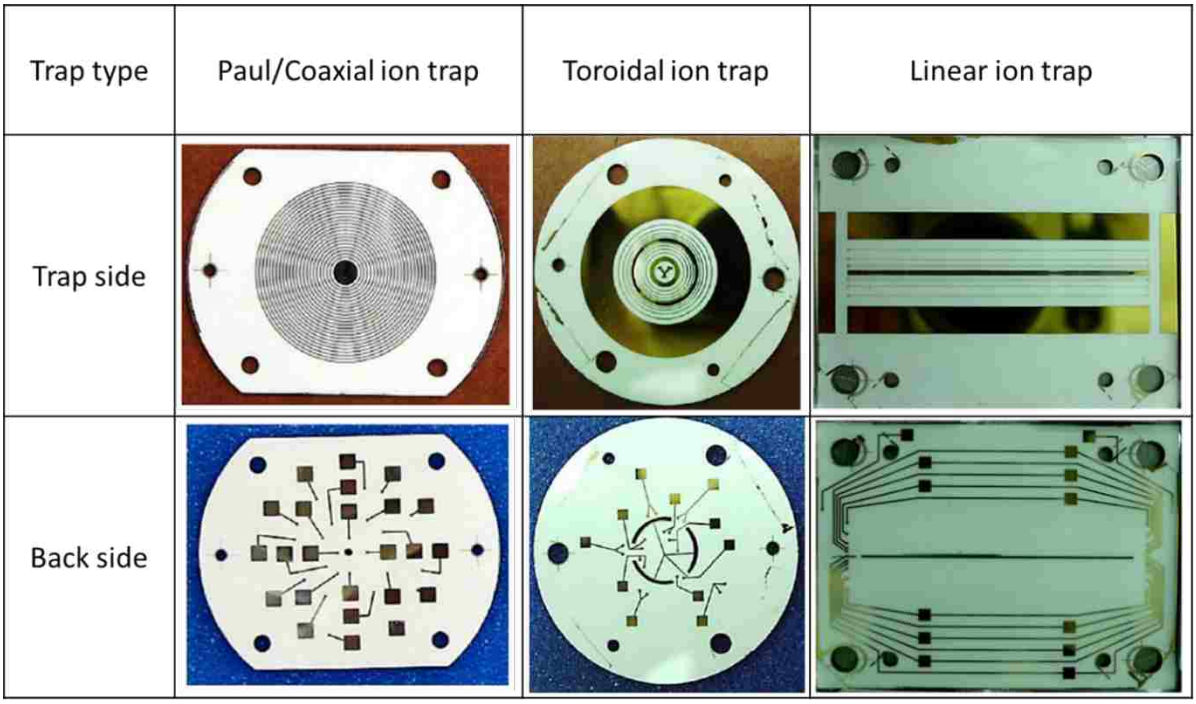

Figure 3-1. The trap and back side view of three different types of ion trap made by two-plate technique, the trap sides are shown without Ge layer. (Adapted from Hansen, B. J. Microfabrication Processes and Innovations in Planar Electrode Ion Traps. Ph.D. Dissertation, Brigham Young University, 2013)

The approach is general: any type of ion trap can be made using two plates with appropriate potential functions on each plate. The accuracy of the electric fields is limited only by the accuracy of 2-D patterning on each plate and the alignment of one plate with respect to the other.

So far, three different types of ion traps by the two-plate technique have been made, including a toroidal ion trap[17], a quadrupole ion trap (Paul trap)[18], a combination of the former two, the coaxial ion trap[19], and a linear ion trap[20]. The photos of these ion traps are seen in Figure 3-1.

3.2 Plate fabrication and experimental results

Plate Fabrication and Ion Trap Assembly

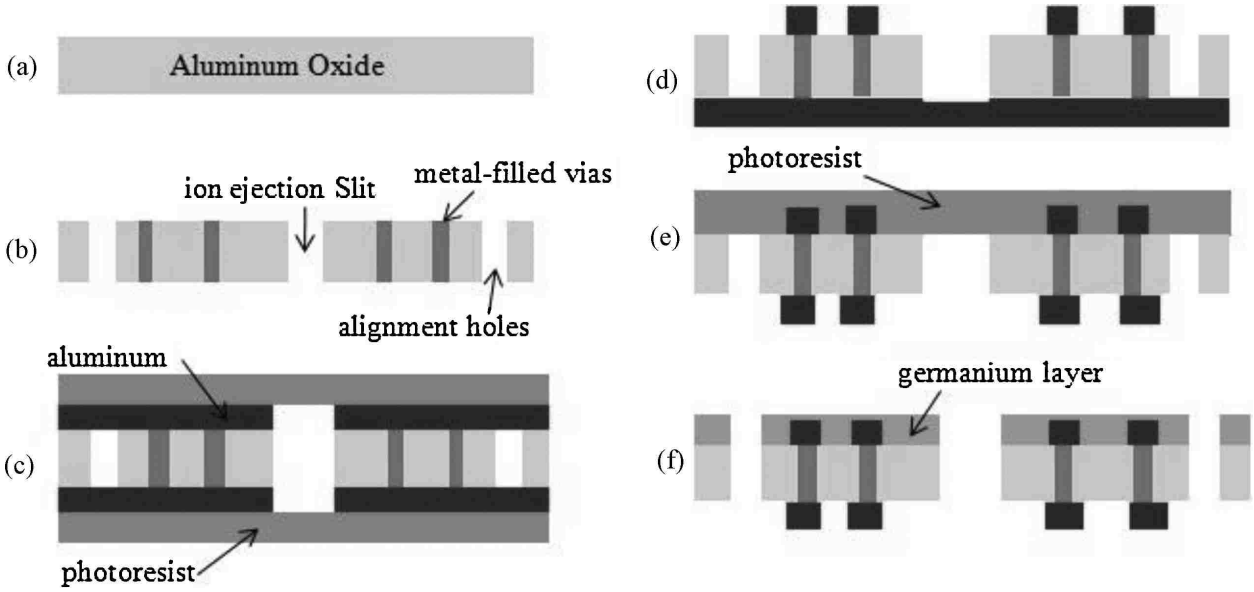

Figure 3-2. Plate fabrication process in linear ion traps. (a) Ceramic plate is polished; (b) ejection slit, mounting and alignment holes are drilled, vias are filled with metal alloy; (c) aluminum layers are deposited on two sides, followed by a layer of photoresist; (d) electrode pattern on the trap side is lithographically etched; (e) photoresist spun on both sides and back side is lithographically etched; (f) Ge layer is deposited on the trap side (From Hansen, B. J.; Niemi, R. J.; Hawkins, A. R.; Lammert, S. A.; Austin, D. E. A lithographyically Patterned Discrete Planar Electrode Linear Ion Trap Mass Spectrometer. *J. Microelectromech. Syst.*, **2013**, 22, 876-883.)

The fabrication work flow is shown in Figure 3-2. First, the aluminum oxide wafers (ceramic plates) were laser-drilled with mounting and/or alignment holes, ejection holes/ejection slits and a series of tiny holes as vias. The vias were filled with gold-tungsten alloys to pass the voltages from the back sides to the trap sides where electrodes would be patterned. Second, the electrode patterns were deposited by photolithography techniques on the trap sides. The back sides were patterned with contact pads and traces connecting the pads to the vias. Third, a thin germanium (Ge) layer at a thickness of 100 nm was evaporatively deposited on top of the electrode patterns on the trap side of each plate. This semi-conductive Ge layer functioned as evenly distributing the potentials across the electrode plane in addition to reducing the charge build-up on the trap side of the ceramic plate.

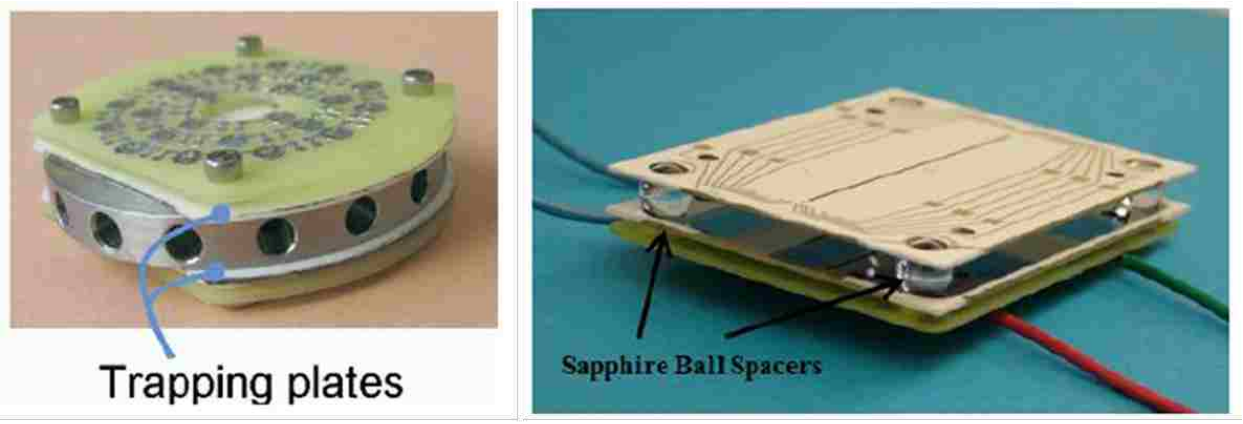

Figure 3-3. (a) Paul/Coaxial Ion trap assembly with metal spacer (From Peng, Y. Novel Ion Trap Made Using Lithographically Patterned Plates. Ph.D. Dissertation, Brigham Young University, 2011); (b) Linear ion trap assembly with sapphire ball spacers (From Hansen, B. J. Microfabrication Processes and Innovations in Planar Electrode Ion Traps. Ph.D. Dissertation, Brigham Young University, 2013.)

Printed circuit boards (PCB) were attached on the back sides of the ceramic plates to conduct the trapping voltages. Each PCB was soldered with capacitors to divide the voltage from the RF

power supply and separately deliver the divided voltage to each electrode ring or line. Spring-loaded pins on the PCBs contacted the patterned pads and conducted the voltages to the ceramic plates. The coaxial ion trap assembly and the linear ion trap assembly with PCBs are shown in Figure 3-3.

Preliminary results with two-plate ion traps

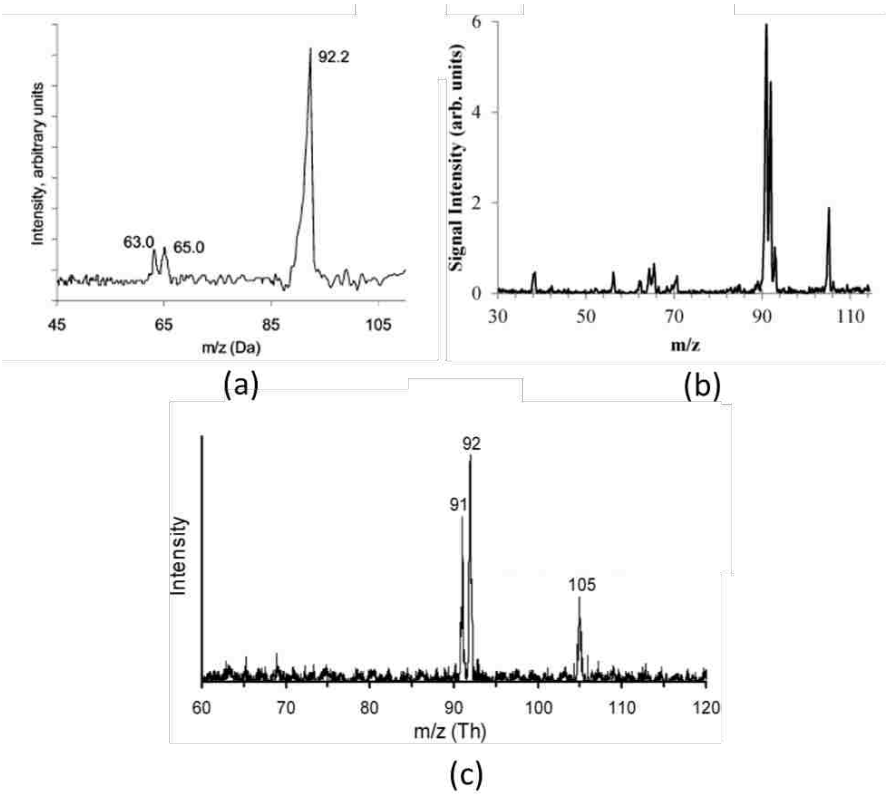

Figure 3-4. Toluene spectra obtained from (a) Halo (Toroidal) ion trap, (Adapted from Austin, D. E.; Wang, M.; Tolley, S. E.; Maas, J. D.; Hawkins, A. R. Halo Ion Trap Mass Spectrometer. *Anal. Chem.*, **2007**, 79(7), 2927-2932.) (b) Linear ion trap (Adapted from Hansen, B. J.; Niemi, R. J.; Hawkins, A. R.; Lammert, S. A.; Austin, D. E. A Lithographically Patterned Discrete Planar Electrode Linear Ion Trap Mass Spectrometer. *J. Microelectromech. Syst.*, **2013**, 22(4), 876-883.) (c) Paul (quadrupole) ion trap (Adapted from Zhang, Z. P.; Peng, Y.; Hansen, B. J.; Miller, I. W.; Wang, M.; Lee, M. L.; Hawkins, A. R.; Austin, D. E. Paul Trap Mass Analyzer Consisting of Opposing Microfabricated Electrode Plates. *Anal. Chem.*, **2009**, 81(13),5241-5248.).

After the electric fields were optimized by independently varying the voltages applied on each electrode ring or line, the toluene spectra obtained from the halo ion trap, the linear ion trap and the Paul ion trap are shown in Figure 3-4. The mass resolution (FWHM) obtained from the halo ion trap was 1.3 Da (Dalton) at a spacing of 4 mm. The linear ion trap showed a FWHM of 0.5-0.6 a.m.u. (atomic mass unit) when the plate spacing was 4.38 mm. The best resolution was obtained from the Paul trap with a FWHM of 0.25 Th (Thompson) when the plates were separated 6 mm apart. This two-plate technique has been demonstrated to work with good performance, and is believed to be a promising method to microfabricate any types of ion traps consisting of only two plates. Among the three types shown above, the two-plate linear ion trap appeared to be the best choice to be miniaturized because of its relatively large ion storage volume at the same trap dimension with 3-D traps[21].

Alignment problems in the two-plate linear ion trap

More recently, the planar linear ion trap plates, with no physical changes, can be moved closer together and function properly as a LIT simply by adjusting the RF voltages applied to each electrode, with a plate spacing of 1.9 mm (y_0 = 0.95 mm)[22]. Results of this experiment are shown in Figure 3-5. Note that the plate design (slit width, location of electrodes) was far from optimal for such a small spacing, but the flexibility in using patterned electrodes with independently-controlled RF allowed this trap to work at an acceptable level. However, at the small spacing, the trap performance was quite different when the plates were disassembled and reassembled, even with the two plates mounted in the same orientation. In addition, the signal intensity varied widely simply by repositioning the plates. In contrast, the 3-D planar Paul trap did not show this behavior.

Resolution in ion traps strongly depends on the precision of the electric field used to separate ions. A decrease in the plate spacing equals a decrease in the ion trap's physical dimension, resulting in a decrease in the alignment accuracy and the field accuracy. A similar problem was reported that resolution was reduced in miniaturized and microfabricated traps and mass filters[23]. Although absolute errors often decrease with smaller fabrication methods, relative errors always increase since fabrication/alignment errors often do not proportionally vary with trap dimensions. In a linear ion trap, if the trap dimension y_0 (equal to r_0) varies over the length of the trapping region, a different mass is selected at one end vs. the other end of the analyzer at any given time. Schwartz[24] suggested that 2-D linear ion traps could be more sensitive to the geometry deviation than 3-D quadrupole ion traps. The alignment in this experiment was realized by the four pre-drilled alignment holes and four precision sapphire balls. To a lesser extent with the full-size planar LIT, that precise alignment was very hard to achieve.

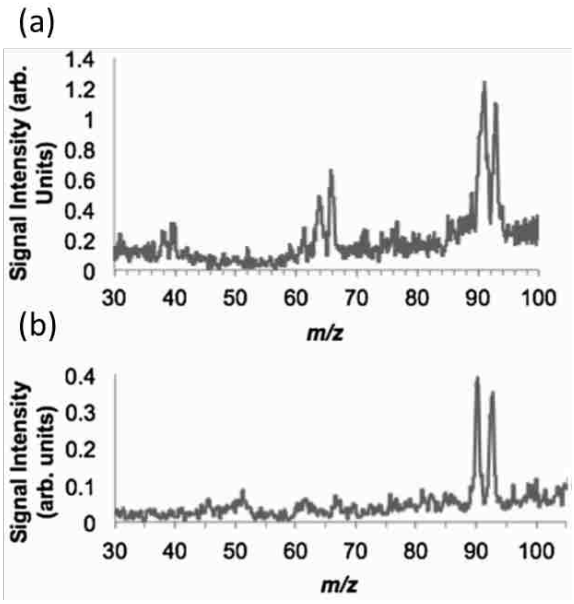

Figure 3-5. Spectra of toluene obtained from the same LIT assembly at a plate spacing of 1.9 mm. (a) and (b) were obtained from two different trials, experimental conditions are the same except plates were disassembled and reassembled.

Electrode alignment could be a serious problem in small 2-D ion traps, but no reports have been found experimentally studying this problem. The following sections focus on studying how the performances of the two-plate planar LIT vary with geometry deviations in simulations and discuss some of the preliminary results obtained by deviating the geometry of the full-size two-plate ceramic LIT in experiments.

3.3 Geometry deviation of two-plate linear ion trap

Degrees of freedom

Unique to two-plate ion traps, and key to this whole approach, is the ability to precisely align the plates relative to each other. With one plate fixed, positioning of the other plate involves only six degrees of freedom (DOF). Table 1 illustrates the different modes of alignment, symptoms of misalignment in each direction, and the approach that can be used to adjust alignment in each direction based on observed signals. Some of these involve shifting the mean location of the ions within the trap by varying the DC axial trapping potentials. This approach was demonstrated[24] on a commercial LIT for observing—but not correcting—misalignment in the electrode rods. Correcting misalignment using this approach can only be done using the two-plate ion traps described above. All other ion traps involve more than two independently movable pieces, and have far too many degrees of freedom for this type of positioning to work. For instance, the CIT and RIT have 12 and 30 degrees of freedom, respectively.

As shown in Table 3-1, the pitch and yaw of the top plate relative to the fixed bottom plate are the most critical to good performance, but are also not difficult to correct. Under these two types of misalignment, ions in different regions of the trap see different electric fields. The signals of

ions ejected from different regions of the trap indicate the type of correction to be made and also inform when these two misalignments are corrected.

Table 3-1. Summary of degrees of freedom on two-plate linear ion trap and proposed strategy.

Degrees of freedom	Types of misalignment	Importance to performance	Symptoms of misalignment	Diagnostic used to correct alignment
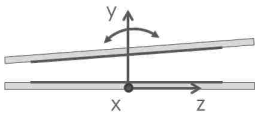	Pitch	High	Measured mass varies along length of trap, resulting in poor resolution	Making voltage on endbars different on two sides pushes ions to one side, shows mass shift; adjust until shift disappears
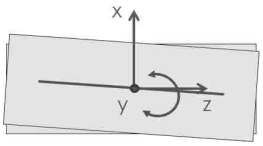	Yaw	High	Resolution and ejection efficiency varies along length of trap, will be optimal at one point	Increasing voltage on endbars together will improve resolution
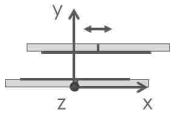	x-displacement	Intermediate	Ion motion will couple in non-ejection direction, leading to reduced signal	Correct before yaw by increasing the potential on the endbars
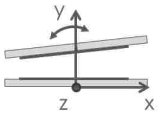	Roll	Intermediate	Possibly ion losses during ejection	Add small CITs on each side of the LIT and see ejected ***m/z***
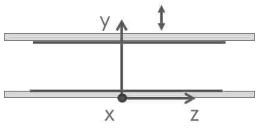	y-displacement	Intermediate	Mass resolution reduced uniformly but gradually	Adjust after all of the above to optimize resolution, mass accuracy
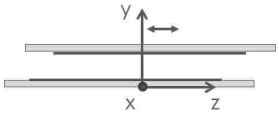	z-displacement	Low	Possible effect on ions towards the ends; no effect in center	After all other degrees of freedom are optimized, can explore this displacement and observe effect, if any

Displacement in the x-direction affects all ions equally, and will lead to reduced ion ejection, but can be corrected with yaw correction. Roll is the most difficult to observe and correct. One option is to include small CITs on the wings of the plates. The signal from these CITs can be compared to make sure that roll is minimized. Alternatively, roll can simply be varied over a wide

range and changes in the signal such as intensity—if an effect is observed, the optimal position can be found after alignment of pitch, yaw, and x-displacement.

Displacement in the y-direction is equivalent to the "electrode stretching" that is commonly done to optimize all other types of ion traps. After the other misalignments are fixed, the plate spacing can be optimized for best mass resolution and accuracy. Finally, it is not known what effects, if any, will be caused by displacement in the z-direction, but it will be easily explored in the experiment. This alignment work may also provide important insight to the tolerances needed for fabrication and assembly of conventional LITs.

Simulation on the misalignment of the two-plate LIT

Simulations might be a good way to verify our predictions on different DOFs before experimental explorations. This section (the remainder of 3.3) was largely taken from Dr. Qinghao Wu's results[25] when he worked in our group.

A model based on the dimension of the full-size ceramic LIT was built in SIMION 8.1, as shown in Figure 3-6. GEM file was used to precisely position the electrodes. The geometric specification of each electrode line and the RF ratio are shown in Table 3-2. Note a Ge layer was also simulated by using a fast-proportional array technique, which inserted many narrow electrode lines in between each two electrodes. Each narrow electrode line was defined to carry a fraction of the RF amplitude difference between the two patterned electrodes so that a smooth voltage gradient was formed. The Ge layer simulated in this way not only allowed fast refining the potential array without taking too much memory, but also enabled the time-varying RF signal to be picked up by every new inserted electrode during the simulation. The #0 electrode surrounded

the 500 μm wide ejection slit. The rest of the electrodes were symmetrically distributed relative to the central ejection slit and were numbered from the slit to the outside rim. The #1 electrode pair were grounded. The #2 and the #3 electrodes were applied with the same fractions of the RF amplitudes. The #4 and the #5 electrodes were applied with the full RF amplitudes.

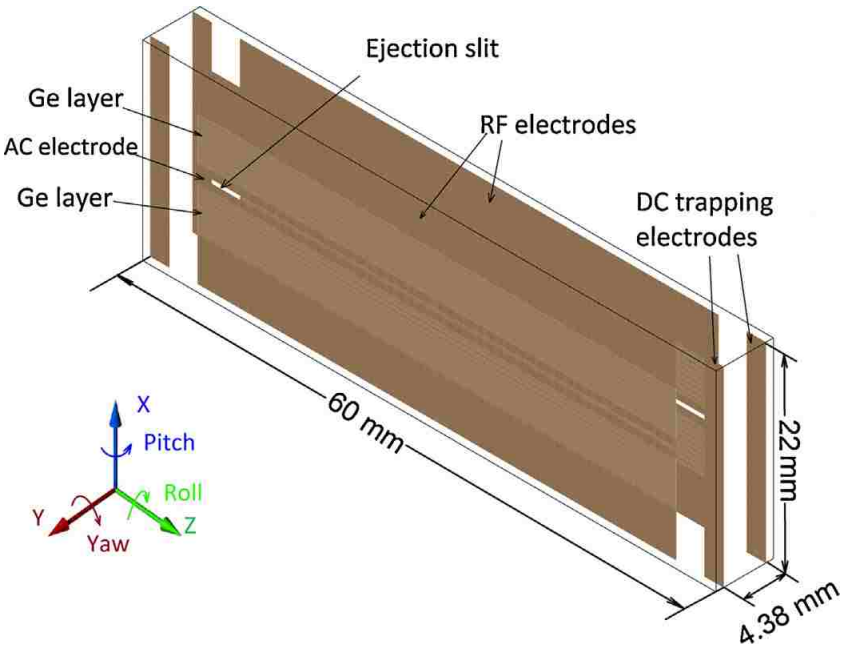

Figure 3-6. Simulation model of two-plate ceramic LIT built in SIMION 8.1. (Adapted from Wu, Q.; Tian, Y.; Li, A.; Austin, D. E. Simulations of electrode misalignment effects in two-plate linear ion traps. *Int. J. Mass Spectrom.* **2015**, 393, 52-57.)

Table 3-2. Geometric parameters and the divided voltage ratio for each electrode line in the two-plate ceramic LIT.

Electrode Line Number	Electrode Line Width/ μm	Distance from slit center to line center / mm	Ratio as a fraction of the full driving amplitude
#0	25	0.0125	0
#1	25	0.91	0
#2	25	1.26	0.1
#3	25	2.19	0.298
#4	25	3.79	1
#5	4500	8.25	1

The simulation process was controlled through user programs where operating parameters were adjusted. Ions at ***m/z*** 150 were created at random positions within a volume and with random initial directions. The initial energy was 0.04 eV. A 2 MHz RF signal was used as the driving frequency. The trapping voltage was 600 $V_{0\text{-}p}$. The scan rate was 26.7 Th/s. Since factors affecting the trap performance involved in boundary ejection are less than that involved in resonance ejection, the results obtained in boundary ejection could be closer to the impact from the geometry defect alone could have on the trap performance. In the simulation, no resonance AC signal was applied. Trapped ions were collisionally cooled down using the hard-sphere collision model from SIMION 8.1 installation package. The collisional gas was He. The pressure used was 0.5 Pa (3.7 mTorr). Each run simulated 2000 ions, but only ions that passed through the slit were counted and recorded. In this section, the resolving power refers to $m/\Delta m$, in which Δm is FWHM, and was used to evaluate the variation of the trap performances. In the simulation, each DOF was independently studied. In other words, each time only one DOF was varied with all the other DOFs kept at the arbitrary zero positions.

The simulation results are shown in Figure 3-7. Note the original coordinates in right (a) and right (b) for the displacements along y-axis correspond to the spacing 4.38 mm. The zero positions in other five DOFs mean that plates were perfectly aligned. In the angular deviations, an abrupt drop in resolving power within only 0.3° of deviation in pitch can be seen in left (a). This matched the prediction in Table 3-1 that pitch is of great importance to the performances of 2-D ion traps. The biggest impactor in the translation deviations seemed to be the plate spacing (y-displacement). Deviation from the optimal spacing within 0.5 mm in either directions would reduce the highest resolving power the trap could reach. However, the optimal spacing depended on the potential

distributions on the trapping side of the plates. On the other hand, the impacts of the ion detection efficiency or the signal intensity from plate spacing and x-displacement seemed to be more obvious than from the three angular deviations. Roll and z-displacement appeared to be the least two important factors, as neither the resolving power nor the ion detection efficiency changed.

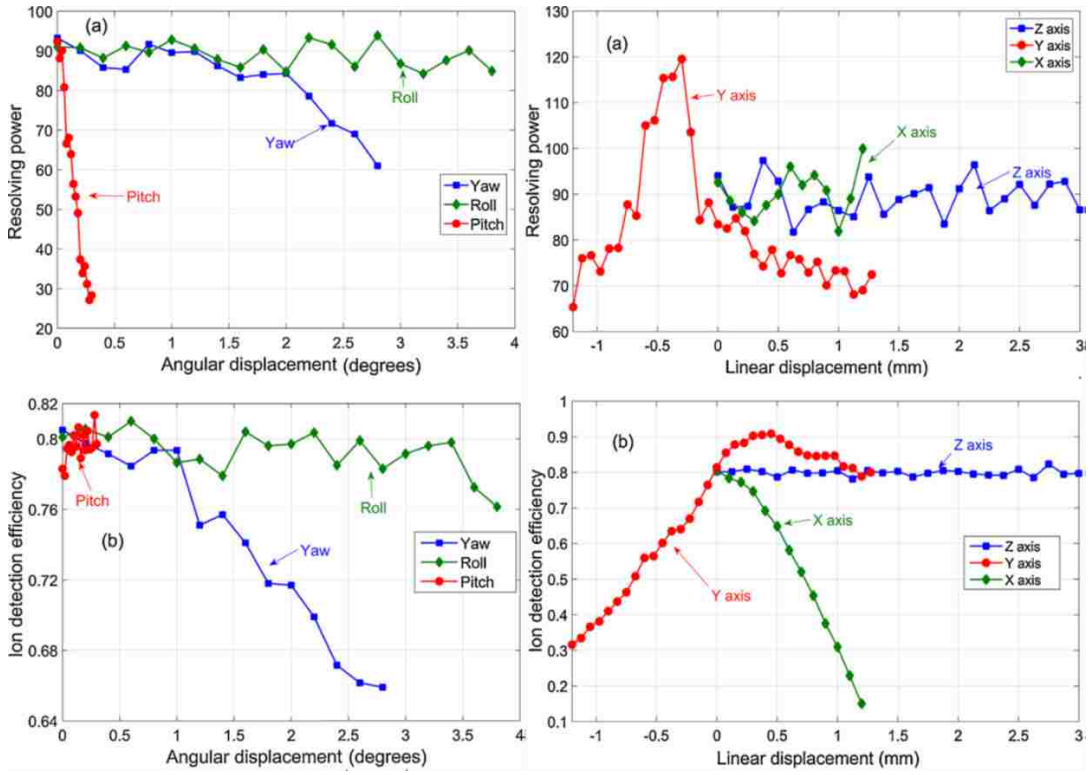

Figure 3-7. Left (a): Variation of resolving power with three angular deviations; Right (a): Variation of resolving power with three translation deviations; Left (b): Variation of Ion detection efficiency with three angular deviations; Right (b): Variation of Ion detection efficiency with three translation deviations. (Adapted from Wu, Q.; Tian, Y.; Li, A.; Austin, D. E. Simulations of electrode misalignment effects in two-plate linear ion traps. *Int. J. Mass Spectrom.* **2015**, 393, 52-57.)

In general, the order of the importance to the trap performance of the six degrees of freedom in the simulation should be: pitch and y-displacement > yaw and x-displacement > roll and z-displacement.

The quadrupole and the components of some of the higher order fields at different plate spacings are shown in Table 3-3.

Table 3-3. Components of the higher order fields at different plate spacings. The components at the plate spacing of 4.38 mm without Ge layer was taken as a comparison. (Adapted from Wu, Q.; Tian, T.; Li, A.; Austin, D. E. Simulations of electrode misalignment effects in two-plate linear ion traps. *Int. J. Mass Spectrom.* **2015**, 393, 52-57.)

Plate spacing (mm)	Geometry					
	Quadrupole	Octapole		Dodecapole		(A4+A6)/A2 (%)
	A2	A4	A4/A2 (%)	A6	A6/A2 (%)	
3.48	−57.97	1.013	−1.747	−9.604	16.57	14.82
3.78	−55.09	0.6781	−1.231	−7.583	13.77	12.53
4.08	−52.10	0.395	−0.7581	−5.777	11.09	10.33
4.38	−49.10	0.1474	−0.3002	−4.246	8.647	8.347
4.68	−46.14	-0.0409	0.0886	−3.109	6.738	6.826
4.38	−46.02	-1.161	2.524	0.2707	−0.5882	1.936

It was reported that in cylindrical ion traps, performance could be best when the sum of the octapole and dodecapole components equals –10% of the quadrupole components[26]. This was known as the "–10% compensation rule". However, in this LIT model, the best performance was achieved when the sum of the octapole and dodecapole components was +10.33%. The simulation results matched the result from the planar Paul trap[27] that the best performance was reached when the octapole and dodecapole components are 0% and +8%, respectively. It is possible two-plate planar ion traps behaved differently from other conventional ion traps.

3.4 Preliminary experimental results

Alignment requires a positioning system capable of both mechanical (coarse) and piezoelectric (fine) movement in each of 6 degrees of freedom. It is an ideal choice to purchase a six-stage positioner that integrates the movements of six DOFs on a single platform. Considering the cost of a six-stage positioner and the fact that some of the DOFs are less important to the trap

performances, it is more applicable to start from the DOF that is predicted to be of greatest importance—for example, pitch and y-displacement (plate spacing).

Alignment platform

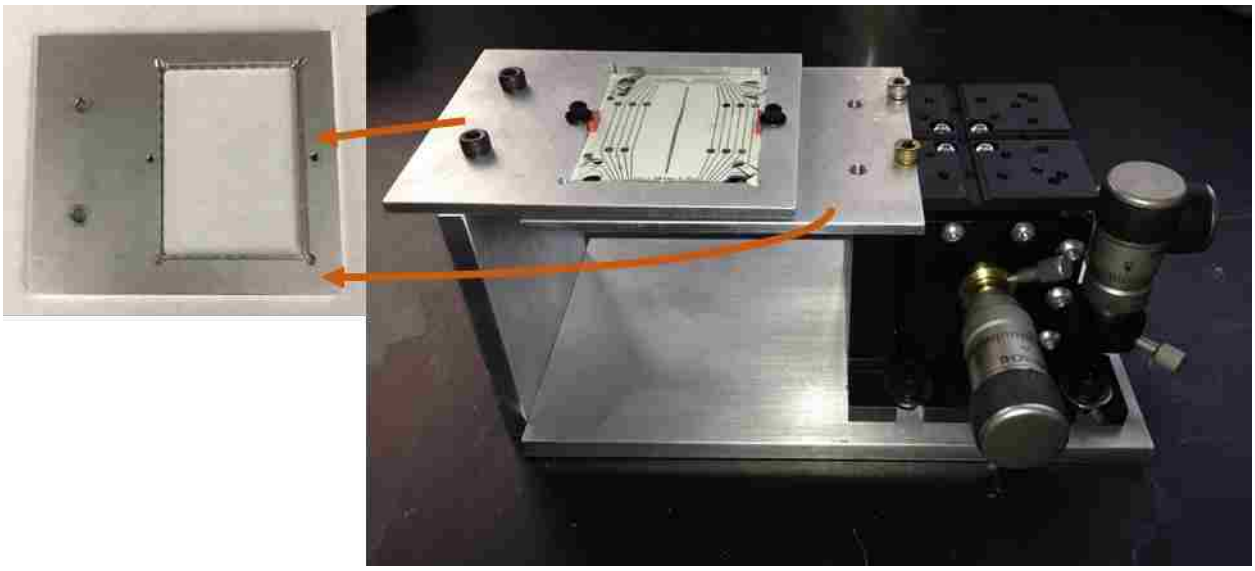

Figure 3-8. First design of the alignment platform. Picture shown on the left is the top/bottom plate holder. This assembly can be manually adjusted in X, Y and Z directions.

The first assembly used screws, nuts, and sapphire balls to mount and align the two plates. In the study of alignment, however, those mounting parts couldn't be used any more as the position of one plate relative to the other should be freely movable. The critical question is how to bring the two plates close enough to each other and align them well by freely moving one of the plate in pitch or y-translation. The solution to solve the free movement issue was to use plate holders. The first alignment platform design is shown in Figure 3-8.

The plate holders were aluminum plates that were machined with slots having the same dimensions as the ceramic plates. The central areas of the slots were made all the way through the plate while leaving narrow edges on four sides of the slots at a thickness of 0.001″. This way the

top plate was held in the slot but was still able to be close enough to the bottom plate. The top plate holder was fixed on a 'leg' support. The bottom plate holder was fixed onto a manual stage that could move in X, Y and Z directions. In this platform, the alignment was changed when the position of the bottom plate was varied by manually adjusting the xyz-stage. An obvious shortcoming of this design is cantilever tilts were inevitable, because both the plate holders were fixed on one side and entirely suspended on the other side. This would affect the alignment accuracy.

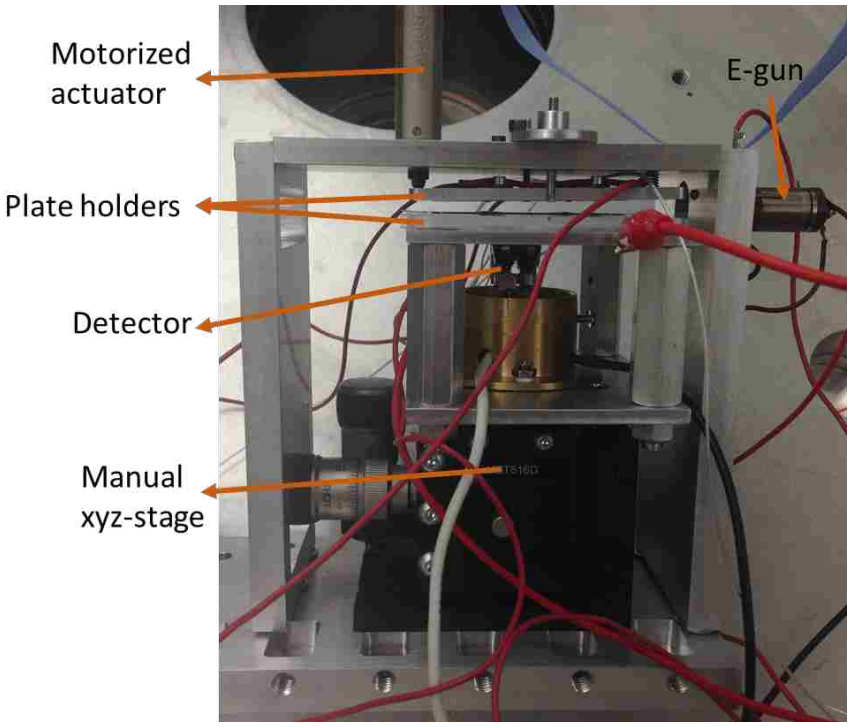

Figure 3-9. The second generation of alignment platform. In this design, pitch could be finely adjusted in vacuum, x-, y- and z- displacements were controlled by manual xyz-stage.

The next generation of the alignment platform is as shown in Figure 3-9. This time the plate holders were made only a little bit larger than the ceramic plates and the PCBs (see Figure 3-10). Two small mounting holes were drilled on two long sides of each plate holder. A top metal piece was supported by two leg supports which were immobilized on a base piece. Two screws were

fixed on the top piece. Each screw had a tiny stainless-steel rod on one end. These tiny rods were inserted into the small mounting holes on the top plate holder to suspended it as well as functioning as the pivots of the movement in pitch. A one-dimensional motorized actuator that could stretch out or retract stood on one short side. A spring was embedded on the opposite side to counterbalance the pressure exerted by the actuator. The bottom plate was immobilzed on a manual xys-stage. A detector was mounted between the stage and the bottom plate by a copper shield.

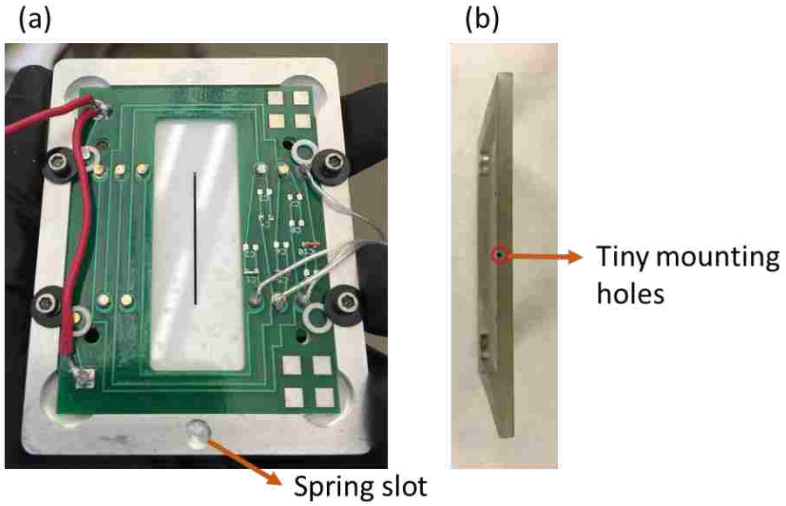

Figure 3-10. (a) Front view of the new plate holder loaded with ceramic plates and PCB; (b) Side view of the new plate holder.

Though the precision sapphire balls (Swiss Jewel Company) cannot be used in the experiment as the movements of the two plates should be independent from each other, they might be used for pre-aligning the plates rather than aimlessly searching for the optimal position by moving the two plates in a big range in vacuum. The process is that first, the top plate was hung onto the top piece but could freely swing in pitch. The bottom plate was loosely placed on a plate adaptor supported by the four posts. Second, the two plates were separated a little bit larger than the ball size by adjusting the manual stage so that the four balls could be placed inside the alignment holes on the

bottom plate. Third, the bottom plate was brought towards the top plate by the xyz-stage until the four balls seat into the alignment holes on the top plate. Fourth, the DOF in pitch on the top plate was immobilized by holding one side with the motorized actuator and inserting a spring on the other side. The bottom plate's position was also immobilized by sticking it onto the bottom plate adaptor with tape. Fifth, the plates were separated apart again to remove the balls from the alignment holes. And lastly, the plates were brought together again until the spacing reached the point spaced by the balls.

Experimental conditions

Since the alignment platform took up a large space, a large vacuum chamber was required. A big cylindrical chamber (cylindrical chamber made from 304 stainless steel with 8 feedthrough collars, Kurt J. Lesker) was used in this experiment. Two aluminum lids (O-ring grooved flanges) were placed on top and bottom to seal the chamber. A turbo pump (TPM 361, Leybold Vacuum) was attached on the bottom lid and was used as the secondary pump. The vacuum connections are shown in Figure 3-11. The detector used was Model XP-2200 from DeTech (Detector Technology, Inc.). The ionization source was an E-gun from Torion (Perkin Elmer, American Fork, UT). The RF power supply was a Model PSRF-100 (Ardara Technologies L.P.) with a built-in frequency of 1.6 MHz. Both the RF arbitrary waveform and the AC signal were created by DS345 30 MHz synthesized function generators (SRS, Stanford Research Systems). The detected signals were sent to a pre-amplifier (Keithley 427 Current Amplifier) at a gain of 10^6, and were then sent to an oscilloscope (LeCroy, WaveSurfer, 42 Xs, 400 MHz, 2.5 GS/s) for analysis. Data were recorded and analyzed in MATLAB.

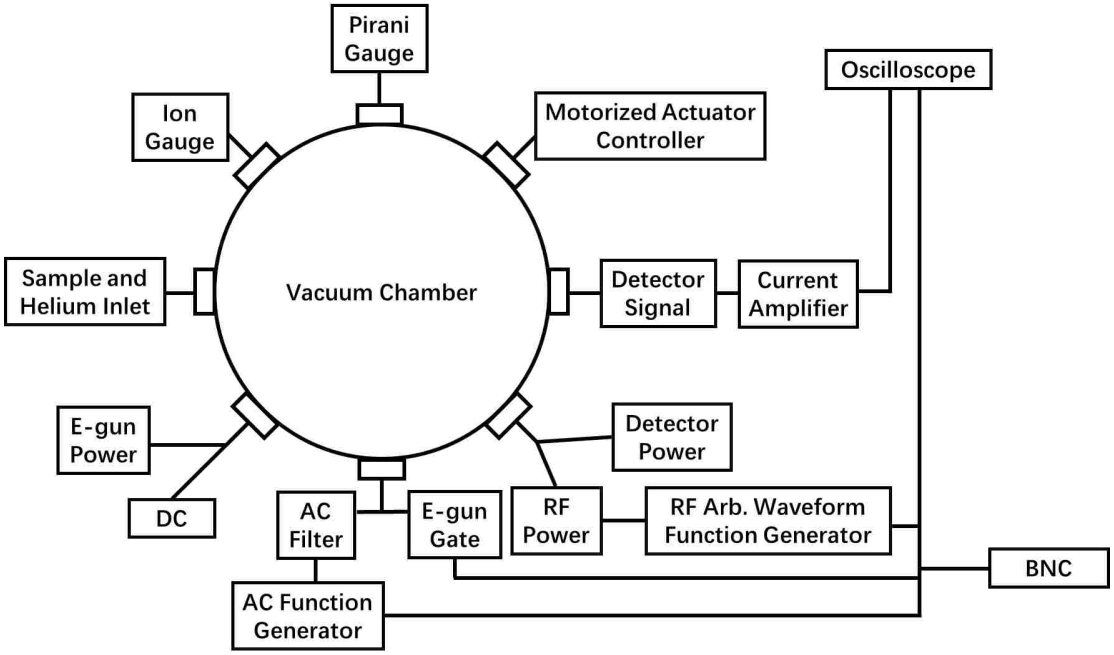

Figure 3-11. Setup of the vacuum and electronic system.

Samples were loaded in a two-inch long glass tube with a 4.4 mm inner diameter. A PTFE cone surrounded the outlet of the sample tube for the seal between the glass-based sample tube and a stainless-steel based leak valve (203 variable leak, Granville Phillips, Boulder, Colorado). When the background pressure in the chamber reached 5×10^{-6} Torr, samples were introduced in vacuum by slowly opening the leak valve until the pressure was stable at around 5×10^{-5} Torr. Helium valve was then opened to raise the final pressure to 1.5×10^{-3} Torr.

The timing control of the electronic system is shown in Figure 3-12. A BNC (Model 565, Pulse/Delay Generator) was used to trigger the function generator, which was used to create the RF arbitrary waveform. The RF arbitrary waveform was then delivered to a high frequency oscillator (RF power supply) and directed its amplitude output. A filter was connected between the AC function generator and the ion trap assembly to prevent feedback of the high RF voltage to the AC function generator. The RF signal and the E-gun gate (GRX-1.5K-B, DEI, Directed Energy,

Inc.) as well as the oscilloscope were simultaneously triggered in each cycle while there was some delay added to the AC channel.

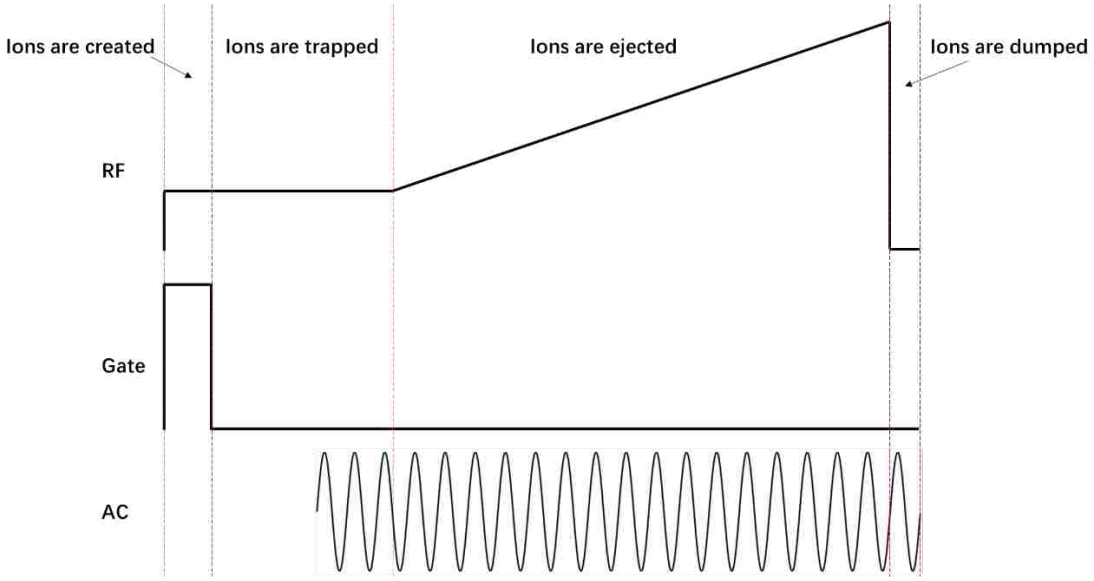

Figure 3-12. Timing control of the electronic system.

Results and discussion

It was necessary to test whether the plates still worked and find out perhaps new operating conditions for two reasons: it had been a long time since the last time the plates were used and the vacuum conditions were completely changed; the optimized voltage ratio for each electrode shown in Table 3-2 were under a 2.3 MHz trapping frequency, whereas the RF power supply used in the following experiment would be 1.6 MHz. Before conducting any experiments on the new alignment platform, the two plates should be assembled on the old platform that incorporated screws, nuts and alignment balls. Voltage ratio on the #2 and #3 electrodes were re-optimized under the new operating conditions in SIMION 8.1 using the model in Figure 3-6. The spacing was still 4.38 mm.

In Figure 3-13 (a), the resolving power referred to m/Δm. In Figure 3-13 (b), the total number of ions simulated was 1000. Considering the results from both the resolving power and the detected ion number, the best performances were achieved when the #2 and the #3 electrodes were both 0.14. The previous operating point (E2 = 0.1, E3 = 0.298), however, fell in the range where the resolving power was much lower though the number of ions detected was a bit higher. To ensure the ion trap was operated at the best condition, the new voltage ratios (E2 = 0.14, E3 = 0.14) were used in the following experiments. The voltage ratios on all the other electrodes were the same as before.

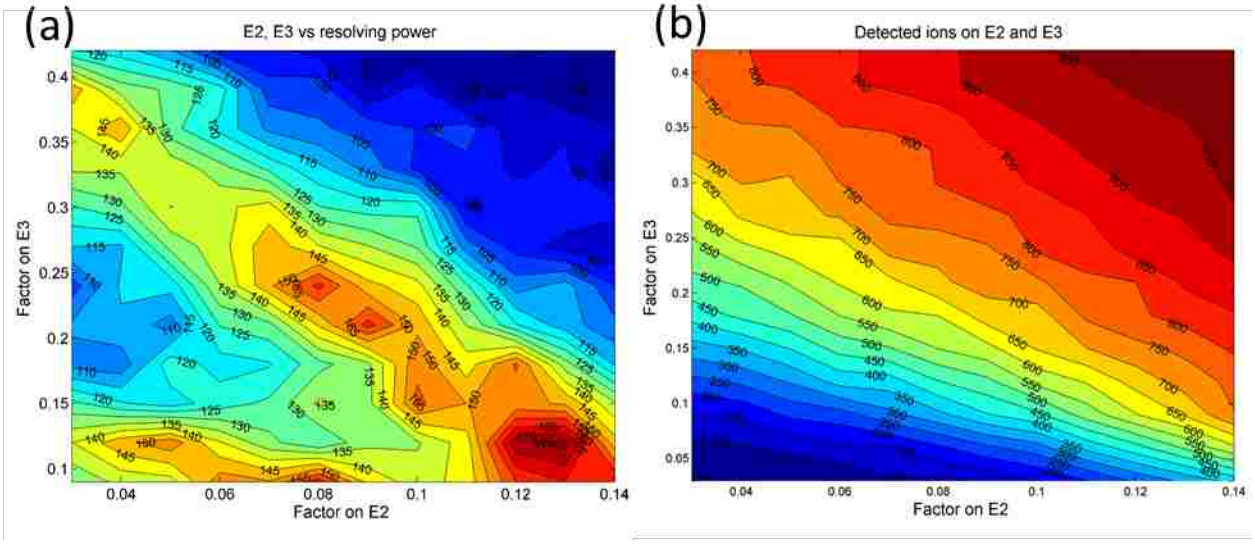

Figure 3-13. (a) The contour view of the resolving power vs. the voltage ratio on the #2 and the #3 electrodes; (b) the contour view of the number of ions detected vs. the voltage ratio on the #2 and the #3 electrodes.

It was unexpected to see that the spectra obtained either by scanning the AC frequency at a constant trapping voltage or by scanning the RF amplitude at a constant AC frequency were not as good as before. Figure 3-14 shows a best spectrum of toluene obtained by scanning the RF amplitude from 275 $V_{0\text{-}p}$ to 825 $V_{0\text{-}p}$ at the constant AC resonant frequency 1700 KHz. The first peak appearing in the 91/92 Th position was likely to come from a mixture of toluene molecular

ions and the ions rearranged in their structures. The second peak showing up around 105 Th could be a mixture of the productions of ion-molecule reactions.

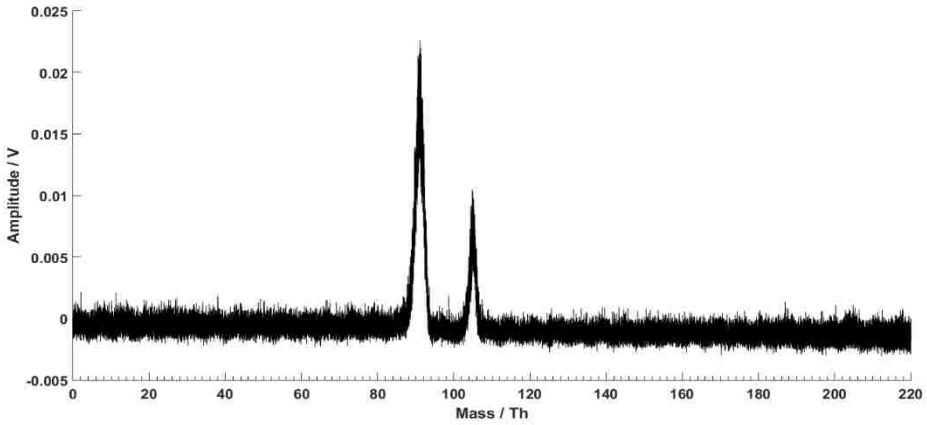

Figure 3-14. Toluene spectrum obtained from the ceramic LIT on the old mounting platform under optimized operating parameters.

One important factor was the alignment of the e-gun and the detector relative to the ion trap assembly. It seemed their alignments were of importance to the signal intensity and should be taken care of in the new alignment assembly.

Next, the ion trap plates were transferred from the old assembly to the new alignment platform. Operating parameters, including the RF trapping voltage, the AC frequency and the plate spacing were all kept the same. Figure 3-15 is a series of mass spectra obtained from toluene by varying the top plate's angular deviation in pitch. The initial position, which was determined by the sapphire balls, was arbitrarily taken as 0°. The misalignment in pitch was varied by the motorized actuator, and by calculating from its travel distance, the variation of pitch in angle was from −1.27° to +3.18° at a step size of 0.6°. The positive and the negative symbols indicated that the actuator was in the process of stretching and retracting, respectively.

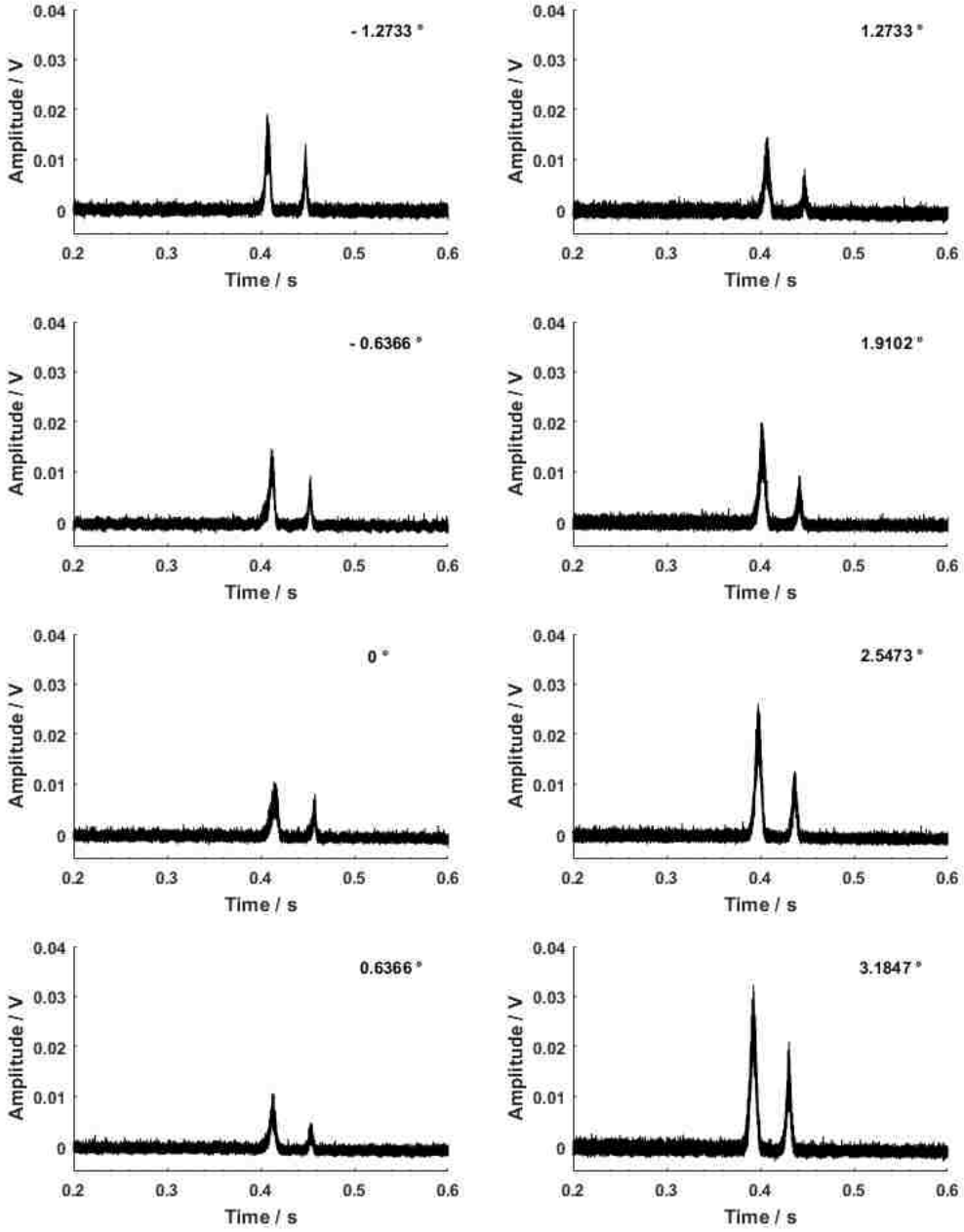

Figure 3-15. Comparison of toluene spectra from different pitch angles.

One of the most obvious variations among these spectra was peak positions. The two peaks shifted backward from −1.27° to 0°, and gradually shifted forward from 0° to +3.18°. Theoretically, peak positions wouldn't change unless the trapping amplitude changed. In this case, the phenomenon that resembled the results of variation of the trapping amplitude was likely to be the

outcome of a slight change in an average plate spacing during the variation process in pitch. This can be inferred from Equation 1-2 that the ejecting voltage V will vary with the trap dimension parameter r_0 (y_0 in 2-D LIT) if the value of the stability parameter q has reached an ejection point. One possible reason why the pitch variation was accompanied with a variation in the average plate spacing was the deviated positions of the tiny mounting holes (the pivot) from the exact middle point on the long side of the plate holders.

Another prominent phenomenon was the variation in peak intensity. It appeared the two peaks were both stronger on the positive end and the negative end than at the arbitrary zero position. An explanation for that could be the relative position of the e-gun to the trap region: as the average height of the top plate varied while the e-gun was immobilized on one of the side supports, the relative elevation to the plate spacing the electrons were shot at varied and would be closer to the trapping center at the large plate spacings than at the small spacings. In the large spacings, more electrons would collide with molecules instead of being lost to the plates.

It was expected that there was little variation in the resolution; even the pitch angle had been deviated by 3°, though the resolution (resolving power) from the simulation results in Figure 3-7 for the deviation in pitch showed an abrupt change within 0.5°. The main problem with these spectra was the poor resolution. There seemed to be two mass peaks, but unfortunately the two peaks were the mixtures of several mass peaks rather than any peaks with a single mass. According to the prediction in Table 3-1 and the discussion in the simulation results, Y-displacement seemed to be another DOF that could have a big influence on the trap performance. In the following experiments, the plate spacing was manually adjusted to three different positions.

Figure 3-16 is the comparison of the variation in peak intensity. The angular deviations in pitch were varied at each plate spacing. The plate spacing was changed by a manual adjuster at a minimum step size of 1 μm. Each time when the plate spacing was varied, the operating parameters, including the RF trapping voltage, the DC and the AC signals, the scan rate and the arbitrary zero position in pitch, remained the same. However, since the vacuum chamber was opened between experiments, there might have been a slight variation in pressure as the sample valve and the helium valve had to be reset.

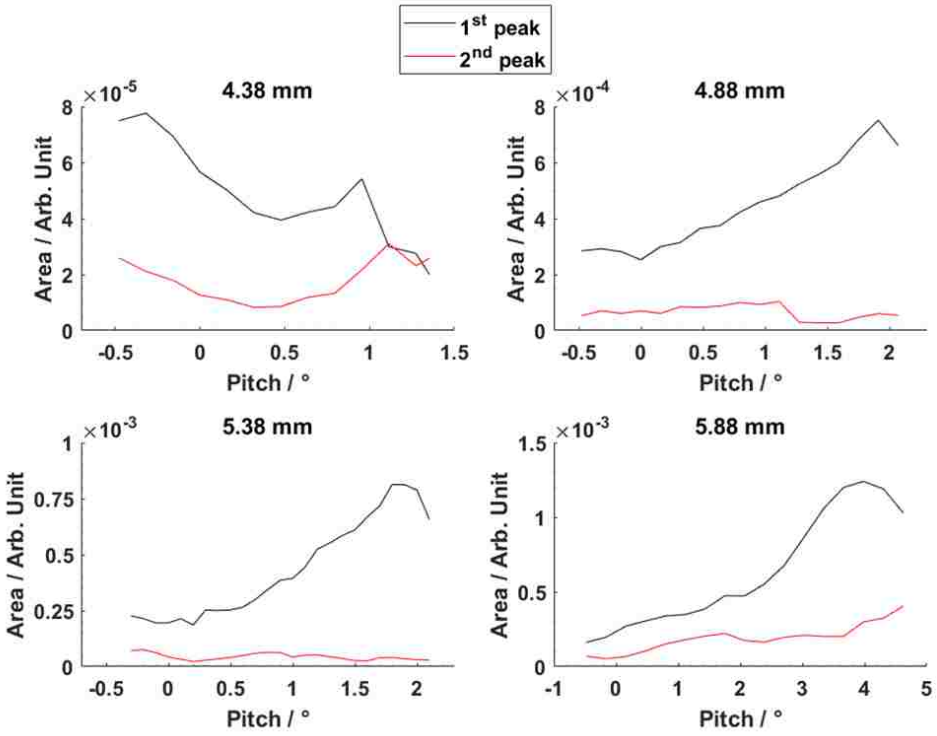

Figure 3-16. Comparison of peak intensities at four plate spacings, the angle in pitch was varied at each spacing.

A clear trend was seen that the peak intensity generally increased with the spacing, though there might be an involvement of a slight fluctuation in pressure. The explanation of this trend was

the same as what happened to the variation in the average plate spacings when pitch was varied. What remained unchanged at these four plate spacings was the resolution.

It seemed there were some other factors limiting the resolution. More efforts are needed on improving the resolution before studying the misalignment impact on trap performance. In addition, a motorized stage that is able to be finely controlled in vacuum is needed to vary the plate spacing in-situ. This way, the variation in peak intensity can better reflect the misalignment effect with less involvement of the uncertainties from the working pressure.

3.5 References

1. Cruz, D.; Chang, J. P.; Fico, M.; Guymon, A. J.; Austin, D. E.; Blain, M. G., Design, microfabrication, and analysis of micrometer-sized cylindrical ion trap arrays. *Rev. Sci. Instrum.* **2007,** *78* (1), 015107.

2. van Amerom, F. H. W.; Chaudhary, A.; Cardenas, M.; Bumgarner, J.; Short, R. T., Microfabrication of cylindrical ion trap mass spectrometer arrays for handheld chemical analyses. *Chem. Eng. Commun.* **2008,** *195* (2), 98 - 114.

3. Chaudhary, A.; van Amerom, F. H. W.; Short, R. T., Development of microfabricated cylindrical ion trap mass spectrometer arrays. *J. Microelectromech. Syst.* **2009,** *18* (2), 442 - 448.

4. Maas, J. D.; Hendricks, P. I.; Ouyang, Z.; Cooks, R. G.; Chappell, W. J., Miniature monolithic rectilinear ion trap arrays by stereolithography on printed circuit board. *J. Microelectromech. Syst.* **2010,** *19* (4), 951-960.

5. Kornienko, O.; Reilly, P. T. A.; Whitten, W. B.; Ramsey, J. M., Micro ion trap mass spectrometry. *Rapid Commun. Mass Spectrom.* **1999,** *13* (1), 50-53.

6. Taylor, S.; Tunstall, J. J.; Leck, J. H.; Tindall, R. F.; P., J. J.; Batey, J.; Syms, R. R. A.; Tate, T. J.; Ahmad, M. M., Performance improvements for a miniature quadrupole with a micromachined mass filter. *Vacuum* **1999,** *53* (1-2), 203-206.

7. Taylor, S.; Tindall, R. F.; Syms, R. R. A., Silicon based quadrupole mass spectrometry using microelectromechanical systems. *J. Vac. Sci. Technol. B* **2001,** *19* (2), 557-562.

8. Sillon, N.; Baptist, R., Micromachined mass spectrometer. *Sens. Act. B* **2002,** *83*, 129-137.

9. Blain, M. G.; Riter, L. S.; Cruz, D.; Austin, D. E.; Wu, G. X.; Plass, W. R.; Cooks, R. G., Towards the hand-held mass spectrometer: Design considerations, simulation, and fabrication of micrometer-scaled cylindrical ion traps. *Int. J. Mass Spectrom.* **2004,** *236* (1-3), 91-104.

10. Madsen, M. J.; Hensinger, W. K.; Stick, D.; Rabchuk, J. A.; Monroe, C., Planar ion trap geometry for microfabrication. *Appl. Phys. B* **2004,** *78*, 639-651.

11. Geear, M.; Syms, R. R. A.; Wright, S.; Holmes, A. S., Monolithic MEMS quadurpole mass spectrometers by deep silicon etching. *J. Microelectromech. Syst.* **2005,** *14* (5), 1156-1166.

12. Pau, S.; Pai, C. S.; Low, Y. L.; Moxom, J.; Reilly, P. T. A.; Whitten, W. B.; Ramsey, J. M., Microfabricated quadrupole ion trap for mass spectrometer applications. *Phys. Rev. Lett.* **2006,** *96* (12), 120801.

13. Austin, D. E.; Cruz, D.; Blain, M. G., Simulations of ion trapping in a micrometer-sized cylindrical ion trap. *J. Am. Soc. Mass Spectrom.* **2006,** *17*, 430-441.

14. Cheung, K.; Velasquez-Garcia, L. F.; Akinwande, A. I., Chip-scale quadrupole mass filters for portable mass spectrometry. *J. Microelectromech. Syst.* **2010,** *19* (3), 469-483.

15. Maas, J. D.; Chappell, W. J., RF planar ion trap for chemical sensing in *IEEE MTT-S International*, 2011.

16. Wright, S.; Malcolm, A.; Wright, C.; O'Prey, S.; Crichton, E.; Dash, N.; Moseley, R. W.; Zaczek, W.; Edwards, P.; Fussell, R. J.; Syms, R. R. A., A microelectromechanical systems-enabled, miniature triple quadrupole mass spectrometer. *Anal. Chem.* **2015,** *87* (6), 3115-3122.

17. Austin, D. E.; Wang, M.; Tolley, S. E.; Maas, J. D.; Hawkins, A. R.; Rockwood, A. L.; Tolley, H. D.; Lee, E. D.; Lee, M. L., Halo ion trap mass spectrometer. *Anal. Chem.* **2007,** *79* (7), 2927-2932.

18. Zhang, Z. P.; Peng, Y.; Hansen, B. J.; Miller, I. W.; Wang, M.; Lee, M. L.; Hawkins, A. R.; Austin, D. E., Paul trap mass analyzer consisting of opposing microfabricated electrode plates. *Anal. Chem.* **2009,** *81* (13), 5241-5248.

19. Peng, Y.; Hansen, B. J.; Quist, H.; Zhang, Z. P.; Wang, M.; Hawkins, A. R.; Austin, D. E., Coaxial Ion Trap Mass Spectrometer: Concentric toroidal and quadrupolar trapping regions. *Anal. Chem.* **2011,** *83* (14), 5578-5584.

20. Hansen, B. J.; Niemi, R. J.; Hawkins, A. R.; Lammert, S. A.; Austin, D. E., A lithographically patterned discrete planar electrode linear ion trap mass spectrometer. *J. Microelectromech. Syst.* **2013,** *22* (4), 876-883.

21. Hager, J. W., A new linear ion trap mass spectrometer. *Rapid Commun. Mass Spectrom.* **2002,** *16* (6), 512-526.

22. Li, A.; Hansen, B. J.; Powell, A. T.; Hawkins, A. R.; Austin, D. E., Miniaturization of a planar-electrode linear ion trap mass spectrometer. *Rapid Commun. Mass Spectrom.* **2014,** *28* (12), 1338-1344.

23. Velasquez-Garcia, L. F.; Cheung, K.; Akinwande, A. I., An application of 3-D MEMS packaging: Out-of-plane quadrupole mass filters. *J. Microelectromech. Syst.* **2008,** *17* (6), 1430-1438.

24. Schwartz, J. C.; Senko, M. W.; Syka, J. E. P., A two-dimensional quadrupole ion trap mass spectrometer. *J. Am. Soc. Mass Spectrom.* **2002,** *13* (6), 659-669.

25. Wu, Q.; Tian, Y.; Li, A.; Austin, D. E., Simulations of electrode misalignent effects in two-plate linear ion traps. *Int. J. Mass Spectrom.* **2015,** *393*, 52-57.

26. Wu, G.; Cooks, R. G.; Ouyang, Z., Geometery optimization for the cylindrical ion trap: Field calculations, simulations and experiments. *Int. J. Mass Spectrom.* **2005,** *241* (2-3), 119-132.

27. Zhang, Z.; Quist, H.; Peng, Y.; Hansen, B. J.; Wang, J.; Hawkins, A. R.; Austin, D. E., Effects of higher-order multipoles on the performance of a two-plate quadrupole ion trap mass analyzer. *Int. J. Mass Spectrom.* **2011,** *299* (2–3), 151-157.

4. Two-Plate Glass Planar Linear Ion Trap and Experimental Study on Its Geometry Deviations

*(The first two sections in this chapter are taken from the journal article "Tian, Y.; Decker, T.; McClellan, J.; Bennett, L.; Li, A.; de la Cruz, A.; Lammert, S. A.; Hawkins, A. R.; Austin, D. E. Improved miniaturized linear ion trap mass spectrometer using lithographically, patterned plates and tapered ejection slit. Journal of American Society for Mass Spectrometry, **in press**". Sections 4.3-4.4 are taken from the journal article "Tian, Y.; Wu, Q.; Decker, T.; Hawkins, A. R.; Austin, D. E. Experimental Observation of the Effects of translational and rotational Electrode misalignment on a Planar Linear Ion Trap Mass Spectrometer. International Journal of Mass Spectrometry. **in preparation**." My individual efforts are proposing the potential problems with the old ceramic plate, designing the pattern on the new glass plate, assembling the third-generation alignment platform, exploring the best performance on the glass plate and conducting the misalignment experiment.)*

4.1 Introduction

Although the dimensional scale of lithographic patterning can easily be reduced to make smaller features and smaller ion traps in the two-plate approach, the plate thickness cannot easily be reduced without compromising the strength and ruggedness of the resulting device. This can lead to problems with ion ejection. In previous efforts (unpublished) we developed and tested a two-plate LIT with plate spacing of 724 μm (y_0 = 362 μm). The ejection slit was fabricated to be 100 μm wide and 20 mm long. The plate thickness was still 0.5 mm as with the larger devices, resulting in an ejection slit that was many times deeper than it was wide. Unfortunately, ions were not successfully ejected through this narrow, deep slit. Two factors likely prevented ion ejection: ions travelling at small angles during ejection would not make it through the slit but would hit the walls, and build-up of charge on the inside walls of the slit repelled subsequent ions. In a LIT,

ions can pick up energy in the non-ejection direction, which has a secular frequency close to the ejection frequency, resulting in ions being ejected with some angular dispersion. In addition, depending on operating frequency and voltage, ion trajectories in miniaturized ion traps can be larger, relative to the available space between electrodes, than in full-size traps, exacerbating the issues with the narrow ejection slit[1].

One possible solution to the above problem is to eject ions parallel to the plates rather than through a slit. However, simulations show that it is more difficult to obtain desirable combinations of higher-order terms in the trapping field when ions are ejected between and parallel to the plates. Early results from the halo ion trap[2-3] showed the same difficulties. A slit allows ions to be ejected with a potential in the ejection direction that is carefully controlled all the way to the point of ejection from the trap.

We have opted for another solution, which is to taper the ejection slit profile just like the ejection slit design for the LIT proposed by Schwartz[4] and the RIT proposed by Ouyang[5]. The slit walls open out, allowing ions to pass through even with a large angular dispersion. Charge build-up on the slit walls is thereby prevented, and ion ejection can proceed. The tapered slits profile also allows the slit walls to be coated with a conducting or semiconducting material, which is impractical in straight-walled slits.

The previous plate design also had several issues in making electrical connections between the front and back-side of the plates, and in making electrical connection with the printed circuit board behind the ceramic plates. These issues were solvable at the dimension scale of the full-size device, but were difficult to miniaturize further. Both of these issues are solved in this new design

by patterning the connections on the trapping side of the plates and wire-bonding the connections from ceramic plate to printed circuit board.

The above issues presented significant challenges in ion trap miniaturization using the two-plate approach. This section demonstrates that a tapered ejection slit combined with single-side patterning and connection solves these issues enabling further miniaturization of this mass analyzer. In addition, performance is significantly improved even for the full-scale device, both in terms of mass resolution and also ruggedness and ability to operate for long periods of time without signal loss due to charge build-up. Further, in characterizing this new design, one of the two plates was mounted on a motorized translation stage so that plate spacing as well as the misalignment in X and Z directions could be optimized in vacuum during operation, enabling the study on the effects of geometry deviation on the trap performance.

4.2 Two-Plate Glass Planar Linear Ion Trap

Design and preliminary simulation

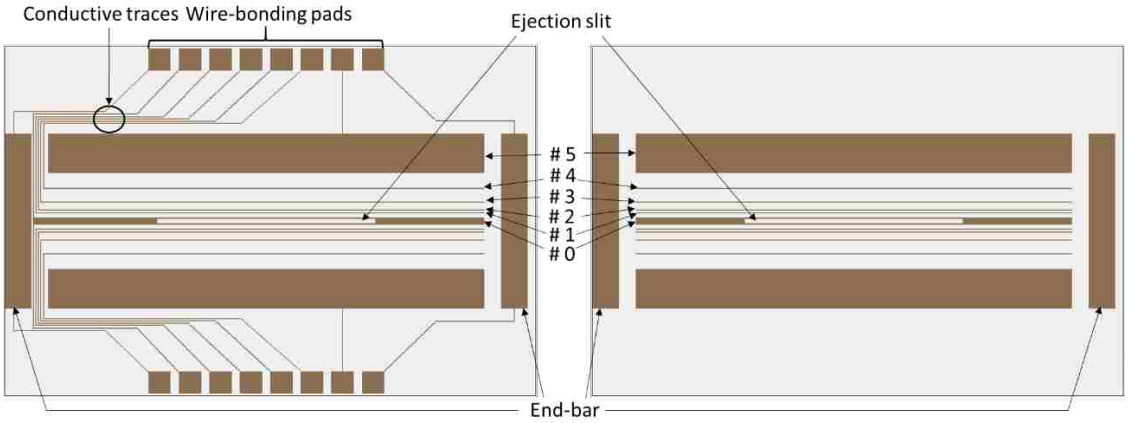

Figure 4-1. Comparison of the simulation models for the new design (left) and the old design (right).

As the connections were patterned on the trap side, a series of traces and bonding areas were added. The electrode pattern is shown in Figure 4-1. Five pairs of RF electrodes are used on each plate, with the positions and dimensions identical to those of the previous ceramic plate design, with a few exceptions. This was done to allow comparison between the designs to be as close as possible. Axial confinement of ions was accomplished using patterned end-bars on each plate.

The specifications and the optimized RF amplitudes for the five pairs of RF electrodes were the same as in the old ceramic plates except the voltage ratio of the #2 and the #3 (see Table 4-1).

Table 4-1. The geometric specification and the optimized voltage distribution on each electrode in the glass planar LIT.

Electrode No.	Electrode Line Width (μm)	Distance from the Ejection slit (center to center) / mm	Voltage as a fraction of the full RF voltage
# 0	300	0	0
# 1	50	0.91	0
# 2	50	1.26	0.14
# 3	50	2.19	0.14
# 4	50	3.79	1
# 5	4500	7.75	1

The electrodes #0 surrounded the ejection slits. In the experiment one of them was grounded on one plate but floated (nominally at ground) with an applied AC resonance waveform on the other, while in the simulation no AC signal was applied. The electrodes #1 pair were always grounded. The #4 and the #5 were always applied with the full RF driving voltage, and the voltages applied on the #2 and #3 electrodes were scaled as 0.14 times the full driving amplitude to adjust the shape of the trapping field[6].

The comparison of the cross-section views of electric fields between the new design and the old design are shown in Figure 4-2. The fields in the central trap regions were almost the same in the two cases. Even though there were two more quadrupolar fields formed on two sides of the

central trapping region, they were not used to trap or select ions, neither did they have any big impacts on the central electric field.

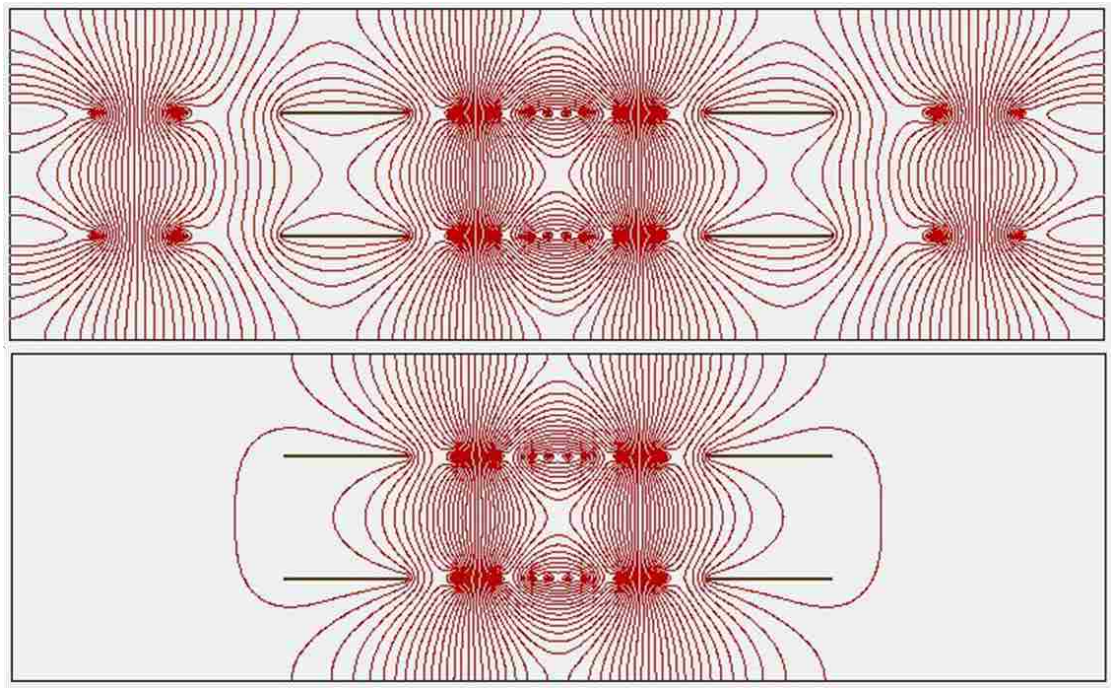

Figure 4-2. Cross-section views of the electric fields of the new design (top) and the old design (bottom).

In both simulation setups, 1000 ions at ***m/z*** 91 and 1000 ions at ***m/z*** 92 were randomly created within the central trapping region. The hard-sphere collision model from SIMION installation package was used. Helium was used as the cooling gas at a pressure of 0.53 Pa (around 4 mTorr). The ejecting voltages of the ions that passed through the slit were recorded for analysis. Results showed that the peak intensity and the peak width were nearly the same in these two models, demonstrating that the new design should work just as the old design did in experiments.

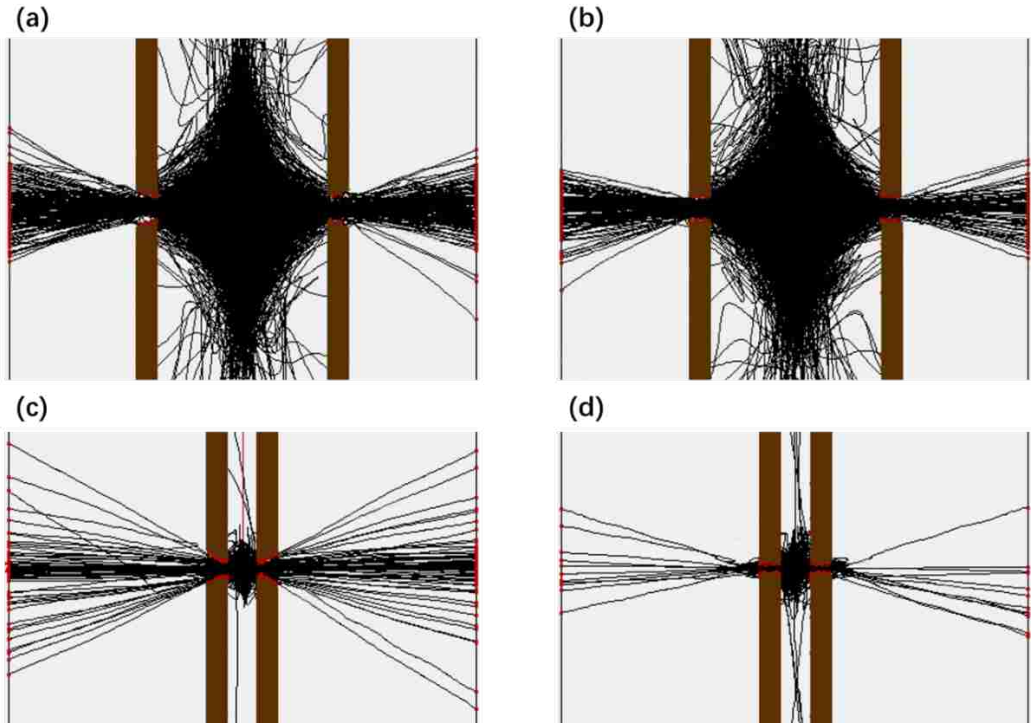

Figure 4-3. Cross-section views of the simulations at the spacing of 4.4 mm with (a) and without (b) tapered slits, and at the spacing of 0.72 mm with (c) and without (d) tapered slits.

The models with and without tapered slits at two different plate spacings were compared as shown in Figure 4-3. Both models were modified from the new design (with traces and pads). All the setups were the same except that the operating parameters (RF amplitude and RF frequency) were optimized for each plate spacing. The slit width in the large plate spacings (a and b) were 0.5 mm and were 0.1 mm in the small plate spacings (c and d). It can be seen that the efficiency of the ions passing through the slit was improved in both tapered cases (a and c). Comparing (a) and (c) or (b) and (d), the passing efficiencies were greater in the large spacings than in the small spacings, indicating the plates used in small spacings should enlarge the slit width instead of proportionally scaling. The thickness may need to be reduced as well to shorten the travel distances of ions passing through the slit.

Design and Fabrication

Whereas prior efforts all used ceramic substrates, in the present study we used borosilicate glass. Glass has similar electrical and structural properties as alumina ceramic, but is more amenable to the tapering cuts used to make the ejection slit. The fabrication process is shown in Figure 4-4. Plates were milled and diced to 57×37 mm, with a thickness of 0.50 mm. A 2.5-mm long, 0.50 mm-wide ejection slit was machined in the glass with a backside taper angle of 45°. Holes were milled into the plates for plate alignment during assembly. Aluminum electrodes and traces were patterned onto the plates using photoresist and photomasks. After patterning, a 100 nm Ge layer was evaporatively deposited on both sides of the plates, covering both the trapping side and the back side of each plate.

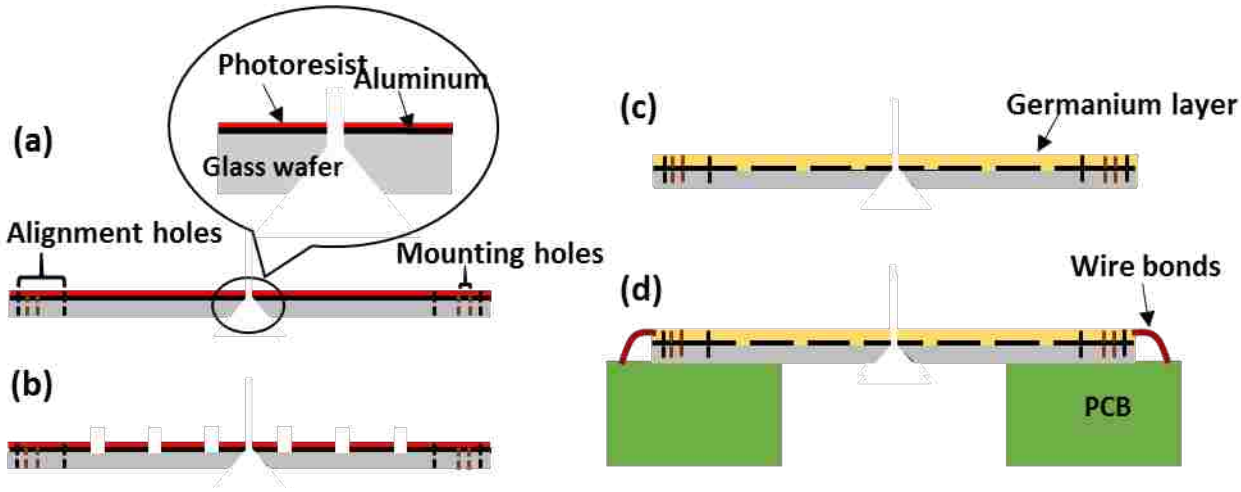

Figure 4-4. Fabrication process of the glass plate with tapered slit.

The PCB and glass plate were assembled as shown in Figure 4-5(b). After patterning, each glass plate was attached to a printed circuit board (PCB) using vacuum-grade epoxy (Torr-Seal, Agilent Technologies, Lexington, MA) as seen in Figure 4-5(a). The connection pads of the plate were then wire-bonded to corresponding pads on the PCB. In addition, a second PCB with

capacitors was attached to the backside of the mounting PCB to establish RF amplitudes and conduct the applied waveforms to the trapping electrodes.

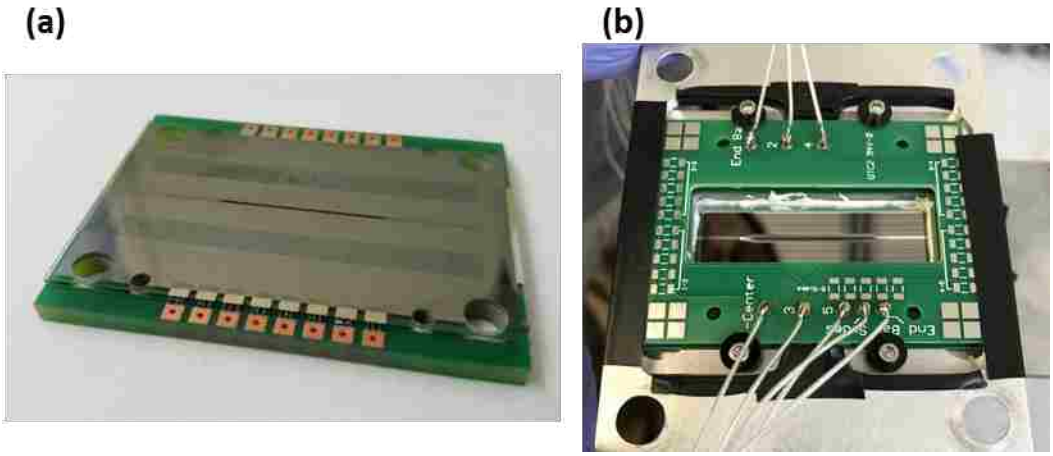

Figure 4-5. (a) Representative of the glass plate with the wire-bonded PCB on its back side; (b) The assembly of the glass plate in the plate holder with the second PCB attached on the back side of the wire-bonded PCB.

Mounting and Assembly

Previous published designs relied on mounting screws and sapphire balls (for plate separation and alignment), resulting in a rigid assembly. The second generation used in Chapter 3 can only vary pitch in vacuum. To provide flexibility with this third generation, one of the two plates was mounted onto a motorized 3-axis stage (MAX 343, Thorlab Inc., Newton, New Jersey, USA) so that plate spacing was adjustable in vacuum. The top plate was still driven by the one-dimensional motorized actuator.

Plate alignment was adjusted prior to putting the instrument in vacuum. The assembly is shown in Figure 4-6. Similarly, the stage was mounted on a base, and the top plate was fixed onto a ceiling piece. The bottom plate was immobilized on the stage together with and right above an electron multiplier (Detector Technology, Inc., Palmer, MA). An electron gun (Torion Inc.,

American Fork, UT) was mounted on the side of the trap with the electron beam directed along the axis of the trap. The two plates were also pre-aligned using the four sapphire balls before the bottom plate was completely immobilized on the stage.

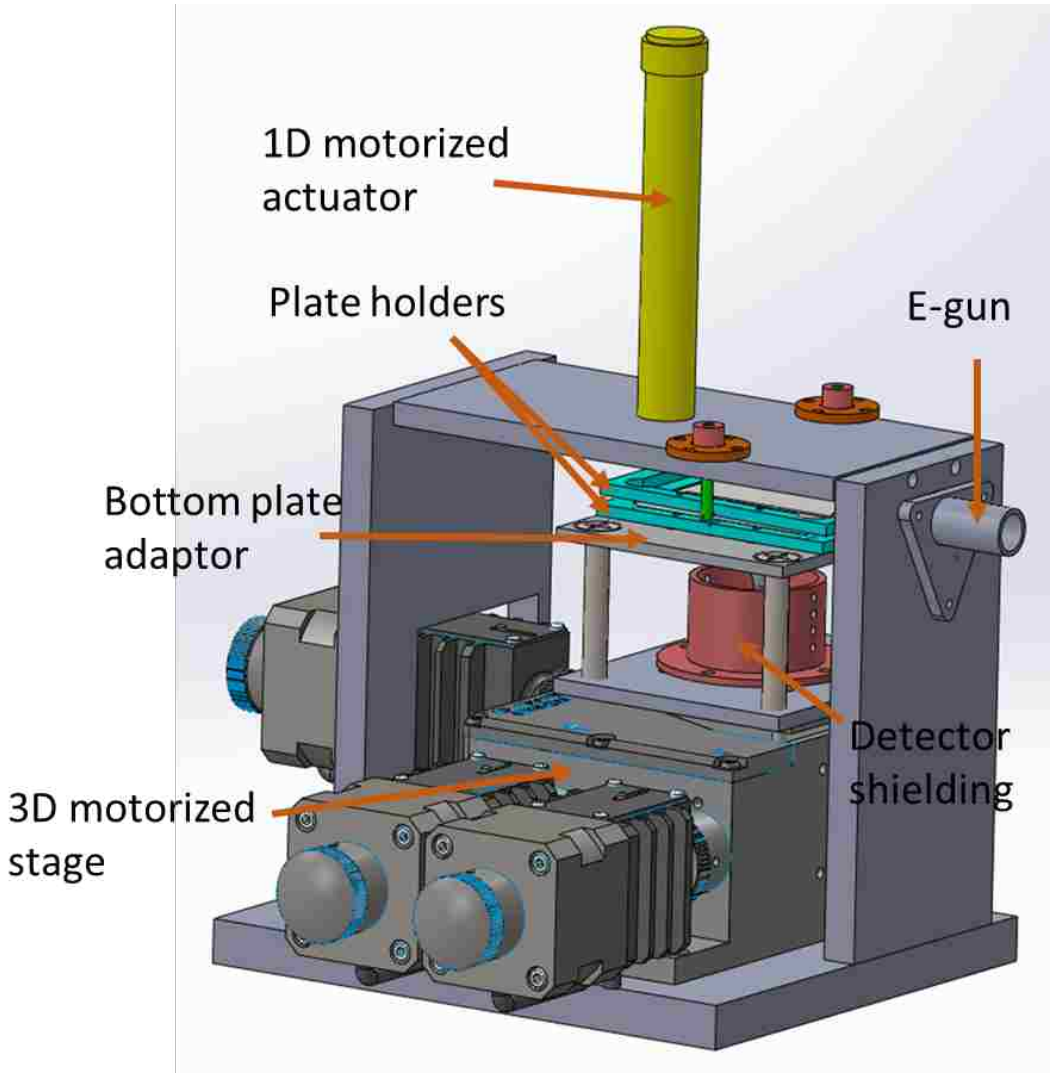

Figure 4-6. 3D view of the third generation of the alignment platform in Solidworks.

The main difference from what was described in Chapter 3 was the position where the top plate was at was digitally represented in APT (software platform). When the bottom plate was

immobilized and the plates were separated apart again, the bottom plate was moved back to the original position which was spaced by balls with fine control.

Experiments

The electronic timing control of resonance ejecting ions was similar to previous experiment[7] (also seen in Figure 3-12) but with a shorter period (60 ms for the whole experiment). The ionization time was reduced to 0.5 ms; ions were trapped with the RF at 200 $V_{0\text{-}p}$ and cooled for 1.825 ms. Ions were then ramped out by sweeping the RF voltage from 200 to 560 $V_{0\text{-}p}$. An AC resonance waveform was applied during the RF ramp with an optimized frequency of 620 kHz and amplitude of 1 $V_{0\text{-}p}$. A +5 V DC voltage applied to the two end-bars contained the ions axially inside in the trap.

The sample used in this experiment was a mixture of toluene and deuterated toluene (D8-toluene) at a volume ratio of 1:1, and a mixture of xylenes (*o-, m-, p-*). Sample pressure for toluene and D8-toluene was $1\text{-}2\times10^{-6}$ Torr, whereas the sample pressure for xylene mixtures was $4\text{-}5\times10^{-6}$ Torr, nearly three times higher than that of toluene mixtures, so that the fragment ions ***m/z*** 91 as well as their isotopic peak ***m/z*** 105 and ***m/z*** 107 could be seen within a wider plate spacing range. The electron gun (e-gun) acceleration voltage was −62 V for toluenes and was decreased to −52 V for xylenes to reduce the fragmentation. A −100 V/+23 V pair of voltages were used on the gate to block or focus the electron beam. The electron multiplier was used with −1600 V applied. As plates and coaxial cables added about 100 pF to the circuit load, the drive frequency was reduced to 1.35 MHz instead of the RF power supply's built-in frequency of 1.6 MHz (Ardara Technologies L.P., Lewiston, NY). The background pressure was in the 10^{-7} Torr level. Sample was preloaded in a glass tube which was connected to a leak valve (203 variable leak, Granville Phillips, Boulder,

Colorado). Sample vapor was leaked into the vacuum. Helium at $3-4\times10^{-3}$ Torr was introduced for collisional cooling of the trapped ions. Variations of plate spacing and scan rate were explored to observe the effect on signal intensity and mass resolution. Computer simulations using SIMION 8.1 were used to plan experiments and anticipate optimal conditions (voltages, plate spacing, etc.).

Results and Discussion

Simulations showed an optimized plate spacing of 4.4 mm with driving frequency at 1.6 MHz, while best resolution was achieved in practice when the spacing was 5.00 mm with the same applied RF. Although end-cap stretching can improve performance in many ion traps due to improvement in higher-order terms of the trapping field[8], these higher-order terms were taken into account in the simulations. It may be that the fields were not exactly as intended, or that some other factor is present that was not adequately accounted for in the SIMION simulations. Such factors may include the effect of the deposited germanium layer, or fabrication tolerances of the slit.

We observed small plate-to-plate differences, including a different optimal AC frequency when different plates were used, which may be the result of fabrication variance or inconsistent alignment. The spectra for the toluene mixture and xylenes are shown in Figure 4-7. The scan rate was 2300 Th/s. The plate spacing was 5.0 mm. The differences in signal-to-noise ratio (S/N) was the differences in the sample pressure.

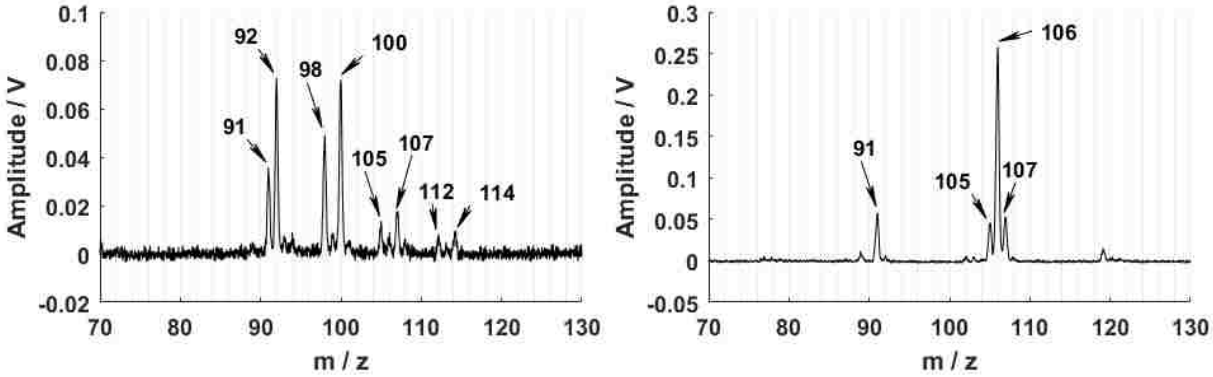

Figure 4-7. Representative spectra of (a) toluene and D8-toluene and (b) xylenes.

In Figure 4-7 (a) the toluene molecular ion peak at ***m/z*** 92 and the H-loss peak at ***m/z*** 91 were completely resolved, as were the corresponding peaks at ***m/z*** 98 and 100 from D8-toluene. Peaks at ***m/z*** 105, 106, 107, 112, 113 and 114 are expected products of ion-neutral reactions (methyl abstraction) within the trap, including the various combinations of deuterated and non-deuterated species[9]. In Figure 4-7 (b), the molecular ion peak at ***m/z*** 106 from xylene is well resolved from the H-loss peak at ***m/z*** 105 and the ^{13}C peak at ***m/z*** 107. The S/N ratio in the xylene spectrum was higher than that in toluene mixture spectrum as the xylene pressure was much higher[10].

Spectra at different plate spacings for the toluene mixture and xylenes are shown in Figures 4-8 and 4-9, respectively. The AC frequency, AC amplitude, end-bar voltage, RF trapping voltage, and RF frequency were the same as above and constant for all these experiments. Plate spacing in this experiment can be changed without having to break vacuum, so a relatively constant pressure was maintained, greatly reducing changes in signal intensity due to sample or helium pressure. Thus the variation of signal intensity should be due primarily to differences in plate spacing.

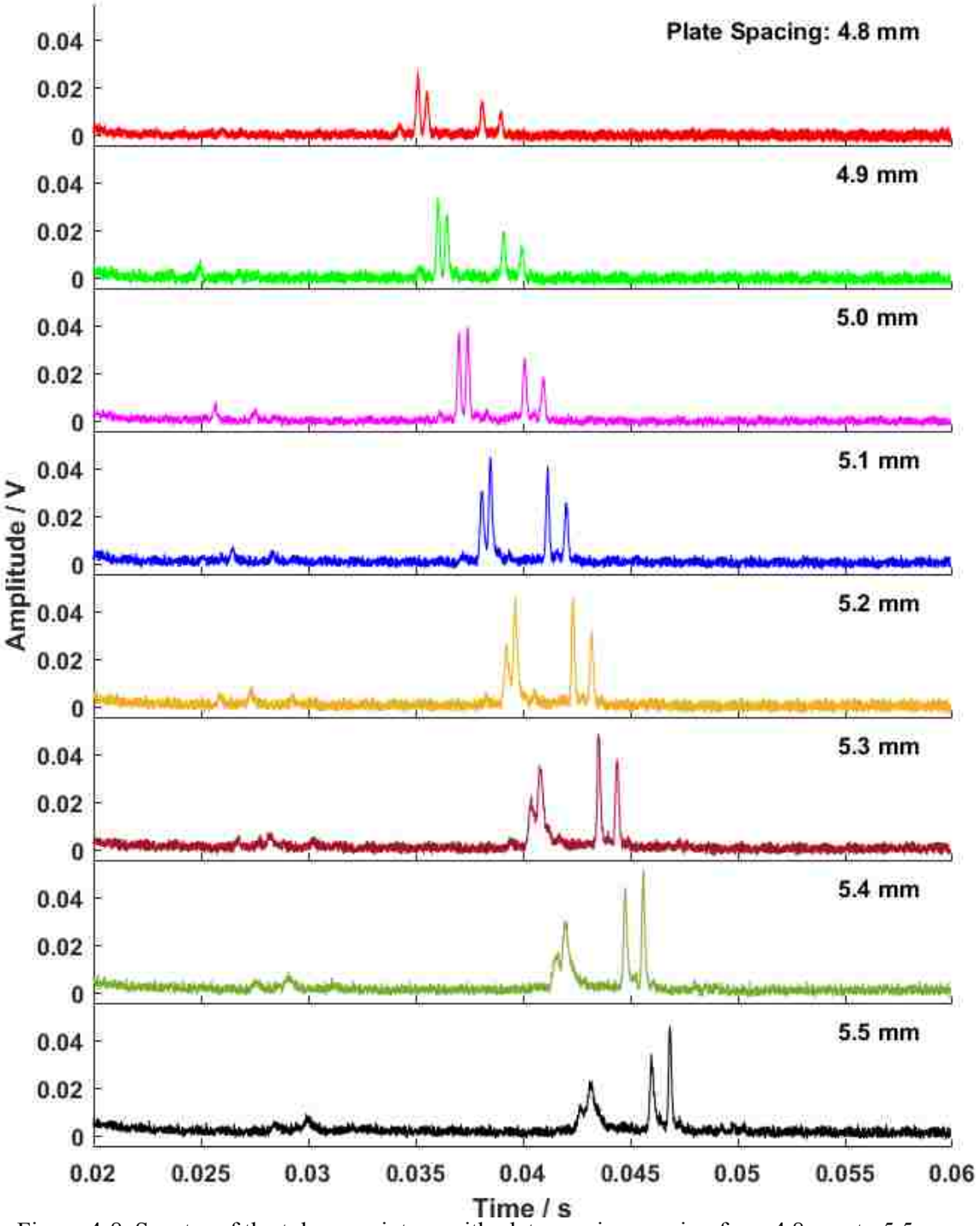

Figure 4-8. Spectra of the toluene mixture with plate spacing ranging from 4.8 mm to 5.5 mm.

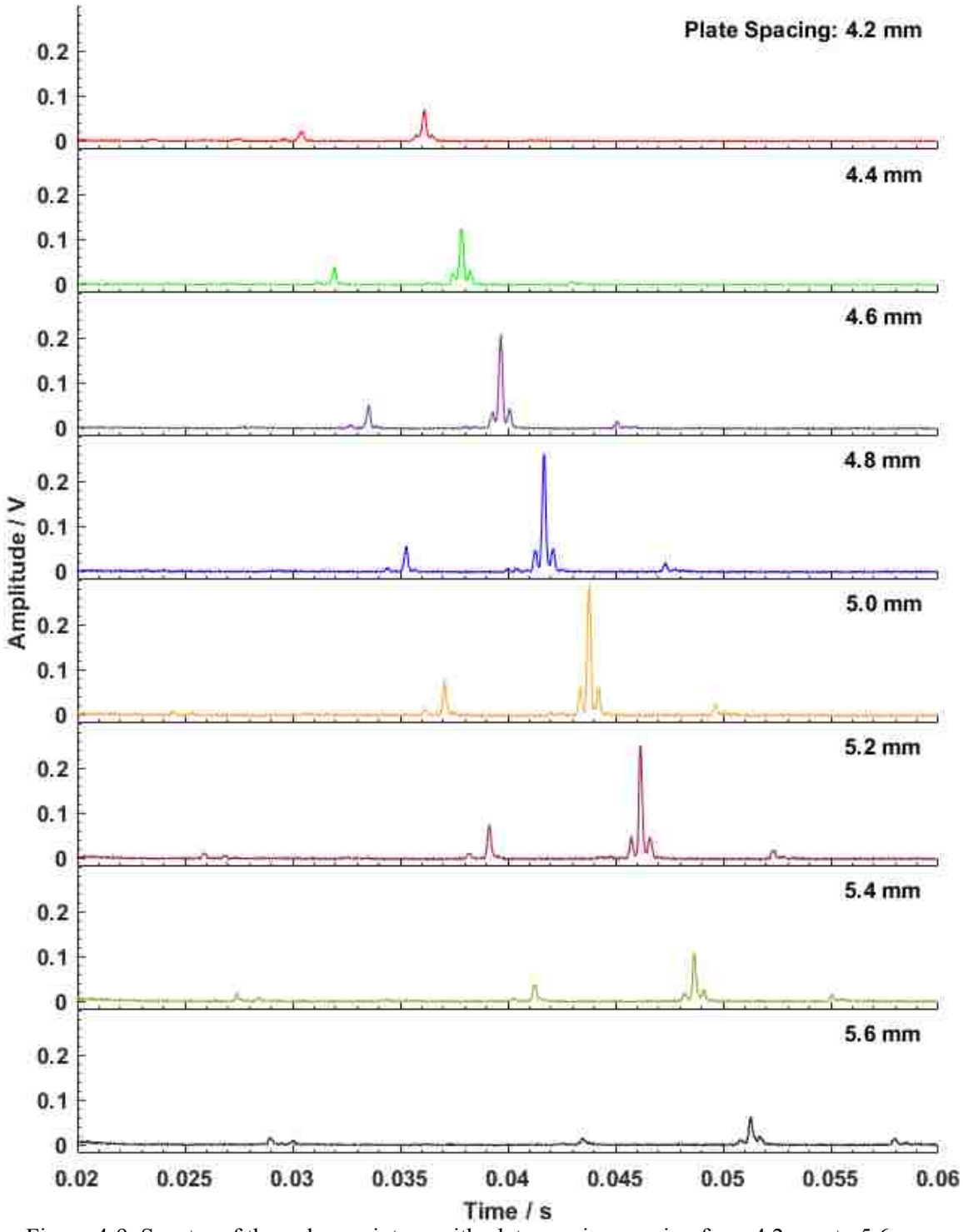

Figure 4-9. Spectra of the xylene mixture with plate spacing ranging from 4.2 mm to 5.6 mm.

In the process of collecting toluene mixture spectra, the smallest spacing was 4.8 mm as the peak intensity was too weak to observe if the plate spacing was closer than 4.8 mm, when the spacing was increased from 4.8 mm to 5.0 mm, a clear increase of signal intensity was observed, so is the case with xylene mixture spectra. On the other hand, the resolution in toluene mixture spectra seemed to vary little at small spacing from 4.8 mm to 5.0 mm, comparing with the resolution variation in xylene mixture spectra when the spacing was increased from 4.2 mm to 5.0 mm.

When the plate spacing was further increased from 5.0 mm to 5.5-5.6 mm, peak intensity from toluene (***m/z*** 91 and ***m/z*** 92) started to decrease more obviously than ion peaks from D8-toluene. A clear decrease in resolution was also seen in spectra of both samples, indicating there was a maximum point for both toluene mixture and xylene mixture within the variation range. That optimal point occurs at 5.0 mm under the current conditions, at which the minimum peak width (full width of a peak at its half maximum, FWHM) was 0.35 Th in toluene spectra (***m/z*** 98) and 0.32 Th in xylene spectra (***m/z*** 106), corresponding to a resolution of 119 and 140, respectively. The variation in resolution with plate spacing was probably due to the variation in higher order components of the trapping field at different plate spacing. The variation in peak intensity might be because the e-gun was fixed relative to the stationary plate, and was not always directed precisely along the trapping center.

However, a more likely explanation is that the ion ejection efficiency changed with the magnitude of the higher-order field components. With a greater contribution of octopole and dodecapole, ions more quickly fall out of resonance during AC excitation, reducing the fraction that gain sufficient energy to be ejected at that point in the scan. Another phenomenon observed

is that when the plate spacing was increased, all the peaks gradually shift to higher ejection RF voltages (as seen in Figures 4-8 and 4-9), consistent with the increased effective trap size (y_0).

Figure 4-10 shows the fraction of octopole and dodecapole as a function of plate spacing, calculated using SIMION and using a previously published procedure for calculating the potential on the germanium surface [11]. This procedure cannot be used for ion trajectory calculations and differs from the procedure used above to predict performance. Interestingly, the optimal experimental performance occurs when the octopole is still negative relative to the quadrupole, and even the sum of octopole and dodecapole is slightly negative.

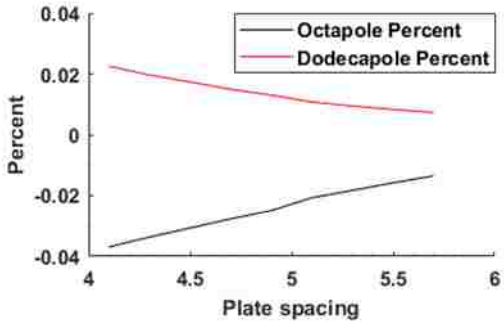

Figure 4-10. Higher order components (octapole and dodecapole) as a fraction of quadrupole field at different plate spacings.

It is well known that resolution in ion traps is dependent on the scan rate[12]. Figure 4-11 shows the spectra for toluene and D8-toluene at different scan rates ranging from 1700 to 12000 Th/s, with each spectrum averaged 50 times. Plate spacing was always at the optimal value of 5.0 mm. It can be seen that the resolution (FWHM) was better with slower scan rate. At 3700 Th/s, the ***m/z*** 91 and 92 peaks started to combine. Peaks at ***m/z*** 98 and ***m/z*** 100 remain resolved even with reduced resolution.

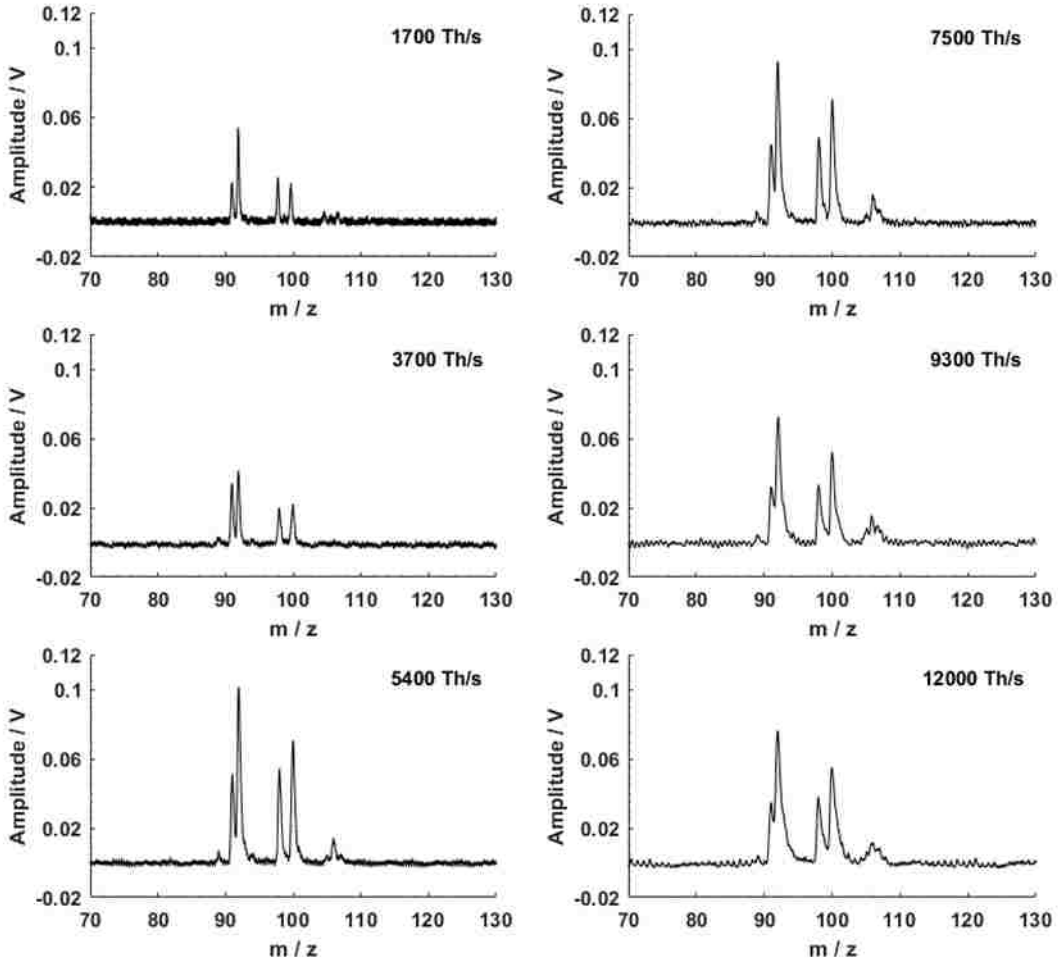

Figure 4-11. Toluene and D8-toluene spectra at different scan rates and spacing of 5.0 mm.

An issue with previous LITs made using patterned plates is that charge build-up in the slits prevented long term operation. Signal intensities would decrease over a timescale of minutes, and would return to normal only after the system was turned off for several tens of minutes. Although the cause of this behavior was previously unclear, the absence of the problem with the present design points to charge build-up as the culprit. With the present design, we saw no reduction in signal even after many hours of continuous operation. This likely is the result of the tapered slit, because other aspects of the design have not significantly changed (e-gun operation, trap design).

From this we also conclude that the signal reduction shown in Figures 4-8 and 4-9 is likely the result of differences in ejection efficiency due to different electric fields with each value of plate spacing, and not due to charge build-up.

The above results demonstrate that the tapered slit design is effective at solving one of the main limitations of miniaturizing the two-plate LIT. Specifically, the taper allows ion ejection to be unimpeded by either collision with the slit wall or by build-up of charge on the slit wall, without compromising plate ruggedness. In addition, the improved electrical connections with the new design proved to be more reliable and easier to miniaturize. The tapered slit can be machined much narrower than what was used in the present study, and smaller versions have already been fabricated, patterned, and mounted and are being prepared for testing.

4.3 Experimental results and discussion in geometry deviations

The experiment setup and the operating parameters were the same as what were used to obtain the spectra in Figure 4-7. In the following experiments, each time only one DOF was changed with all the other DOFs at ball-aligned positions.

The angular deviation in pitch, as expected, is the most serious factor affecting both the resolution and the intensity. Figure 4-12 shows the spectra at different pitch angles for the toluene mixture and xylenes. The 0° position was an arbitrary position determined by the alignment balls. It is subject to change in practice as there might be some extra pressure exerted on the spring with the rigid balls. The top plate could be bounced back after removing the balls. The "+" symbol represents the movement of stretching with the one-dimensional actuator. The "–" symbol represents the movement of retraction. In this design, the actuator stood on the opposite side of

where the electron beam entered, which means in the negative process electron beams might be blocked if pitch was deviated too much. This would not happen in the positive process. During the experiment, the actuator traveled within a range of 0.5 mm, corresponding to the variation from −0.40° to +0.40° in pitch. The step size was 0.16°.

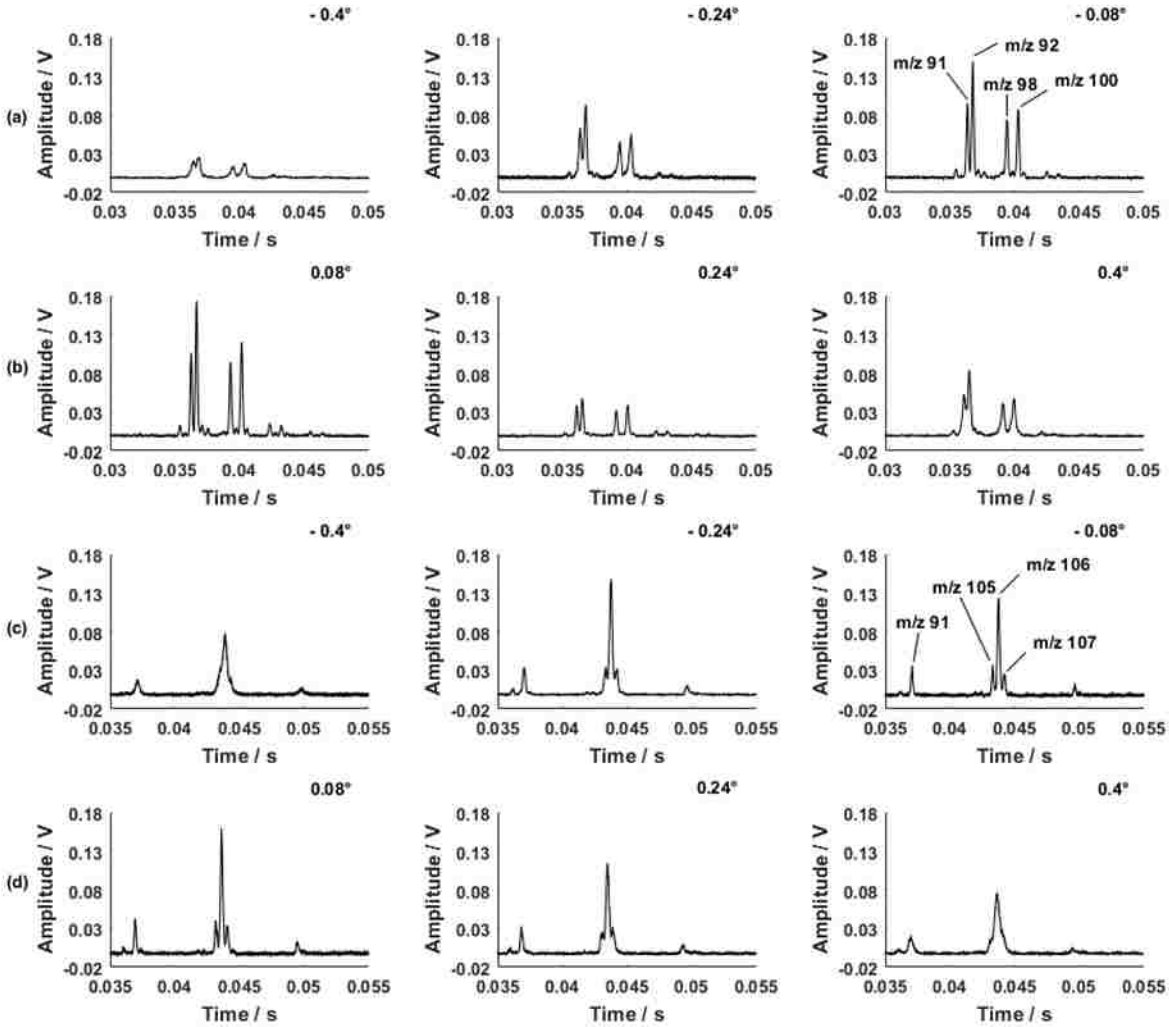

Figure 4-12. The spectra variation with pitch varied from –0.40° to +0.40°. (a) and (b) are the spectra of the toluene mixture; (c) and (d) are the spectra of the xylenes.

A clear variation in mass resolution can be seen in both the toluene mixture and xylenes. The ***m/z*** 91 and 92 peaks were completely separated at 0° and +0.08°. Peak intensities were also the

strongest in the range between these two positions, but the performances decreased when the top plate was further deviated. The ***m/z*** 91 and 92 peaks started to join when the pitch angle was larger than +0.16° or was smaller than −0.08°. Though ***m/z*** 98 and 100 from D8-toluene were always separated, the peak widths were broadened at large pitch angles and the intensity varied so much that they almost disappeared at +0.40°. Same results were observed in xylenes spectra. Performances were the best at 0° and +0.08°, since ***m/z*** 105, 107 peaks were separated from the molecular ion peak ***m/z*** 106 though they mixed together at large pitch angles.

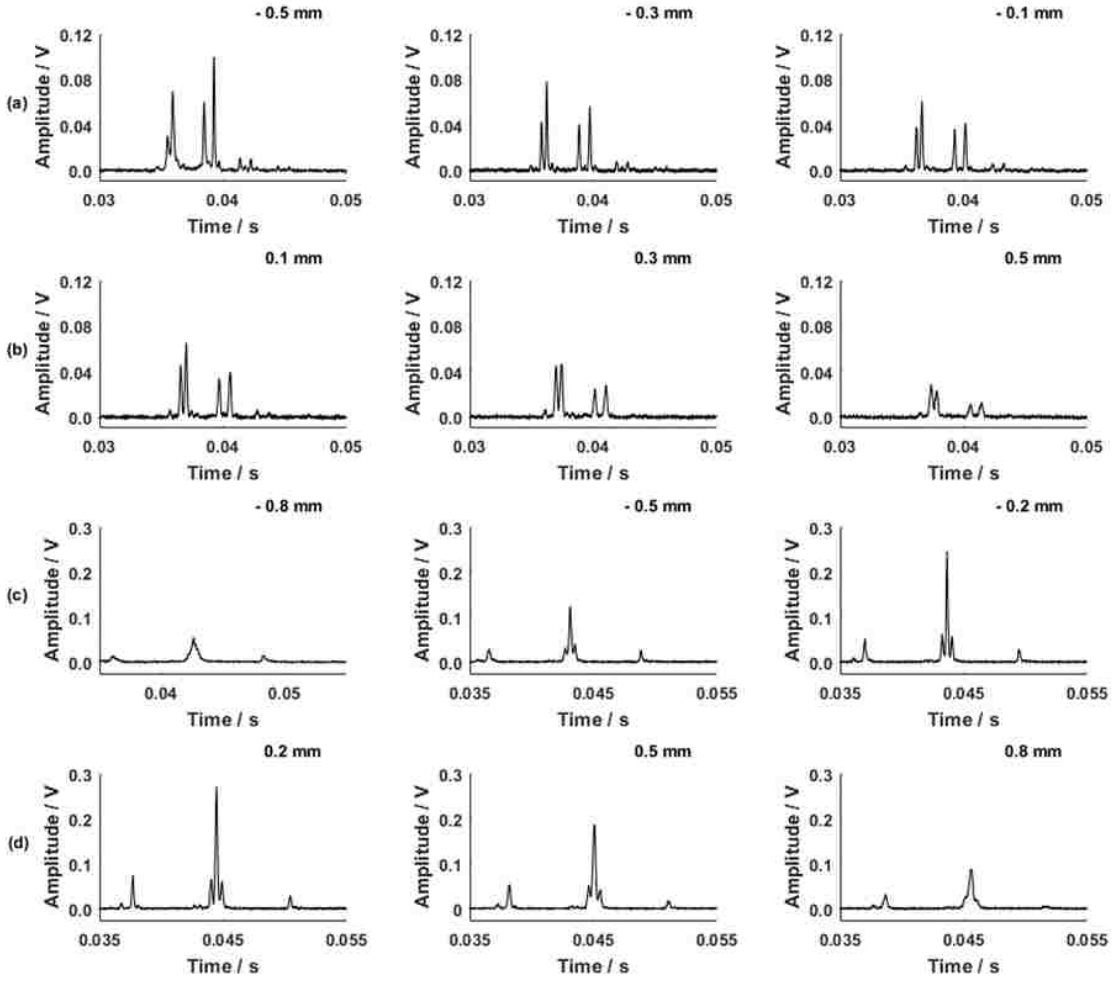

Figure 4-13. (a) and (b) are the spectra for the toluene mixture with x-displaced from −0.50 mm to 0.50 mm; (c) and (d) are the spectra for the xylenes with x-displaced from −0.80 mm to +0.80 mm.

The x-displacement, as predicted, should have less impact on the performance if it's not displaced too much. Figure 4-13 shows the spectra for the two samples at different degrees of x-displacement. The pitch angle was always at the arbitrary 0° position. The "0 mm" position was also an arbitrary point defined by the sapphire balls. The stage moved forward in the positive positions, and moved backward in the negative positions. Theoretically, these two directions are basically the same and the variations in the performances should be the same, whereas the results turned out to be quite different in these two directions. In the spectra from the toluene mixture, the peak intensities varied less from −0.5 mm to 0 mm than from 0 mm to 0.5 mm, but the resolutions varied a bit more from −0.5 mm to 0 mm than from 0 mm to 0.5 mm. Similar trends were also observed in xylenes' spectra, which was a little out of expectation. The variation in the peak areas followed what were predicted in the simulation—it generally decreased when x-displacement became larger.

Displacement from z direction, as expected, had the minimum effect on the trap performance. Figure 4-14 are the spectra displaced from –2.5 mm to +1.5 mm in z direction. Again, the positive symbol means the actuator moved forward, corresponding to the process the bottom plate traveled towards the E-gun. The negative symbol means the bottom plate moved away from the E-gun. The travel range and the staring position were limited by the travel range of the actuator (4 mm) as well as by the spacing between the bottom plate adaptor and the side support which the E-gun was attached on.

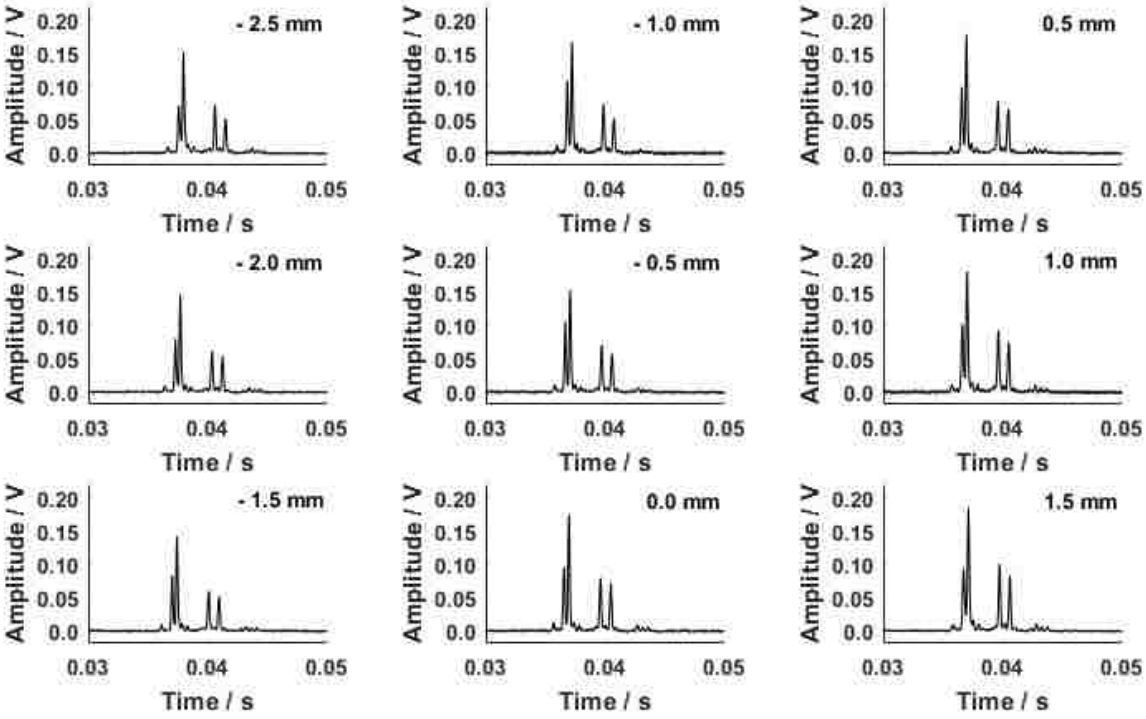

Figure 4-14. The spectra for the toluene mixture at different z-displacements.

It turned out the peak intensity almost remained the same with a minor fluctuation in peak intensity. Considering that the plate was 60 mm long with a 25-mm long ejection slit and a series of 50-mm long electrode lines, the effective trap length was affected little by just displacing 2.5 mm. It is possible the performance would be affected a lot if the bottom plate was displaced by 1/3 or 1/2 of the effective trap length. The fact is this big deviation is unlikely to happen in practical alignment work unless the plates are very small or the aspect ratio of the plates are small.

Experimental results and the simulation results[13] are compared in Figure 4-15. In Figure 4-15 (a) and (b), the resolution obviously dropped when the pitch angle varied from 0° to +0.3° in both the experiment and simulation. However, the number of ions being detected slightly decreased in the experiment while increased in the simulation. It is possible pitch has some impacts on the peak area or the ion detection efficiency but it's not statistically important. The trends of the variations

in the resolution and the peak area or detection efficiency from x-displacement were the same. Compared with pitch, x-displacement, as expected, has more influences on the ion ejection efficiency and less influences on the mass resolution.

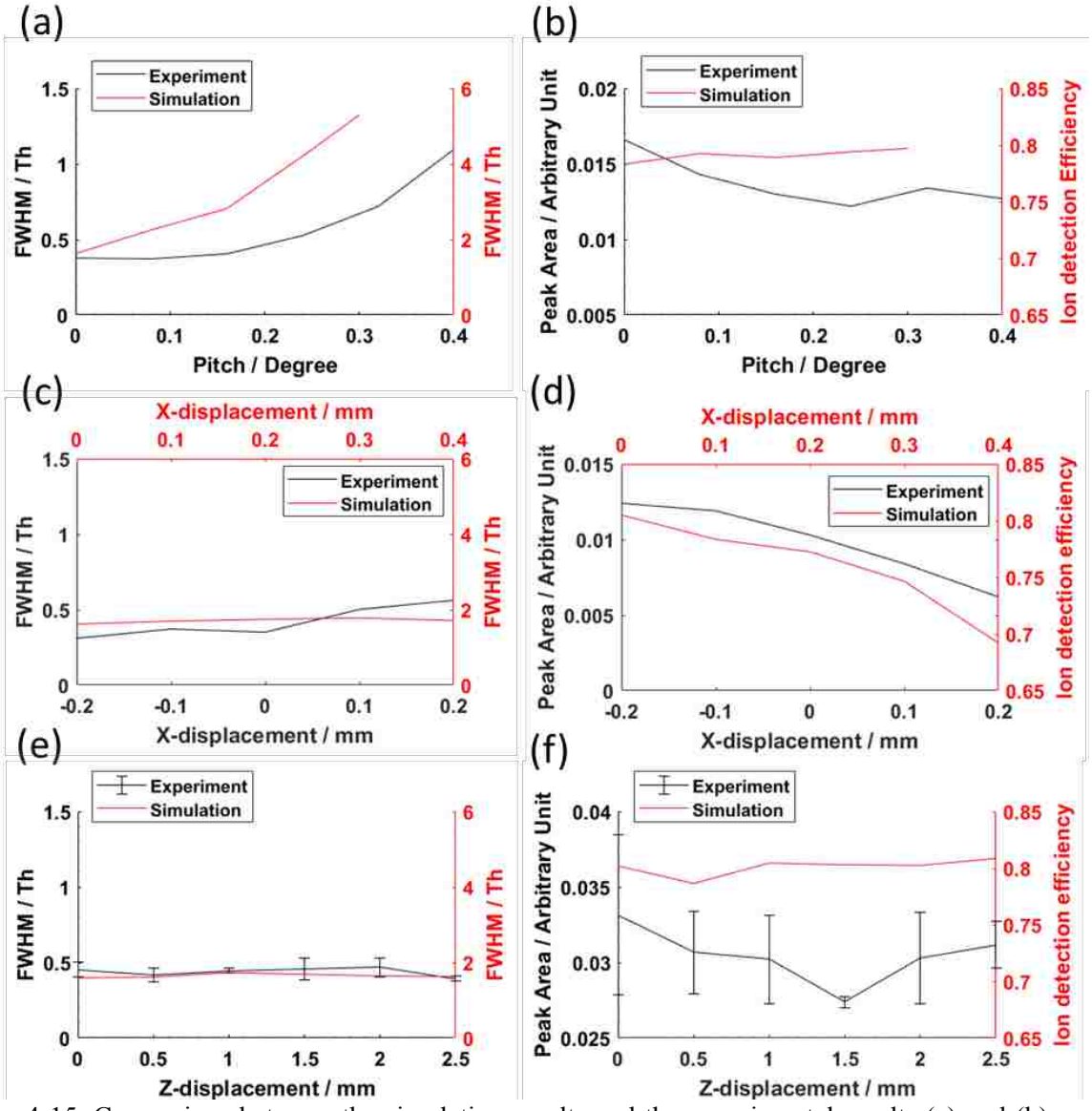

Figure 4-15. Comparison between the simulation results and the experimental results (a) and (b) are the results in pitch; (c) and (d) are the results from x-displacement; (e) and (f) are the results from z-displacement. The ***m/z*** 98 peak was used to calculate the data points. Simulation data was taken from previously reported[13].

The impact on the resolution from z-displacement seemed to be the least important among these three DOFs. There was a little fluctuation in the peak area in the experiment in Figure 4-15 (f). Note the factors affecting the ion detection efficiency in the simulation may be less. This is because each time only one ion was created in the trap region and simulated without any AC signal so that no space-charges were involved. In addition, the total number of ions simulated didn't change in each run. In the experiment, however, things were different: the variation of the number of electrons entering the trap region, the variation of the maximum trapping capacity affected by the space-charge effect, and the decrease in the resolution as an outcome of the broadened peak widths could all contribute to a reduction in the detected ion number. It might also be possible the detected ion number was less affected in boundary ejection than in resonance ejection when the pitch angle was changed. All these factors could lead to the differences between simulation results and experiment results.

It is possible the trapped ions could still be ejected through the ejection slits even though the two slits were completely staggered. But the variation in the resolution with different x-displacements needs further explanation. One possible reason is there was yaw involved, and the variation in the resolution could be the result of a combination of x-displacement and yaw. When a little in-plane rotation happened on one of the plates relative to the other, taking a random point as its rotation center, the two slits were no longer parallel and a cross point was formed. The electric fields formed around that cross point was the effective region where ions were trapped and ejected. The cross point would shift along the two ejection slits' lines when the bottom plate moved back and forth in the x direction. If the cross point was formed near both slits' middle points, the electric fields were less distorted by any electric fields nearby as the electric fields on the two sides of the

cross point were symmetric. As a result, the trajectories of the trapped ions were less affected. But if the cross point was close to one end on either plate or both, ions were more affected by the field distortion because the side fields could not be balanced out. The influence from yaw, in the prediction, is not as important as from pitch, but it may still make a big difference with the help of x-displacement. The consequence of this mixed misalignment could be more serious than the prediction for yaw alone. Another phenomenon is there was a slight shift in peak position when the displacement in x direction varies, indicating there might be a little pitch involved. This is because the equivalent plate spacing was the spacing where the cross point was formed, and pitch would change that equivalent spacing in the process of translation in X direction.

To explore whether an increase in DC would help improve or diagnose the misalignment in pitch, we intentionally displaced the top plate in pitch at –0.24° and gradually increased the DC volt from 5 V to 20 V. The positions in x and z directions were set to the arbitrarily defined zero positions. As seen in Figure 4-16 (A), the resolution was improved with a higher DC. But if the DC was over 10 V, the signal intensity was largely reduced which was probably the result of severer space charge as ions were more tightly constrained. For comparison, we turned the pitch angle of the top plate back to the arbitrary 0° position so there was less pitch involved and repeated the experiment. As seen in Figure 4-16 (B), there were not many changes in the signal resolution, but the intensity seemed to decrease all the time. Therefore, the limited improvement in the resolution as in Figure 4-16(A) should be largely due to the deviation in pitch other than any other misalignments or factors.

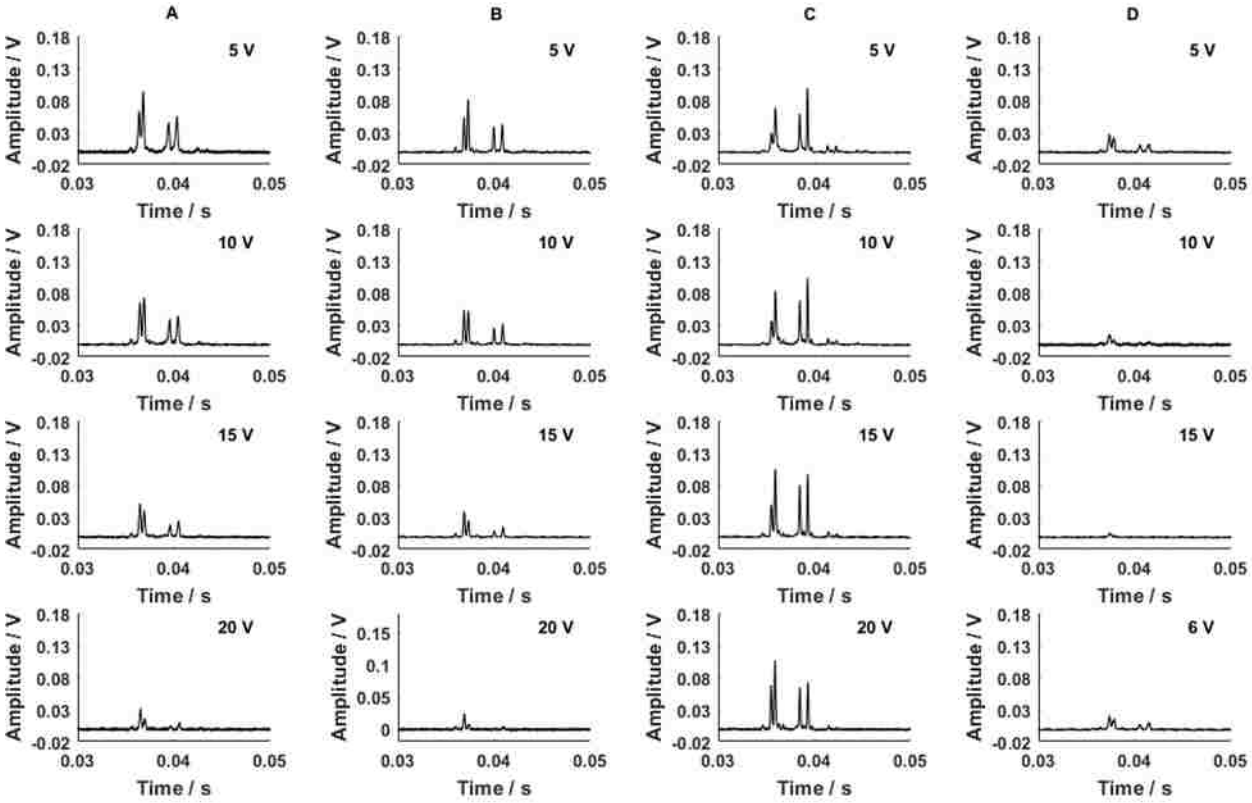

Figure 4-16. The spectra for toluene mixture with different DC volt at different displaced position: (A) −0.24° in Pitch; (B) 0.00° in Pitch; (C) −0.50 mm in x-displacement; (D) +0.50 mm in x-displacement.

In Figure 4-16 (C) and (D), a comparison between x-displacements with different DC volts on two sides of the zero position was conducted. During this process pitch was always set to the arbitrary 0° position. The performances were entirely different on two sides although the plates were intentionally displaced by the same distance (0.5 mm). This is very likely to be another proof of the presence of yaw. If the cross point was closer to the middle points of the ejection slits on both plates, then an increase in DC would help improve the performance a little bit. However, if the cross point was far from that mid position on either plate, a higher DC just jeopardized the performance. If yaw was involved in the experiment of x-displacement, all the experiments done by far were under the presence of some sort of yaw as there were no actuators installed that could

change that DOF. If the discussion above were all true, the limited improvements in the resolution degraded by pitch with a higher DC was probably because the cross point was close to the middle position when the alignment in x direction was placed at that arbitrary zero position.

4.4 Conclusion

Key improvements for a two-plate planar LIT were demonstrated to work and to provide solutions encountered in efforts to miniaturize the previous design. Better than unit resolution was achieved by optimizing the plate spacing under a given voltage distribution at a scan rate of 2300 Th/s. This new design consistently showed stable spectra with good resolution. The fabrication process for this one-side ion trap is easier and faster, and the connections are more durable than those of the old one, again an advantage for further miniaturization efforts.

In the misalignment experiment, the two-plate LIT is demonstrated to be sensitive to the misalignment in pitch as predicted. The poor resolution due to pitch could be recovered by increasing the DC volt on the End-bars though at a sacrifice of the peak intensity. There was a maximum value DC can be applied, otherwise the performances would degrade. The effect from x-displacement alone was still unknown, but it would play an important role in affecting the performance once yaw was involved. This mixed misalignment turned out to have a clear impact on the peak intensity and affect the resolution if the formed cross point was far from the middle points of the two ejection slits, though its variation was not as obvious as in pitch. Improving the poor resolution caused by the mixed misalignment by increasing the DC volt only worked when the cross point was near the trapping center. On the other hand, the phenomenon that the resolution was improved by increasing the DC volt was not sufficient to diagnose whether there were

displacements either in pitch or in yaw. z-displacement had little impact on either the resolution or the intensity within a practical range.

Limitations of the new alignment platform are: first, yaw itself could affect the resolution and intensity a lot, but no actuator was applied to adjust that DOF in the experiment. A motorized rotation stage is needed to help study the impacts from x-displacement and yaw separately; second, misalignments could incorporate roll whereas this DOF was ignored in this experiment. It is possible the performance will be further improved if roll can be aligned. Future work should install a rotation stage to adjust yaw and/or another actuator to adjust roll if possible.

4.5 References

1. Tian, Y.; Higgs, J.; Li, A.; Barney, B.; Austin, D. E., How far can ion trap miniaturization go? Parameter scaling and space-charge limits for very small cylindrical ion traps. *J. Mass Spectrom.* **2014,** *49* (3), 233-240.

2. Austin, D. E., Wang, M.,Tolley, S. E., Maas, J. D., Hawkins, A. R., Halo ion trap mass spectrometer. *Anal. Chem.* **2007,** *79*, 2927-2932.

3. Wang, M.; Quist, H. E.; Hansen, B. J.; Peng, Y.; Zhang, Z.; Hawkins, A. R.; Rockwood, A. L.; Austin, D. E.; Lee, M. L., Performance of a halo ion trap mass analyzer with exit slits for axial ejection. *J. Am. Soc. Mass Spectrom.* **2011,** *22* (2), 369-378.

4. Schwartz, J. C.; Senko, M. W.; Syka, J. E. P., A two-dimensional quadrupole ion trap mass spectrometer. *J. Am. Soc. Mass Spectrom.* **2002,** *13* (6), 659-669.

5. Ouyang, Z.; Wu, G.; Song, Y.; Li, H.; Plass, W. R.; Cooks, R. G., Rectilinear ion trap: Concepts, Calculations, and Analytical Performance of a New Mass Analyzer. *Anal. Chem.* **2004,** *76* (16), 4595 - 4605.

6. Zhang, Z.; Quist, H.; Peng, Y.; Hansen, B. J.; Wang, J.; Hawkins, A. R.; Austin, D. E., Effects of higher-order multipoles on the performance of a two-plate quadrupole ion trap mass analyzer. *Int. J. Mass Spectrom.* **2011,** *299* (2–3), 151-157.

7. Brett J. Hansen, R. J. N., Aaron R. Hawkins, Stephen A. Lammert, Daniel E. Austin, A lithographically patterned discrete planar electrode linear ion trap mass spectrometer. *J. Microelectromech. Syst.* **2013,** *22*, 876-883.

8. Gill, L. A.; Amy, J. W.; Vaughn, W. E.; Cooks, R. G., In situ optimization of the electrode geometry of the quadrupole ion trap1. *Int. J. Mass Spectrom.* **1999,** *188* (1–2), 87-93.

9. Zhang, Z. P.; Peng, Y.; Hansen, B. J.; Miller, I. W.; Wang, M.; Lee, M. L.; Hawkins, A. R.; Austin, D. E., Paul trap mass analyzer consisting of opposing microfabricated electrode plates. *Anal. Chem.* **2009,** *81* (13), 5241-5248.

10. Moxom, J.; Reilly, P. T. A.; Whitten, W. B.; Ramsey, J. M., Sample pressure effects in a micro ion trap mass spectrometer. *Rapid Commun. Mass Spectrom.* **2004,** *18* (6), 721-723.

11. Li, A.; Hansen, B. J.; Powell, A. T.; Hawkins, A. R.; Austin, D. E., Miniaturization of a planar-electrode linear ion trap mass spectrometer. *Rapid Commun. Mass Spectrom.* **2014,** *28* (12), 1338-1344.

12. Kaiser, R. E.; Cooks, R. G.; Stafford, G. C.; Syka, J. E. P.; Hemberger, P. H., Operation of a quadrupole ion trap mass spectrometer to achieve high mass/charge ratios. *Int. J. Mass Spectrom. Ion Processes* **1991,** *106*, 79-115.

13. Wu, Q.; Tian, Y.; Li, A.; Austin, D. E., Simulations of electrode misalignent effects in two-plate linear ion traps. *Int. J. Mass Spectrom.* **2015,** *393*, 52-57.

5.Linear Wire Ion Traps

(The simulation and experiment on the half-size WIT in this chapter are taken from "Wu, Q.; Li, A.; Tian, Y.; Zare, R. N.; Austin, D. E. Miniaturized Linear Wire Ion Trap Mass Analyzer. Anal. Chem. 2016, 88(15), 7800-7806" and "Wu, Q.; Tian, Y.; Li, A.; Andrews, D.; Hawkins, A. R.; Austin, D. E. A Miniaturized Linear Ion Trap with Electron Ionization and Single Photon Ionization Sources. Journal of American Society for Mass Spectrometry. 2017, 28(5), 859-865." My contribution to these two papers is helping collect data from the half-size wire ion trap. The discussion about the geometry deviation on WIT and the preliminary work on WIT miniaturization are my individual efforts.)

5.1 Introduction

As was mentioned in Chapter 1, LIT is a promising choice for developing portable MS due to its relatively large ion storage volume. Traditional LITs or the simplified version, RITs, use machined metal electrodes which makes the traps unnecessarily heavy. In addition, it is possible some ions are lost to the electrodes near the ejection slit. The two-plate planar LIT effectively reduces an assembly's weight in addition to restoring the storage volume at a small trap dimension. The higher order components in the electric field can also be optimized by independently dividing the RF voltage applied on each electrode. However, the lithographically patterned planar plates (ceramic and glass plates) are fragile and must be handled with care. Meanwhile, the electrical connections on the two-sided patterned ceramic plates can easily go wrong, but they are hard to check or to repair.

To reduce the trap weight, simplify the fabrication process, and make the ion trap robust, our group introduced a new ion trap, the linear wire ion trap (WIT), that had a similar structure with a traditional quadrupole mass filter. The WIT was made by arraying a number of wires held taut

between two identical plastic plates. The wires were arranged in a hyperbolic pattern on each one of the four sides so that the cross section view of the wire array looked like that in the traditional LIT (see Figure 5-1 (b)). Each of the two plastic plates was embedded with a metal ring as an end-electrode. After straightening the wires and applying the desired voltages on each wire group (wires on the same side belong to the same group), a quadrupolar field was created in the center that possessed the same trap ability as a traditional LIT had. Section 5.2 which includes the design, the fabrication and the experimental results of a half-size WIT is substantially taken from Dr. Qinghao Wu's publications[1-2].

5.2 WIT simulation and experimental results

WIT simulation

The model was built in SIMION 8.1 as shown in Figure 5-1 (a) to optimize the hole positions in the simulation before machining the plastic plate. The planar parts surrounding the wires were grounded shields to prevent the interference of any electric fields from outside regions, such as those created by the detector or the RF signals in the experiment. The quadrupolar field was created by four virtual electrodes, each of which was formed by six wires arrayed with the desired curvature.

There were 24 wires in all with 6 wires on each side in both the full-size and half-size WIT. The wire array was symmetric relative to the X and Y axes crossed at the trapping center. Since the position of each hole was determined by the coordinates in X and Y directions, the number of independent variables were 12. In fact, it was the Y coordinates of the wires in B group and the X coordinates of the wires in A group that determined the trap dimension and the curvature of the virtual electrodes.

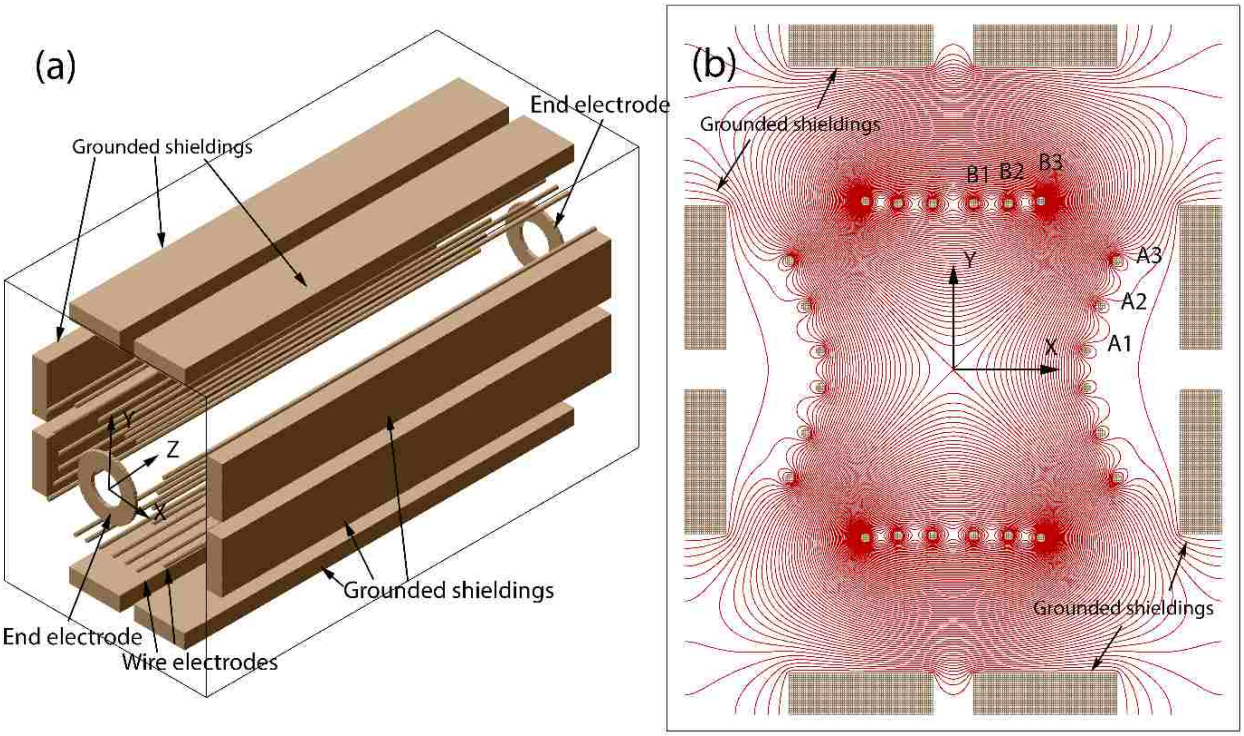

Figure 5-1. (a) The model built in SIMION 8.1; (b) Cross-section view of the field contour. (Adapted from Wu, Q.; Li, A.; Tian, Y.; Zare, R. N.; Austin, D. E. Miniaturized Linear Wire Ion Trap Mass Analyzer. *Anal. Chem.*, **2016**, 88, 7800-7806.)

To simplify the optimization process, the X coordinates of the wires in B group and the Y coordinates of the wires in A group were made constant. A geometry file was written to finely control the wire positions at a scale of 0.1 mm per unit for the full-size WIT and 0.05 mm per unit for the half-size WIT. The relative geometry optimization was done by varying one of the six variables each time within a reasonable range.

All the electrical parameters and recorded data were controlled by user programs. The simulated RF frequency was 1.53 MHz with an initial voltage 380 $V_{0\text{-}p}$. There are 3000 ions created in each run all at a mass-to-charge ratio of 91. Ions were boundary ejected and their ejection voltages were recorded to calculate the resolution.

Simulations showed that the performance was not affected too much by the absolute coordinates but by the relative ratio between the X coordinates of the wires in A group and the Y coordinates of the wires in B group. If the wires' Y coordinates were generally larger, more ions would be ejected in X direction, otherwise more ions would be ejected in Y direction. The optimized geometrical parameters are shown in Table 5-1. This optimized case had the best resolution that ejected most of the ions in X direction.

Table 5-1. Geometrical specification for the half-size wire ion trap. The origin of the coordinate was at the trapping center, the rest wires were mirrored about the x and y axes based on the following six wires.

Position	Wire Number					
	A1	A2	A3	B1	B2	B3
X/mm	3.25	3.6	4	0.5	1.35	2.15
Y/mm	0.45	1.55	2.65	3.8	3.8	3.85

WIT fabrication

Two 30×24 mm plastic plates were laser drilled with 24 holes at a diameter a little larger than 0.2 mm at the positions shown in Table 5-1. The two plates were immobilized by four screw rods to support the ion trap structure as well as to separate and position the wires. A large circle was drilled right at the center of the wire hole array on each plate to attach a washer as the end-cap. A series of stainless-steel wires at a diameter of 0.008″were passed through these holes to form the virtual electrodes. Each wire group was tightened by twisting all the wires in that group together on one side. The straightness of the wires was adjusted by the nuts threaded on the mounting rods as shown in Figure 5-2.

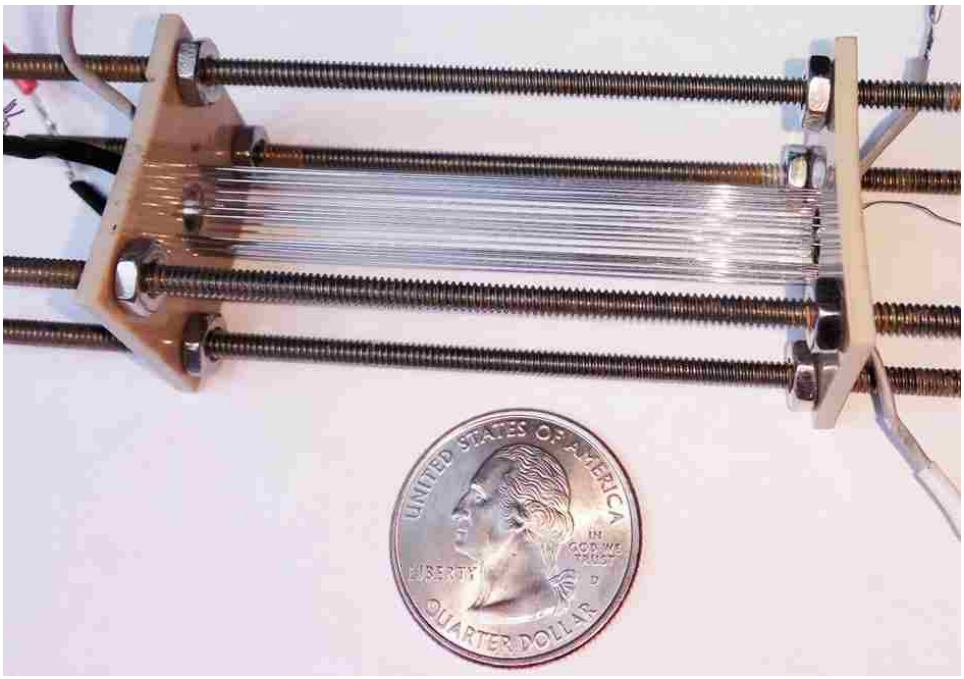

Figure 5-2. Photo of the completed half-size WIT. (Adapted from Wu, Q.; Li, A.; Tian, Y.; Zare, R. N.; Austin, D. E. Miniaturized Linear Wire Ion Trap Mass Analyzer. *Anal. Chem.*, **2016**, *88*, 7800-7806.)

Experiments were primarily done on the half-size WIT. The cross section view of the WIT assembly with two ionization sources is seen in Figure 5-3. The four shields all had bulges on the inner surfaces so that they were close enough to the wires without being impeded by the mounting rods. Two detectors were mounted on the grounded shields to compare the signal intensities on two directions. One was attached on the X direction, and the other one was on the Y direction. There were two ionization sources mounted on two opposite ends, an electron-gun (E-gun) and an ultraviolet lamp (UV lamp).

The E-gun was used to dissociate the neutral molecules into more fragment ions by bombarding them with electrons at high kinetic energies; the UV lamp produced a pulse of photons so that neutral molecules were soft ionized by absorbing the energy of each single photon they met, yielding more molecular ions.

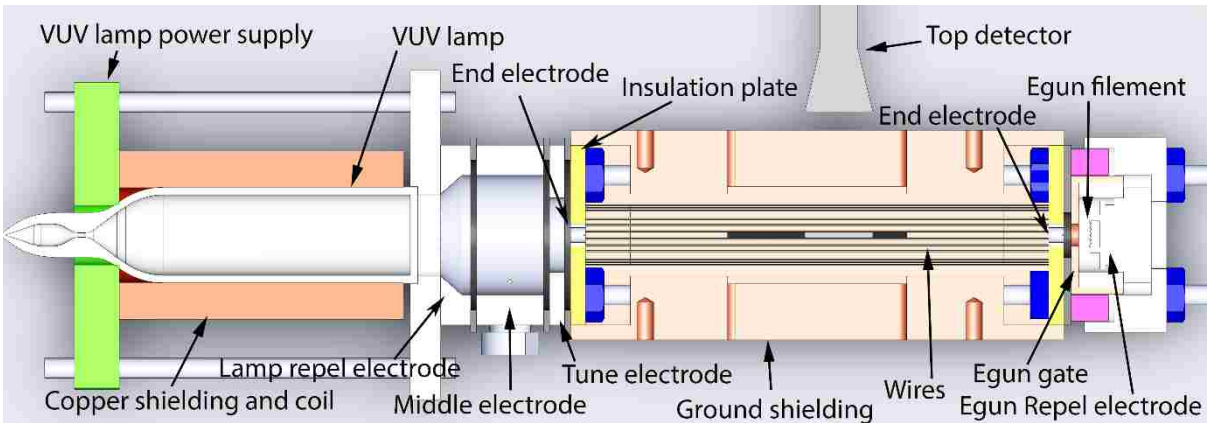

Figure 5-3. Schematic view of WIT assembly with two ionization sources. (Adapted from Wu, Q.; Tian, Y.; Li, A.; Andrews, D.; Hawkins, A. R.; Austin, D. E. A Miniaturized Linear Ion Trap with Electron Ionization and Single Photon Ionization Sources. *J. Am. Soc. Mass Spectrom.* **2017**, *28*(5), 859-865.)

Comparison experiment was conducted between these two ionization sources to determine which one performed better. Three focal lenses, repel electrode, middle electrode and tune electrode, were arranged in line between the UV lamp and one of the WIT end-caps. The thickness, the central hole size and the applied voltage of each lens were optimized in SIMION to obtain the highest efficiency ions passing through the end-cap hole. Silicon rubbers were spaced between each two lenses and between the tune lens and one of the WIT plastic plate. The E-gun was mounted by a self-designed mounting: the filament of the E-gun was surrounded and insulated by a ceramic ring, which was surrounded by a magnetic ring to focus the electron beam. The magnetic ring was placed into a copper cylinder that was also used as the e-gun gate. The copper cylinder sat into a PTFE mount which was threaded on the four WIT screw rods. To make use of the sample molecules more efficiently, a fused-silica tube was used to connect the sample inlet to the center hollow region of the middle electrode. Helium gas was also transferred to the middle electrode region through a Teflon tube rather than expanding in the whole chamber.

Experiments

A RF voltage at 1.53 MHz (Ardara Technologies, L.P.) was applied on the top and bottom B groups. The supplementary AC signal was generated by a function generator (SRS DS345, Stanford Research Systems. Sunnyvale, CA) and was applied on one of the A group. The other side of A group where the side detector was attached was grounded. The AC frequency was tuned to 525 KHz at an amplitude of 2.2 $V_{0\text{-}p}$. The AC signal was biased by 1.3 V to improve the ion ejection efficiency. A 12 V DC was applied on the two end-bars. Samples were introduced in vacuum and raised the background pressure from 10^{-6} mbar to 10^{-5} mbar by a leak valve (Granville-Phillips Co., Boulder, CO). Helium pressure was kept at $5x10^{-4}$ mbar. The e-gun acceleration voltage was set to −60 V. A pair of +23 V and −100 V was alternatively applied on the gate to control the electron beam. Both the top and side detector voltages (electron multiplier, Detector Technology, Inc.) were set to −1400 V. Signal was amplified by 10^7 times in a pre-amplifier (Keithley 427 current amplifier, Beaverton, OR) before sent to an oscilloscope. The UV lamp used in this experiment created photons with 10.6 eV (117 nm) (Heraeous Noble Light, PKR 106, GmbH, Germany). It was pulsed on and off by a gate at +23 V/0 V DC power. The FWHM of the produced photon is 0.1 eV. The voltage on the repel electrode, the middle electrode and the tune electrode were 23 V, 20 V and 15 V, respectively, to focus and push the created ions into the trap region.

Achievements on the half-size WIT

Unit resolution was achieved by resonance ejecting the toluene and deuterated toluene mixture as Figure 5-4 (a) shows.

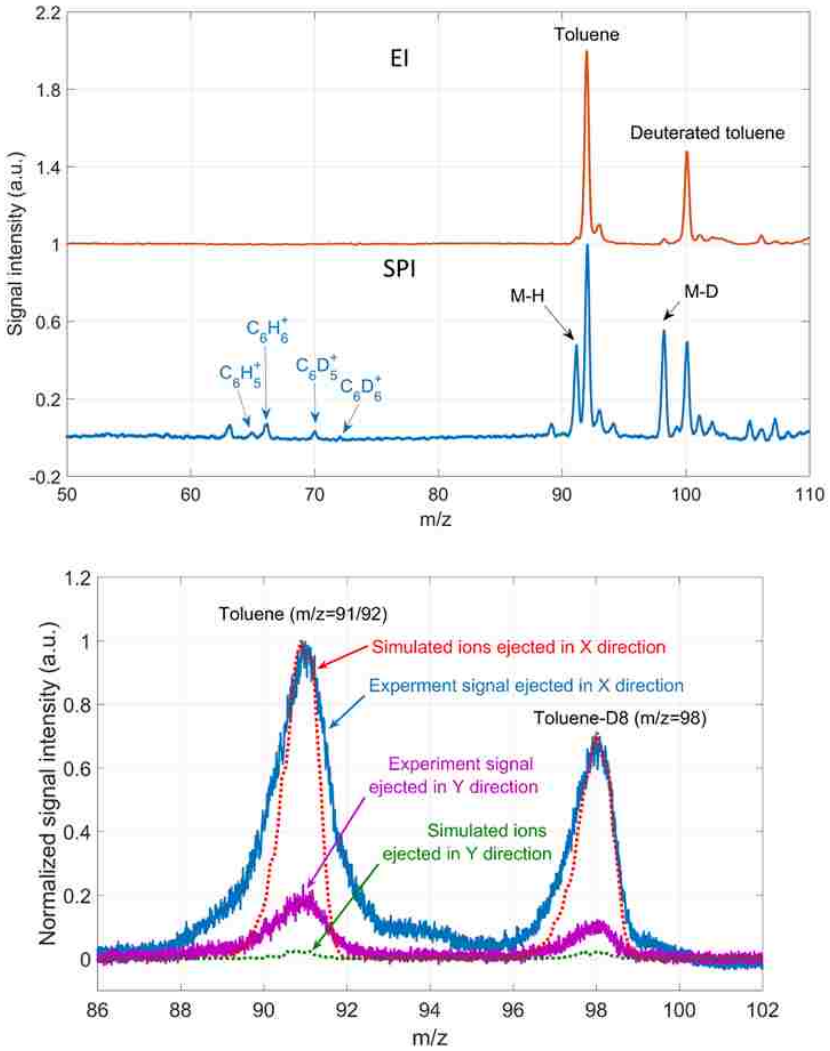

Figure 5-4. (a) Spectra obtained by electron ionization (EI) and by single photon ionization (SPI); (Adapted from Wu, Q.; Tian, Y.; Li, A.; Andrews, D.; Hawkins, A. R.; Austin, D. E. A Miniaturized Linear Ion Trap with Electron Ionization and Single Photon Ionization Sources. *J. Am. Soc. Mass Spectrom.*, **2017**, *28*(5), 859-865.) (b) Comparison of the signal intensity in X and Y directions in both the experiment and the simulation. (Adapted from Wu, Q.; Li, A.; Tian, Y.; Zare, R. N.; Austin, D. E. Miniaturized Linear Wire Ion Trap Mass Analyzer. *Anal. Chem.*, **2016**, *88*, 7800-7806.)

The spectrum was averaged over 50 scans. The scan rate was 3830 Th/s. The reported FWHM of the result obtained with electron ionization (EI) could be as small as 0.37 Th. However, comparing the result from EI with that from single photon ionization (SPI) under the same operating conditions (including the same sample and helium pressures, the same trapping, ejecting and detecting parameters), SPI seemed to perform better both in the resolution and the sensitivity.

Figure 5-4 (b) compared the signal intensity in X and Y directions in the experiment with the number of ions ejected in these two directions in the simulation. The experimental result matched the simulation result that most of the ions were ejected in X direction.

5.3 Geometry deviations on the WIT

Although WITs are relatively easier and cheaper to make compared with ceramic or glass planar linear ion traps, geometry deviations could easily happen during the process of straightening the wires. Making the two plastic plates exactly parallel with each other is difficult, partly because the trap structure entirely depends on manually positioning the eight nuts that are flexible during the fabrication. The main reason is one of the corners of the two plates had to be intentionally pushed more apart to straighten some of the wires that were looser than others. However, the half-size WIT with an apparent geometry deviation still showed good performance. It would be interesting to find out whether LITs made in this structure would be less sensitive to geometry defects.

Five DOFs in a WIT

The types of geometry deviation that could happen in a WIT include the three angular deviations pitch, roll, yaw, and two translation deviations x- and y- displacements (see Figure 5-5). The only difference between the WIT and the two-plate LIT was there was no z-displacement in the WIT. The wire electrodes were affected in a different way from other types of linear ion traps: all the “electrodes” were affected with some of their curvature squeezed no matter which displacement happened.

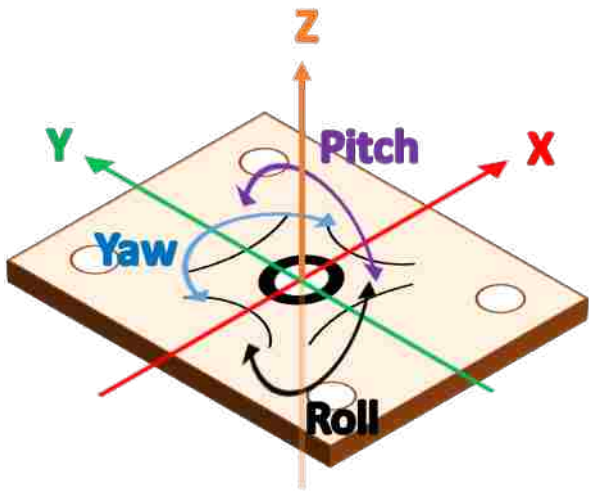

Figure 5-5. Representative of geometry deviations involved one of the plate relative to the other in a WIT.

Simulations of the geometry deviations on the full-size WIT

SIMION 8.1 was used to study the full-size WIT's performance with the presence of only one of each displacement. The relative positions of the wires were the same as Table 5-1 showed but the absolute values were doubled. The two end-caps were separated by 60 mm apart. The geometry deviation was made by moving one of the plate with the other plate fixed. The geometries with different levels of displacements were finely controlled in GEM files. RF signal was made at 1.6 MHz, which started to ramp from 1500 $V_{0\text{-}p}$ at a scan rate of 4320 Th/s. The end-cap rings were always applied with 12 V to confine the ions. In each run, there were 10,000 ions created at ***m/z*** 91 at the same position in the center of the trapping region. The collision gas was helium at 4.3 mTorr. Ions were boundary ejected without any AC resonance voltages. The ejection voltage, as well as the x, y and z coordinates where ion stops moving were recorded. As the geometry was intentionally made to eject most of the ions in X direction, only ions ejected in X direction were analyzed. Considering the fact that WITs might be insensitive to the geometry deviation, the deviations in the simulation were varied within a large range: the translation distances in X and Y

directions were varied from 0 to 30 mm at a big step size of 5 mm. Pitch and roll were changed from 0 to 30° at a step size of 5°. Yaw was varied from 0 to 10° at a step size of 1°.

Results and discussion

The two opposite virtual electrodes became closer in radial direction when x-displacement occurred and closer in axial direction when y-displacement occurred. What followed was a little increase of the curvature on the other two sides of the electrodes.

As seen in Figure 5-6, the resolution was almost the same no matter how the y-displacement varied. In the X direction, however, the FWHM gradually increased when the plate was displaced from 0 mm to 30 mm. This indicated the performance of the resolution in x direction was affected more from the displacement in x direction than in y direction. Similar experimental results had been reported on a quadrupole ion trap[3] that the axial dimension in which ions were ejected had a big impact on the ion trap's performance. Nevertheless, the performance was quite stable within 10 mm, considering the plate had been deviated by 35% of its width. The FWHM became obviously larger only when the displacement was over 10 mm. The impact from roll and pitch were quite similar. The FWHMs varied from 0.87 Th to 1 Th when the angles were changed from 0° to 10° in both cases. The explanation of these variations were similar to what happened to pitch in the two-plate LIT[4]. The difference is pitch and roll had equal impact on the resolution whereas roll was less important than pitch in the case of the two-plate LIT. Roll and pitch need to be taken with extra care during the fabrication as they are easy to occur and appear to have the biggest impact on the resolution.

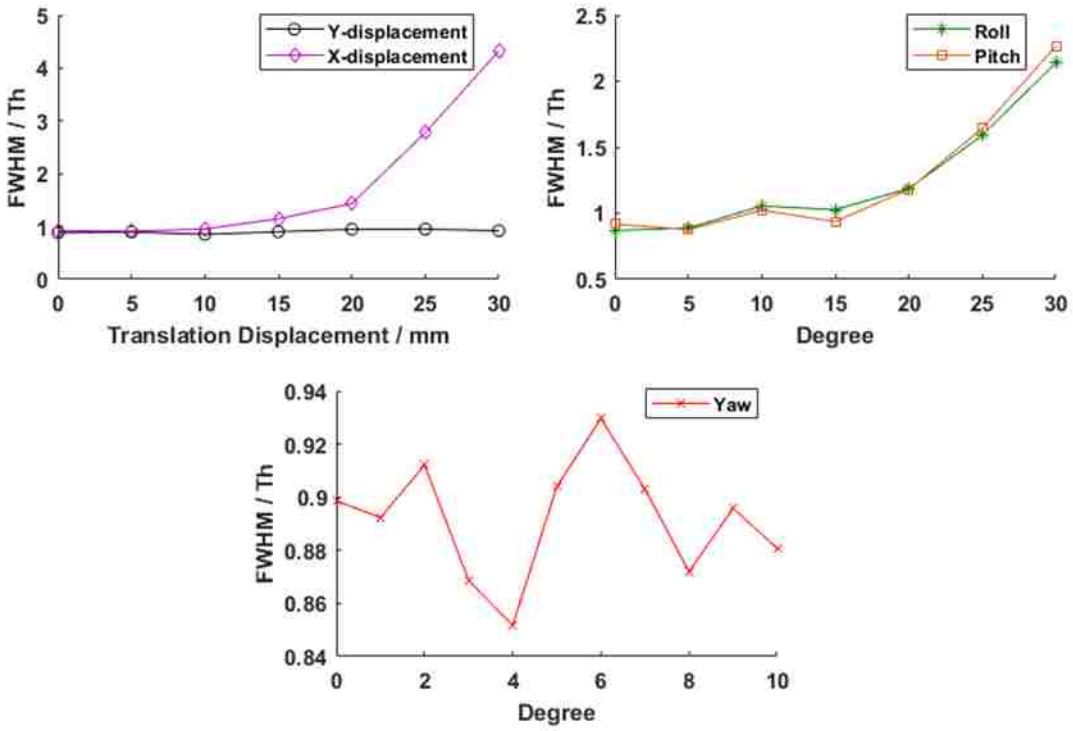

Figure 5-6. Plot of FWHM as variations in five DOFs, including (a) y- and x-displacements, (b) Roll and Pitch and (c) Yaw.

The cross section became tighter in the center than those near the two ends when yaw occurred. The tightness depended on how much yaw was displaced. For instance, imagine the trap length evenly divided into an infinite number of tiny sections. Though the cross section of each tiny section varied in size and had a small angle relative to the next two sections on two sides, the curvature of the four virtual electrodes remained the same on four sides. It was interesting to see that ions could still be trapped in such a distorted structure. The FWHM fluctuated but was always below 1 Th within 10° of displacement in yaw. The misalignment in yaw was largely determined by the tolerance in the positions of the mounting holes between the two plates. Since the precision

in the two-dimensional machining process was typically high, yaw was less likely to happen and was less important to the resolution.

Another phenomenon observed in the simulations for all five DOFs was the mass shift. This was due to the similar reason in the two-plate LIT, that a variation of average trap dimension would lead to a variation in the ejection voltage for the same ion mass according to Equation 1-2.

5.4 Preliminary work on WIT miniaturization

It can be inferred from the simulation that WITs have robust structures and tend to be less affected by the geometry deviation compared with the two-plate LIT in term of the resolution. The relatively easier and cheaper fabrication on plastic plates with relatively high precision make them more competitive in developing miniaturized ion traps, even though the straightening process would be a challenge at small scales.

Digital Ion Traps

So far, the trapping voltage used in most of the ion traps are sinusoidal waveforms. Ions are ejected by ramping the sinusoidal RF amplitude while keeping the RF frequency constant. However, the HMCO (high mass cut-off) of an ion trap operated in this amplitude scan mode is limited by the maximum voltage that can be applied. On the other hand, small ion traps often work at high frequencies while the choices of high frequency oscillators are limited by the resonant network[5]. The other way to eject ions according to Equation 1-2 would be sweeping the RF frequency at a constant RF amplitude. However, sinusoidal waves oscillated at high frequencies would be unstable, jeopardizing the mass resolution. Ding and co-workers proposed a way of trapping ions under a rectangular waveform which was created and controlled by digital circuitry[6-

[7]. The waveform was generated by switching a MOSFET (metal-oxide-semiconductor field-effect transistor) between two independent DC voltages (Positive V1 and Negative V2) as shown in Figure 5-7 (top). By varying the switch speed and the duration of time the MOSFET stayed at each DC voltage, the output rectangular waveform was generated as shown in Figure 5-7 (bottom). ***T*** represents the period of a rectangular waveform. ***d*** is duty cycle which determines the ratio of the residence time in V1 and V2.

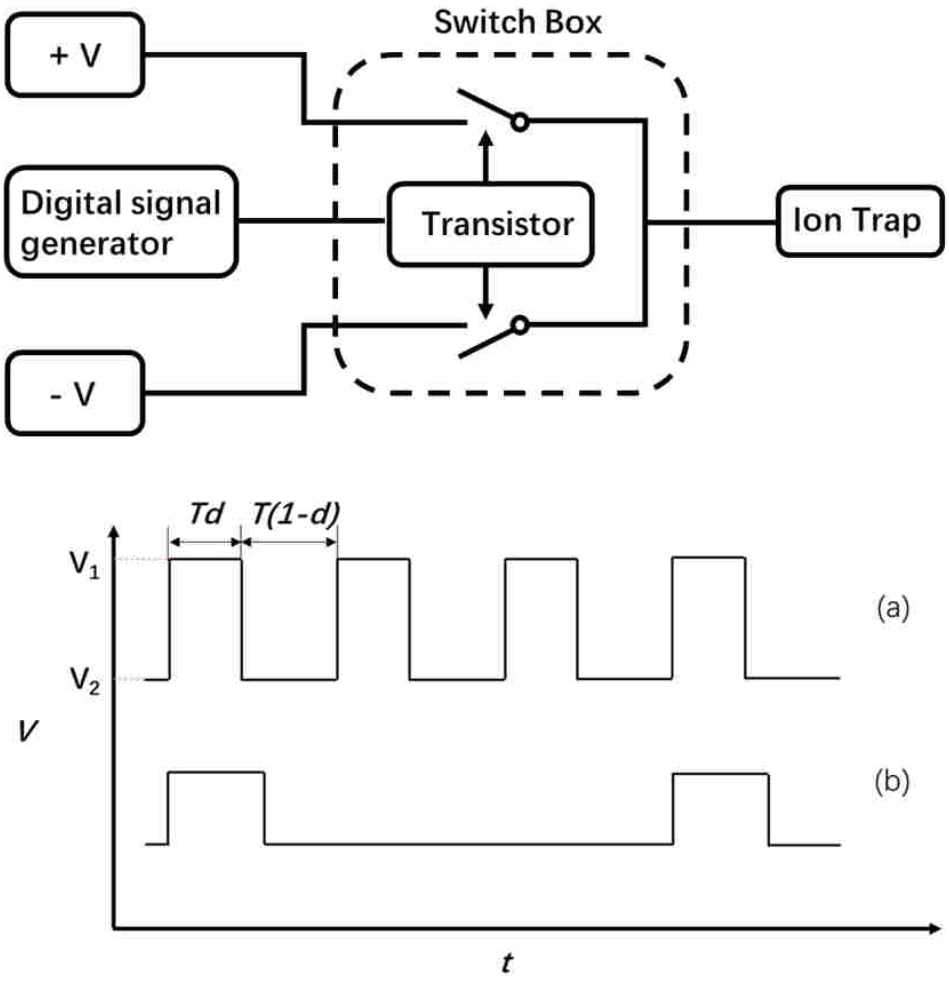

Figure 5-7. Representative of the digital circuitry (above) and timing control of the digital waveform (below): (a) Driving/Trapping waveform; (b) Supplementary resonance waveform.

The definition of the trapping amplitude in the rectangular waveform thus becomes

$$U = dV_1 + (1 - d)V_2 \qquad \textit{Equation 5-1}$$

The name "digital" comes from the fact that the rectangular waveform is generated by a digital circuit. Ion traps operated with waveforms that are controlled by the digital circuits are called digital ion traps (DITs). The ability of trapping heavy ions with relative low amplitudes and the character of easily sweeping trapping frequencies with high stability make DITs attractive in the development of small ion traps.

WIT operated with digital circuitry

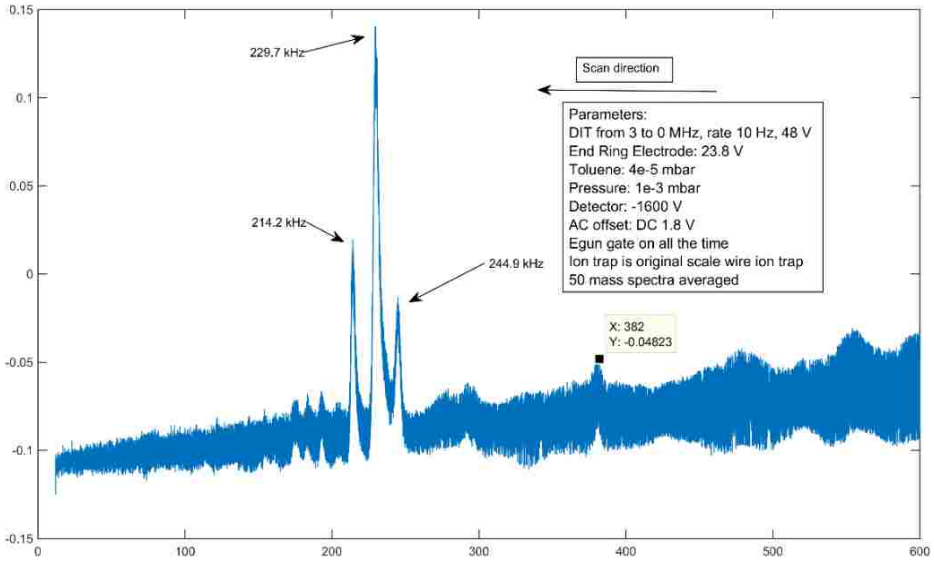

Figure 5-8. Toluene ion peaks obtained by applying digital waveform on the full-size WIT.

A self-made digital power supply was constructed based on the idea proposed by Ding's group[7]. This digital power supply had been demonstrated to work with the full-size WIT though nothing had been obtained from the half-size WIT. The signal from toluene ions was obtained with

the appropriate parameters as shown in Figure 5-8. The trapping amplitude was always 48 V. The trapping frequency was scanned from 3 MHz to 1 Hz at a rate of 10 Hz.

Since the transistor in this digital power supply could not stand high voltages at high frequency range. Small ion traps that typically operate at relative low amplitudes would be better choices to work with.

Preliminary work on small WITs

The next small ion traps we targeted were quarter-size WITs. The wire positions of the quarter-size WITs were determined directly by scaling down the pattern from the full-size or the half-size WITs. The relative positions among the wires were remained the same. Since the dimensions of the virtual electrodes in quarter-size WITs were four times smaller than those in the full-size WITs, either the number of wires on each side should be reduced or the diameter of wires used should be smaller. Otherwise, these wires would be too close to each other. As the stainless-steel wires with the maximum diameter allowed by the 24-wire array space would be too narrow to bear the tension during the straightening process, a better option is reducing the number of wires used on each side instead of reducing the wire diameter.

Table 5-2. Geometric specifications for the original four wires A1, A2, B1 and B2 in the 5/16-size WIT.

Position	**Wire Number**			
	A1	**A2**	**B1**	**B2**
X/mm	2.12	2.25	0.44	1.25
Y/mm	0.5	1.32	2.25	2.25

The second small WIT we designed has four wires on each side as seen in Figure 5-9. The trap dimension was scaled as 5/16 of the full-size WIT. The geometry specifications for this new pattern are shown in Table 5-2.

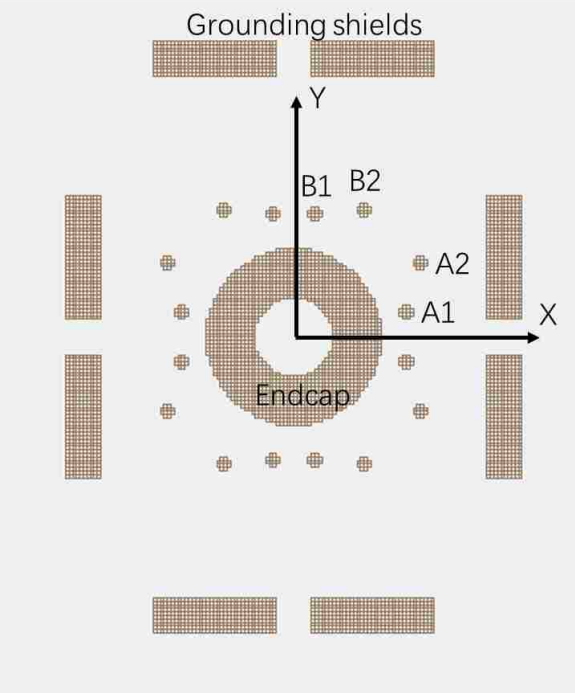

Figure 5-9. Simulation model of four-wire WIT in SIMION.

The support plates used in the quarter-size and the 5/16-size WITs were both made of printed circuit boards. All the boards were pre-drilled with holes at diameters of 0.15 mm. Wires at diameters of 0.005″ were used to make the 5/16-size WIT. It is a bit challenging to connect the inside end-cap rings to the outside power cables without touching the surrounding wires. In the quarter-size WIT, the end-cap rings were made by coating a layer of silver-epoxy covering the surfaces of the central holes (see Figure 5-10 (b)). The epoxy layers were connected to the patterned traces which led out of the central area. In the 5/16-size WITs, metal tubes were pre-inserted in the central holes as the end-caps (see Figure 5-10 (c)).

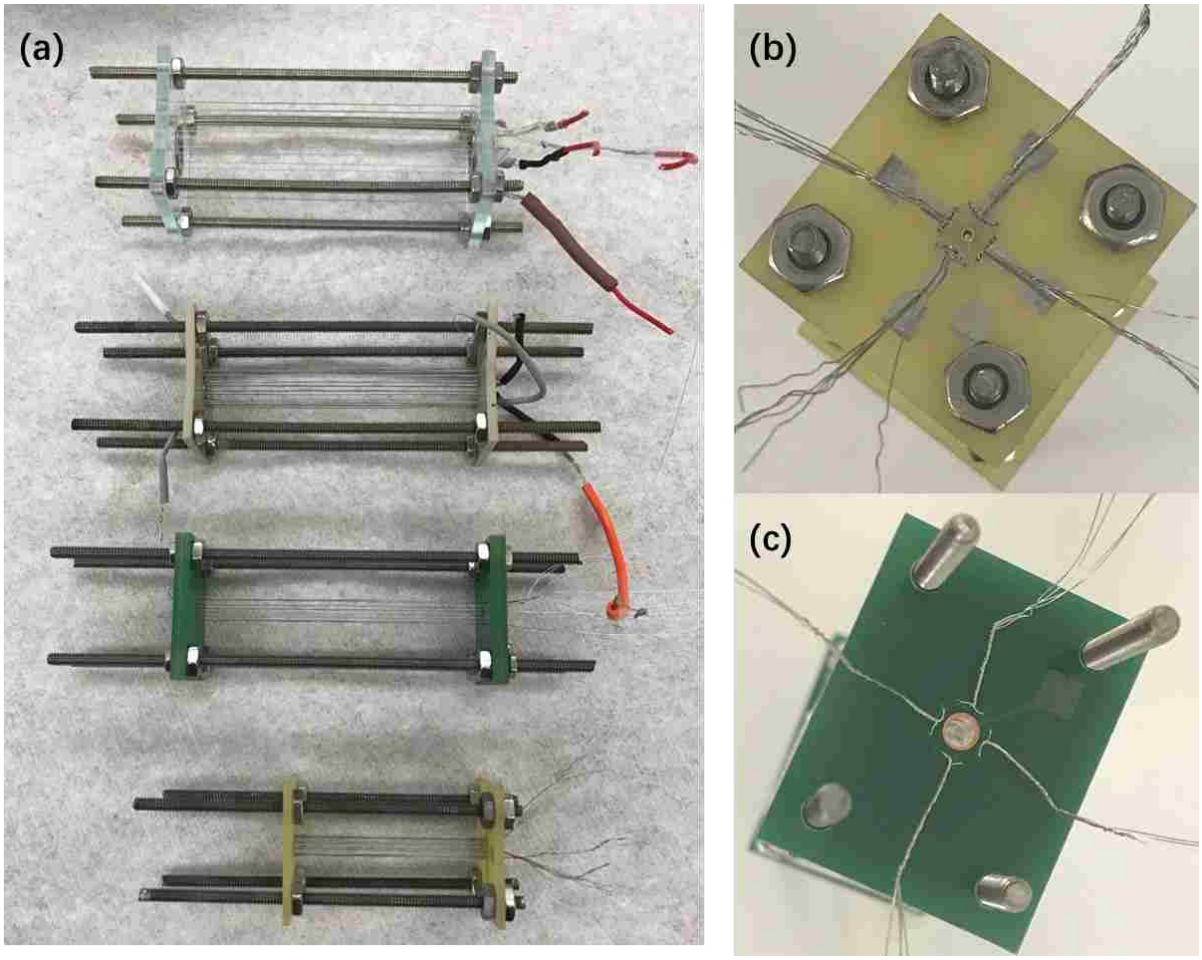

Figure 5-10. (a) Overview of different WIT sizes: from top to bottom are Full-size, Half-size, 5/16-size and Quarter-size WIT; (b) Photo of the quarter-size WIT with six wires on each side; (c) The 5/16-size WIT with four wires on each side.

Experiments on the 5/16-size WIT had been done by sweeping the RF amplitude at the constant frequency 3 MHz, yet no signals have been obtained. Future efforts can be made on exploring the optimal RF frequency, increasing the current on the E-gun's filament, using the SPI source instead of the EI source, or applying the digital power supply which is suitable for ion traps at small dimensions.

5.5 References

1. Wu, Q.; Li, A.; Tian, Y.; Zare, R. N.; Austin, D. E., Miniaturized linear wire ion trap mass analyzer. *Anal. Chem.* **2016,** *88* (15), 7800-7806.

2. Wu, Q.; Tian, Y.; Li, A.; Andrews, D.; Hawkins, A. R.; Austin, D. E., A miniaturized linear ion trap with electron ionization and single photon ionization sources. *J. Am. Soc. Mass Spectrom.* **2017,** *28* (5), 859-865.

3. Gill, L. A.; Amy, J. W.; Vaughn, W. E.; Cooks, R. G., In situ optimization of the electrode geometry of the quadrupole ion trap1. *Int. J. Mass Spectrom.* **1999,** *188* (1–2), 87-93.

4. Wu, Q.; Tian, Y.; Li, A.; Austin, D. E., Simulations of electrode misalignent effects in two-plate linear ion traps. *Int. J. Mass Spectrom.* **2015,** *393*, 52-57.

5. Brancia, F. L.; Ding, L., Rectangular waveform driven digital ion trap (DIT) mass spectrometer: Theory and applications. In *Practical Aspects of Trapped Ion Mass Spectrometry*, March, R. E.; March, R. E., Todd, J. F. J., Eds. CRC Press: Boca Raton, FL, 2010; Vol. IV, pp 273-307.

6. Ding, L.; Sudakov, M.; Kumashiro, S., A simulation study of the digital ion trap mass spectrometry. *Int. J. Mass Spectrom.* **2002,** *221* (2), 117 - 138.

7. Ding, L.; Sudakov, M.; Brancia, F. L.; Giles, R.; Kumashiro, S., A digital ion trap mass spectrometer coupled with atmospheric pressure ion sources. *J. Mass Spectrom.* **2004,** *39* (5), 471-484.

6.Summary and Future Work

The process of miniaturizing ion traps as a part of the effort for developing portable mass spectrometers is accompanied with several issues. The most significant issues are electric issues, space charge effect, and mechanical tolerance. Electric issues include high-field electron emission, parasitic capacitance, and gas breakdown. Extra care must be taken with these potential problems when designing small ion traps. The space-charge effect is a physical phenomenon that occurs when dealing with small, charged systems. This effect can never be eliminated, only minimized or alleviated. The main problem caused by the space-charge effect is the reduction in the ion storage volume, which often brings down the sensitivity or even the resolution of a mass analyzer. Although the linear ion traps is the topic of this dissertation, trap arrays are equally important as an alternative to expand the trapping capacity and have been substantively explored to develop portable mass spectrometers. Mechanical tolerance refers to the surface roughness, quality of the shape, and the electrode alignment. The mechanical tolerance affects the performance by reducing the field accuracy. Though this dissertation only talks about the alignment issues with a simple model—the two-plate linear ion trap—the six degrees of freedom involved in this two-plate ion trap can be analogized to many other traps with more than two independent parts. There are six degrees of freedom between each two independent parts. The alignment issues in these traps can be viewed as an accumulation of individual degrees of freedom that can arise from each pair of electrodes. The microfabrication method discussed earlier relied on a Micro-electro mechanical

system (MEMS) that could provide tolerance in ranges far beyond conventional machining techniques, which can provide promising ways of fabricating ion traps at very small scales. As a way of making the most use of the in-plane high precision feature of MEMS and reducing the dependence on the out-of-plane fabrication with less precision, the two-plate technique is a promising method for ion trap miniaturization with low tolerance.

The two-plate linear ion trap has the advantage of a large trapping capacity at small scales in addition to high field precision due to low tolerance in the electrode fabrication. Even though the alignment of the two plates in the linear ion trap has been demonstrated as an important issue affecting the trap performance, a resolution of better than one unit could still be obtained by aligning them only in four degrees of freedom.

In the future, the angular dispersion of the ions, the charge build-up on the ejection slit wall, the aspect ratio, and the thickness of the plate should be considered in miniaturizing small plates. Thin plates with high-aspect ratios, and tapered slits with conductive layers coated on the inner walls would be optimal at small scales.

On the other hand, the wire linear ion trap appeared to be another promising type of ion trap to be miniaturized due to its relatively high tolerance to the electrode misalignment. Its high performance and easy and cheap fabrication also make it attractive for future study.